APPENDIX A

IDENTIFICATION OF FACTORS CONTROLLING THE DEVELOPMENT OF SUBSIDENCE IMPACTS FORECASTING METHODOLOGY TO THE I-70 ALIGNMENT OVER LONGWALL MINING OF THE TUNNEL RIDGE MINE, WASHINGTON COUNTY, PA

Task 1: Pre-Undermining Activities Report
Submitted 2 July 2019; Finalized 19 January 2020

The University of Pittsburgh Master Agreement
Contract No. 4400018535

Anthony Iannacchione, Associate Professor, Principal Investigator
Email ati2@pitt.edu
Phone: 412-624-8289

Luis Vallejo, Professor, Co-Principal Investigator
Mingzhou Li, Graduate Research Student
Emily Adelsohn, Graduate Research Student
Robert Winn, Graduate Research Student

Task 1 Report Outline

SECTION I – INTRODUCTION

Subsection Ia – Project Scope

1.0 Background

Longwall coal mining was introduced to Pennsylvania in the late 1960's. Since that time, almost 800 hundred longwall panels have extracted huge reserves of coal. Of this total, twenty-five panels have undermined parts of two interstate highways, I-70 and I-79. These twenty-five panels were located in four mines: Gateway, Eight-Four, Cumberland, and Emerald.

Over the last five decades, there has been a great deal of effort to understand how longwall subsidence basin formation impacts surface features, such as buildings, water supplies, streams and wetlands. Less is known as to how subsidence can impact interstates and even less about the embankments and cuts that carry these highway alignments. In some areas, careful monitoring of conditions and asphalt re-surfacing repaired the subsidence damage with only minimal impact to highway traffic. In other cases, bridges carrying I-79, as well as certain overpass structures, had to be replaced (Iannacchione, et al., 2011). Traffic delays were most noticeable during milling and paving activities. It should be stated that the University is not aware of any subsidence impacts causing an accident or injuring the traveling public.

2.0 Contract

The University of Pittsburgh (herein referred to as the 'University') submitted a proposal to PennDOT in May 2018. This proposal has the University studying data collected by PennDOT and its contractors during periods where an interstate was impacted by longwall subsidence. It also requires the University to assess the risk to other areas along Pennsylvania interstate alignments that might be impacted by longwall subsidence in the future.

The University received a notice to proceed with this effort on 3 October 2018. The contract was to end, no later than, 4 January 2021 at a cost of $516,348.30. The project is administered by Teresa Swisher with Roy Painter is the technical advisor. The project Kickoff meeting occurred on 23 October 2018 with work activities started in late November after the necessary University approvals were in-place. Communication and reporting on contract activities occur through regularly scheduled monthly meetings and through required reporting activities. This report is an example of a required reporting task.

The five major reporting tasks are listed below:

- Task 1: Pre-Undermining Activities - A report containing a summary of the pre-undermining activities, along with a PowerPoint presentation of research findings by 5 August 2019
- Task 2: Undermining Activities - A report containing a summary of the undermining activities, along with a PowerPoint presentation of research findings by 3 April 2020
- Task 3: Post-Undermining Activities - A report of the Subsidence Forecasting, along with a PowerPoint presentation of research findings by 3 October 2020
- Task 4: Draft Final Report by 17 November 2020
- Task 5: Final Report by 19 December 2020

The Final Report will summarize the most important information contained in Tasks Reports 1, 2 and 3. This report, referred to as the Task 1 Report, focuses on pre-undermining activities associated with the extraction of Tunnel Ridge's Panel 15.

Subsection Ib – Project Objective

Alliance Coal's Tunnel Ridge Mine has plans to undermine I-70 with the longwall mining method in both Pennsylvania and West Virginia over the next two decades. One of their panels, Panel 15, undermined I-70 early in 2019 and more are planned in the future.

1) Investigate the influence of longwall mining on highway alignments and associated slopes and embankments.
2) Evaluate how the highway deforms during undermining with a focus on determining its transient characteristics.
3) Utilize models to better understand subsidence impacts to the highway alignment, and where possible,
4) Determine how other future highway alignments could be impacted.

Subsection Ic – Initial Study Area Overview

The Tunnel Ridge Mine undermined a relatively small portion of I-70 in Pennsylvania in early 2019. Panel 15, especially where it crosses the western most extent of I-70 in Pennsylvania, defines the initial focus of this study. This panel lies less than one mile southwest of the West Alexander I-70 interchange. The initial study area is hereby designated as the 3,300-ft of I-70 (Figure Ic.1). Panel 15 underlies approximately 2,130-ft of I-70. The gate entries underlie another 520-ft of highway with another 325-ft buffer zone over the unmined coal. The western end lies some 700-ft within the State of West Virginia and the remaining 2,600-ft within the Commonwealth of Pennsylvania.

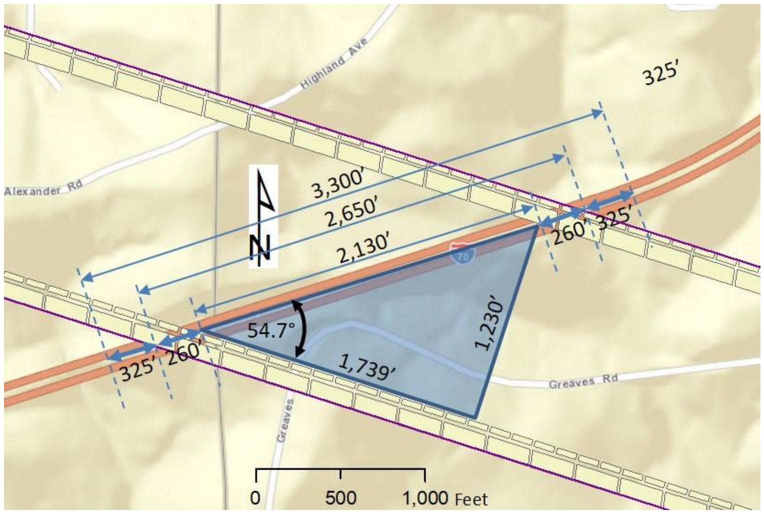

Figure Ic.1 - Location and dimensions of the initial study area

SECTION II – MOTIVATION FOR STUDY

Subsection IIa – History of Longwall Mining beneath Pennsylvania Interstate Alignments

Over the last four decades, two of Pennsylvania's interstates in Greene and Washington Counties have been undermined by longwall mines in five separate episodes. Two of these episodes undermined I-70 and the remaining three episodes undermined I-79. Considering all five episodes, there have been a total of 25 panels that undermined or influenced interstates, which can be seen below in Figure IIa.1. The third Act 54 report titled "The Effects of Subsidence Resulting from Underground Bituminous Coal Mining on Surface Structures and Features and on Water Resources, 2003 to 2008" contained a section summarizing the occurrences of undermining interstates prior to 2008 (Iannacchione, et al. 2011). This report and the Pennsylvania Spatial Data Access (PASDA) database were utilized to review the history of undermining Pennsylvania interstates.

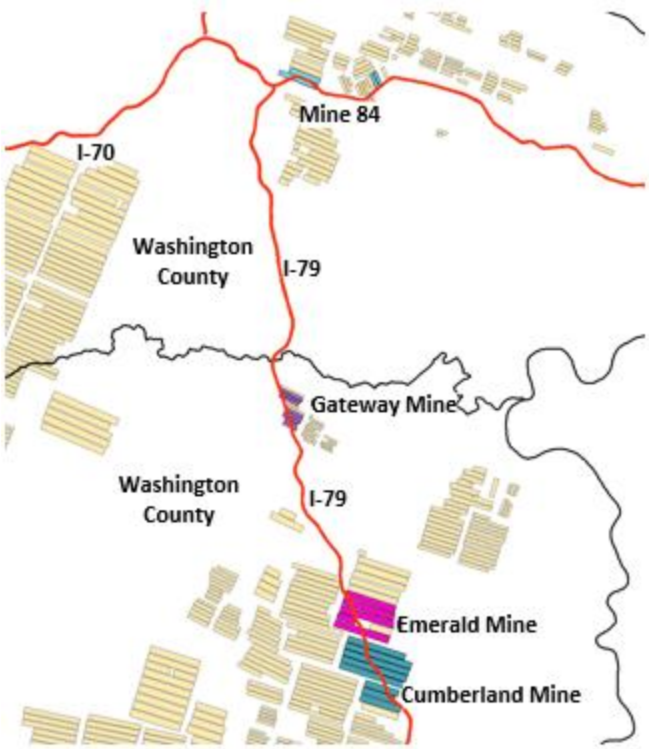

Figure IIa.1 – Longwall panels that have undermined Pennsylvania Interstates

1.0 Gateway Mine

The first experience with undermining interstates came from the Gateway Mine. Between June 1982 and September 1989, Gateway mined eight longwall panels that crossed I-79 just north of the Ruff Creek Interchange at Exit 19. The panels cut the road at an average angle of 41 degrees. These panels were mined from south to north, with two panels in the middle of the block that did not cross the interstate (Figure IIa.2). The Gateway panels that undermined I-79 were smaller than future panels, with an average size of about 47-acres, an average length of 4,100-ft, and an average width of 511-ft (Table IIa.1).

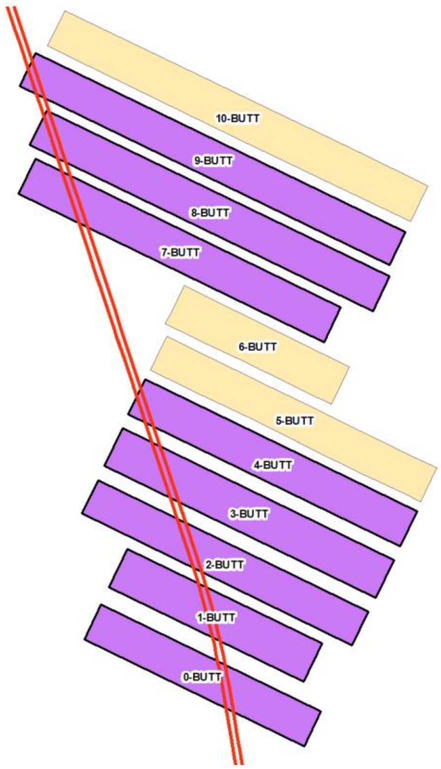

Figure IIa.2 – Section of I-79 undermined by Gateway mine longwall panels

Though the Gateway panels were small, they were among the deepest panels that undermined interstates in Pennsylvania. These panels had an average overburden of 788 feet (Table IIa.1) with minimum and maximum overburdens of 648-ft and 945-ft respectively. The standard deviation of overburdens for each panel individually ranged from 50 to 94-ft, demonstrating variation in overburden within each panel. Due to the small panel width and large overburdens, the width to overburden ratios for all these panels averaged 0.70, which classified the subsidence basins formed through the mining of these panels as subcritical (Section IVa).

Table IIa.1 – Characteristics of Gateway Mine panels that undermined I-79

Panel ID	Days to Mine	Acres	Dates Mined		Days to Mine 1 acre	Panel Dimensions		Overburden, ft			Width to height Ratio
			Start	Finish		Width, ft	Length, ft	Min	Max	Avg	
0-Butt	336	38	1982	1983	8.8	522	3,218	648	863	770	0.68
1-Butt	235	37	1983	1984	6.4	567	2,842	657	934	742	0.76
2-Butt	258	45	1984	1985	5.7	504	3,957	655	915	759	0.66
3-Butt	344	45	1985	1986	7.6	534	3,969	648	909	786	0.68
4-Butt	179	46	1986	1987	3.9	503	3,967	667	945	820	0.61
7-Butt	158	51	1988	1988	3.1	499	4,468	696	902	780	0.64
8-Butt	170	56	1988	1989	3.0	489	4,995	701	918	831	0.59
9-Butt	227	58	1989	1989	4.0	470	5,386	716	890	813	0.58
Average	238	47			5.3	511	4,100	673	910	788	0.70

A study performed by Yancich at West Virginia University (1986) analyzed the subsidence characteristics of the first three of the Gateway panels to impact the interstate: 0-Butt, 1-Butt, and 2-Butt. This study included the regular monitoring of fixed survey monuments along the northbound lanes of I-79 and ultimately compiled a final subsidence profile for the three panels (Figure IIa.3).

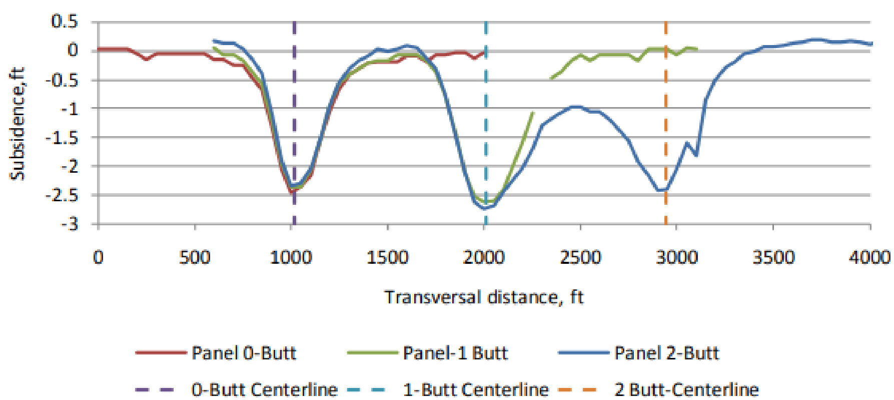

Figure IIa.3 – Final subsidence profiles for three Gateway panels undermining northbound I-79 (Yancich, 1986)

The surveys clearly depict three separate subsidence basins, all of which that come to a point around a maximum vertical subsidence of 2.5-ft. It is also noteworthy that, after the completion of all three panels, there is a foot of vertical subsidence over the gateroads between Panel 1-Butt and Panel 2-Butt; this amount of vertical subsidence indicates yielding pillars in the gateroads between these two panels.

The study went on to examine the slope and curvature of these panels derived from the final subsidence basins (Figure IIa.4). The maximum slope ranged from +1.9% to -1.56% and the points of zero slopes were located at the approximate location of the center of the panels and the gateroad entries. The maximum curvature ranged between $+2x10^{-4}$/ft and $-2x10^{-4}$/ft, with the areas of highest curvature between the edges and centers of the panels. Most impacts on I-79 were expected to occur in these areas of highest slope and curvature.

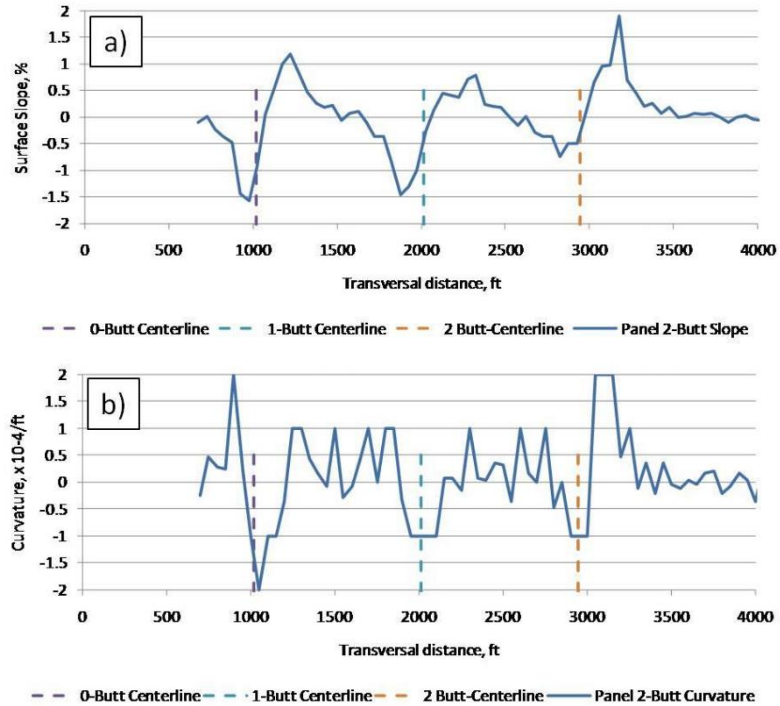

Figure IIa.4 – Profiles of a) surface slope and b) curvature from three Gateway panels undermining I-79 northbound (Yancich, 1986)

Despite these higher slopes and curvatures, only minor damage was reported on the northbound lanes of I-79 as a result of undermining. Figure IIa.5 depicts repaired damage to I-79 a) between the centerline and southern edge of panel 0-Butt, b) near the southern edge of panel 1-Butt, and c) near the northern edge of panel 2-Butt. However, the Yancich study only described a subset of the impacts, making it difficult to determine the overall magnitude of damage and repairs associated with this undermining event.

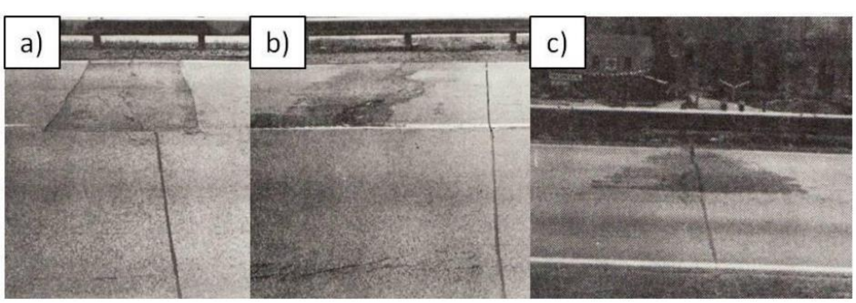

Figure IIa.5 – Photographs of impacts to northbound lanes of I-79 over a) 0-Butt, b) 1-Butt, and c) 2-Butt panels of the Gateway Mine (Yancich, 1986)

2.0 Mine Eighty-Four (84)

The interstate I-70 was first undermined by Mine 84. There were four panels that influenced this interstate that were mined in two separate episodes (Figure IIa.6).

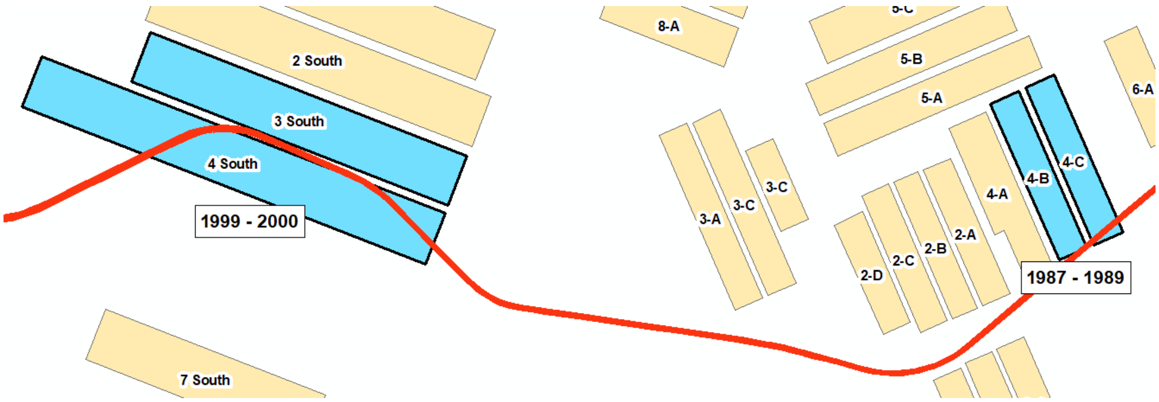

Figure IIa.6 – Mine 84 longwall panels that undermined I-70

The first of these episodes occurred between 1987 and 1989 with the mining of two longwall panels, panels 4B and 4C, whose extreme southern tips intersected the road at an angle of 17 degrees. Like the panels from the Gateway mine, these two panels were relatively small, with an average size of 49 acres. The panels averaged a length of 3,436-ft and a width of 622-ft. However, unlike the Gateway panels, these panels formed supercritical subsidence basins. They were in a shallower section of the Pittsburgh Coalbed with an average overburden of 579-ft and minimum and maximum overburdens of 451 and 692-ft respectively (Table IIa.2). The lower overburden and slightly wider panel combined for an average width to overburden ratio of 1.08, making them subcritical. No information on the impacts of this initial episode of mining under I-70 was found.

Table IIa.2 – Characteristics of Mine 84 panels that undermined I-70, 1987 to 1988

Panel ID	Acres	Dates Mined		Panel Dimensions		Overburden, ft			Width to height Ratio
		Start	Finish	Width, ft	Length, ft	Min	Max	Avg	
4-B	48	NA	1987	612	3,428	451	635	556	1.10
4-C	49	NA	1988	632	3,445	459	692	602	1.05
Average	49			622	3,436	455	664	579	1.08

NA – Not Available

The second episode of undermining I-70 occurred between 1999 and 2000, with the mining of two longwall panels: 3-South and 4-South. The layout of these panels was designed to minimize the impacts to the interstate; as a result, there was approximately 0.75 miles of interstate that ran over the gate road entries between the two panels. These two panels were significantly larger than any panels that had previously undermined interstates with an average size of 191 acres. The panels averaged a length of 7,779-ft and a width of 1,071-ft. They were located at a similar overburden as the previous panels, with an average overburden of 597-ft and minimum and maximum overburdens of 498 and 775-ft respectively (Table IIa.3). The larger widths of these panels generated an average width to height ratio of 1.79, causing the resulting subsidence basins to be classified as supercritical.

Table IIa.3 – Characteristics of Mine 84 panels that undermined I-70, 1999 to 2000

Panel ID	**Days to Mine**	**Acres**	**Dates Mined**		**Days to Mine 1 acre**	**Panel Dimensions**		**Overburden, ft**			**Width to height Ratio**
			Start	**Finish**		**Width, ft**	**Length, ft**	**Min**	**Max**	**Avg**	
3-South	258	166	1999	2000	0.61	1,061	6,843	465	788	587	1.81
4-South	344	215	2000	2000	1.03	1,081	8,715	498	775	607	1.78
Average	301	191			0.82	1,071	7,779	481	782	597	1.79

A study completed by O’Connor in 2001 analyzed the second undermining event of I-70. For this study, a series of 32 tiltmeters were installed along the highway to detect hazardous deformations during undermining. These tilt meters were outfitted with real-time data acquisition systems and triggered an alarm if levels of tilt exceeded 0.002-ft/ft. To minimize damage to the road during undermining, PennDOT implemented a plan that temporarily supported the Zediker Station Road overpass, dismantled some overhead signs, decreased the speed-limit to 40-mph, provided for lane closures and detours, and visually monitored highway conditions (O’Connor, 2001). Due to these mitigation techniques, there were no accidents caused by the undermining of this section of I-70.

After reviewing the data, O’Connor (2001) reported that the vertical subsidence measured was different than that predicted –

> “…The ground surface ultimately deformed into a trough with a maximum subsidence of three to five feet with surface tilting occurring around the margins of the trough. Precursor movement occurred ahead of the mine face, and outside the edges of the panel being mined. Predicted subsidence profiles, however, differed from the actual measured subsidence. As a consequence of differential tilt, (the) ground surface, pavement, and structures were subjected to greater curvature and larger curvature strain than anticipated. Buried culverts and an overpass along the undermined section of I70 were not damaged, but longitudinal cracks developed between lanes, as did transverse bumps. This led to temporary lane closures as cracks were filled and bumps were milled down. Along the secondary roads, some transverse cracking occurred and the wall blocks in a railroad bridge abutment cracked and shifted…”

Some damage occurred to I-70 as a result of this undermining event. Movement was seen both inside and outside of the panels mined. Damage observed included small compression bumps, longitudinal cracks, and transverse cracks. It was reported that this damage occurred in areas with high residual strains and that some of the cracking occurred on joints between lanes (O'Connor, 2001).

3.0 Emerald and Cumberland Mines

Between 2003 and 2010, 13 longwall panels operated by Alpha Resources undermined I-79. These panels were located in the Emerald and Cumberland Mines and will be further characterized by mine.

3.1 <u>Characterization of Cumberland Panels</u>

The Cumberland Mine extracted eight panels that crossed beneath I-79 (Figure IIa.7). The panels were mined from north to south and crossed the road at an average angle of 39 degrees. The distance between panels LW53 and LW54 is greater than that between other panels due to the main entries in that location.

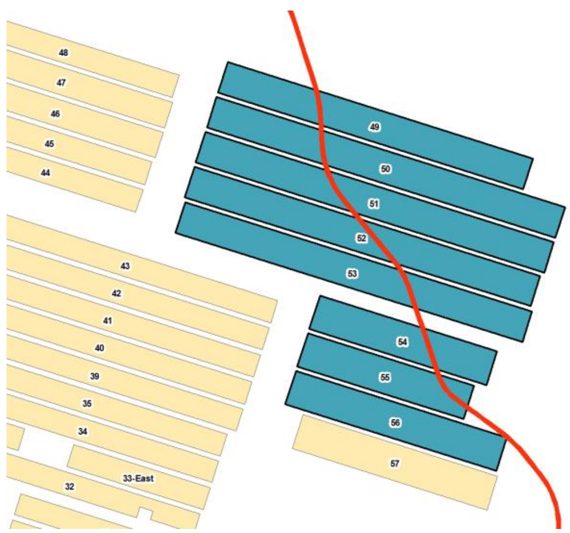

Figure IIa.7 – Eight Cumberland longwall panels undermining I-79

The Cumberland panels were the largest to undermine an interstate, with an average size of 349 acres, an average length of 11,722-ft, and an average width of 1,317-ft. The average overburden for these panels is 717-ft with minimum and maximum overburdens of 543 and 960-ft respectively (Table IIa.4). The standard deviation for the overburden of these panels ranges from 80 to 92, meaning that the variation in overburden across panels is both consistent and significant. The average width to overburden ratio for these panels is 1.84, characterizing the subsidence basins for these panels as supercritical.

Table IIa.4 – Characteristics of Cumberland panels that undermined I-79

Panel ID	Days to Mine	Acres	Dates Mined		Days to Mine 1 acre	Panel Dimensions		Overburden, ft			Width to height Ratio
			Start	Finish		Width, ft	Length, ft	Min	Max	Avg	
49	354	371	2003	2004	1	1,270	12,732	579	921	741	1.71
50	290	425	2005	2005	0.7	1,276	14,525	551	884	728	1.75
51	284	425	2005	2006	0.7	1,276	14,528	543	877	709	1.80
52	281	419	2006	2007	0.7	1,272	14,415	554	904	728	1.75
53	271	416	2007	2008	0.7	1,271	14,453	569	901	693	1.83
54	NA	235	2008	2008	0.8	1,394	7,390	558	910	709	1.96
55	NA	221	2008	2009	NA	1,394	6,935	585	960	713	1.96
56	NA	280	2009	2009	NA	1,388	8,796	543	915	716	1.94
Average	296	349			0.8	1,317	11,722	560	909	717	1.80

NA – Not Available

3.2 Characterization of Emerald Panels

The Emerald mine undermined an additional five panels that crossed I-79. These panels crossed the road at an average angle of 44 degrees. As depicted in the layout of the Emerald panels that interacted with I-79 shown in Figure IIa.8, the fourth panel to be mined, B-6, was cut into two smaller panels, with the majority of I-79 in this section passing over the unmined area.

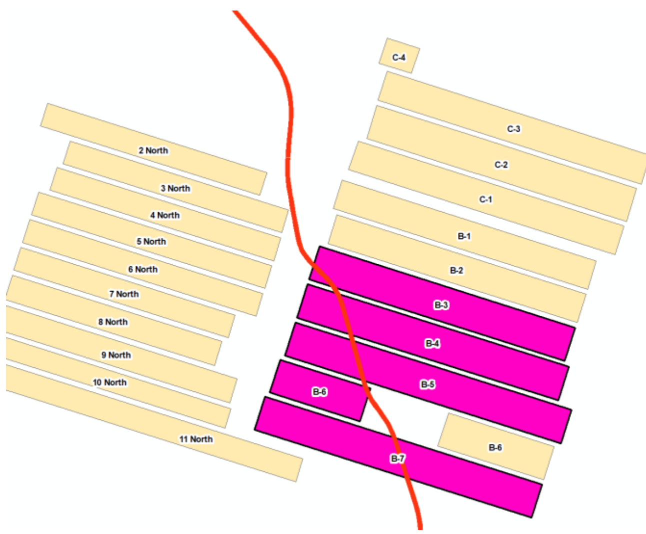

Figure IIa.8 – Five Emerald longwall panels undermining I-79

The Emerald panels were also very large, with an average size of 331 acres, an average length of 10,067-ft, and an average width of 1,435-ft. The average overburden for these panels is 723-ft with minimum and maximum overburdens of 541 and 946-ft respectively (Table IIa.5). The standard deviation for the overburden of these panels ranges from 76 to 101, meaning that the variation in overburden across panels is significant but not consistent. The average width to overburden ratio for these panels is 2.0, classifying these panels' subsidence basins as supercritical.

Table IIa.5 – Characteristics of Emerald Mine panels that undermined I-79

Panel ID	**Days to Mine**	**Acres**	**Dates Mined**		**Days to Mine 1 acre**	**Panel Dimensions**		**Overburden, ft**			**Width to height Ratio**
			Start	**Finish**		**Width, ft**	**Length, ft**	**Min**	**Max**	**Avg**	
B-3	252	365	6/30/05	3/9/06	0.7	1,438	11,094	541	925	739	1.95
B-4	274	374	3/20/06	12/19/06	0.7	1,440	11,333	574	916	755	1.91
B-5	328	395	12/31/06	11/24/07	0.8	1,439	11,983	550	946	739	1.95
B-6	NA	128	2008	2009	NA	1,429	3,910	544	840	659	2.17
B-7	NA	393	2009	2010	NA	1,428	12,017	547	928	725	1.97
Average	285	331			0.7	1,435	10,067	551	911	723	2.00

NA – Not Available

A study completed by Vallejo and Lin in 2010 analyzed the undermining of I-79 through the examination of two Emerald panels and six Cumberland panels. Survey data was collected for the highway alignments that crossed all eight panels on multiple dates during the undermining process. This data showed not only the final subsidence basin underneath the highway, but also the dynamic subsidence as the basin formed. The data collected for Cumberland panels LW51 and LW52 can be seen below in Figure IIa.9.

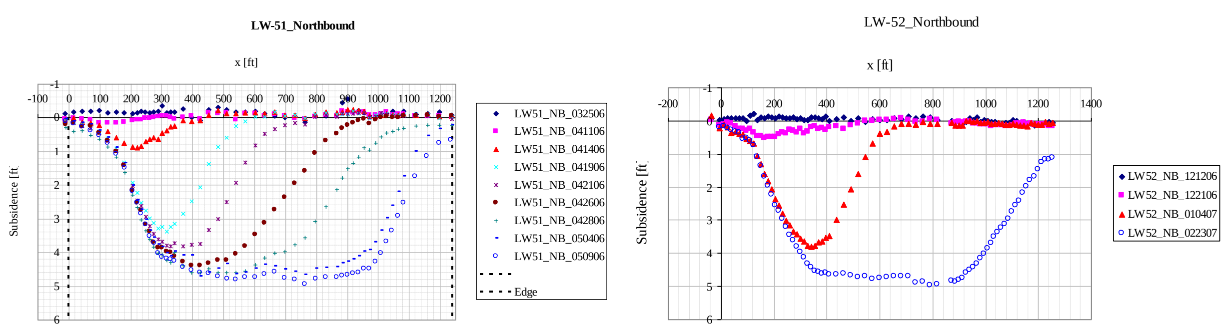

Figure IIa.9 – Measured subsidence profiles over time of Cumberland panels LW51 (left) and LW52 (right) (Vallejo and Lin, 2010)

Prior to undermining, the Pennsylvania Department of Transportation (PennDOT) implemented several mitigation techniques to lessen the impact of subsidence on drivers. Sections of concrete were removed from beneath the asphalt pavement in areas of predicted high stresses and strains to provide the road with additional flexibility to adapt to the subsidence event. During active mining and repair periods, speed-limits were reduced to 45-mph and lanes were reduced from two to one in both directions. In addition, the interstates were under constant observation and monitoring to ensure that damage was fixed before it could cause accidents or injury.

Throughout the undermining process of these panels for both the Cumberland and Emerald mines, the Pennsylvania Department of Environmental Protection (PADEP) and PennDOT staff routinely visited I-79. During these visits, they observed a variety of types of damage on the highway surface during the undermining process including compression bumps, transverse cracking, longitudinal cracking, joint faulting, and lane-to-shoulder separations. Some examples of these failures can be seen in below in Figure IIa.10. Most of the damage was considered to be localized and was repaired during or following the undermining period.

Figure IIa.10 – Examples of surface damage on I-79 caused by Emerald and Cumberland undermining a) compression bump, b) transverse crack, c) joint faulting, and d) lane-to-shoulder separation (Iannacchione, et al., 2011)

4.0 Financial Analysis

As described above, both Pennsylvania interstates that were influenced by longwall mining experienced numerous localized effects. Some of these effects were permanent, while others were transitory, and the damage was lessened once the subsidence wave moved through the area. In order to mitigate these effects, monitoring, traffic control, and temporary support measures were implemented. Damage was repaired through milling, temporarily patching, repaving, and straightening of guiderails. It is estimated that Pennsylvania spent almost 20 million dollars (Painter, 2010) monitoring and rehabilitating sections of I-79 that were impacted by longwall mining between 2002 and 2008 (Table IIa.6).

Table IIa.6 – Estimated cost to monitor, maintain, and repair I-79 during undermining (Painter, 2010)

Year	Detour Preparation	Monitor and Equipment	Construction	Total
2002 - 2003	$6,263,597			$6,263,597
2004		$244,048	$467,608	$711,656
2005		$65,309	$1,644,856	$1,710,165
2006		$239,176	$3,192,371	$3,431,547
2007		$152,871	$3,090,231	$3,243,102
2008		$230,131	$4,016,737	$4,246,868
Total from 2002 to 2008				$19,606,935

5.0 Summary

Since the early 1980s, 25 longwall mining panels have undermined I-70 and I-79 in southwestern Pennsylvania. The characteristics have changed drastically over this time period due to improvements to the longwall mining technology. The longwall panels in the 1980s were much narrower than later panels and tended to produce subcritical subsidence basins. Contrarily, the 13 panels that undermined I-79 between 2002 and 2010 were very wide, producing supercritical subsidence basins. In addition, the rate of longwall mining also increased with time, meaning that the more recent panels were mined quicker and the time needed for the longwall subsidence basin to form and reach equilibrium has decreased.

Despite all the panels that have been mined, there are still many unknowns regarding the impact of subsidence on an interstate's alignment. In general, extensional damage, such as longitudinal and transverse cracking, began before and as the longwall face passed beneath an area, and compression damage, such as bumps and heaves, formed once the longwall face had passed a section of highway. However, in the past, little to no information was collected regarding the dynamic effects of subsidence.

In order to better understand and characterize the risk mining has on an interstate, information documenting the vertical movement, horizontal movement, strains, and damage to the surface must be recorded frequently and compared to the location of the longwall face at the time of observation. For this reason, an in-depth monitoring process was implemented to obtain all this information and more for the Tunnel Ridge longwall panel that undermined I-70 in early 2019. Through the synthesis of this data, more sophisticated models and estimates will be able to be produced to predict the location and severity of damage to the highway and a timeline for rehabilitation of the highway for any longwall mining that may impact interstates in the future.

Subsection IIb – Investigation of Southwestern Pennsylvania Interstate Slope Instabilities

An effort was made to investigate past slope instabilities that have impacted southwestern Pennsylvania Interstate alignments. This assessment found a range in the magnitude and occurrence of slope instabilities impacting highways in the regions. It also helped to stress the importance of this issue.

In November of 2018, Cheryl Moon-Sirianni (PennDOT, District 11 Manager) was quoted (see below) as saying approximately 80 landslides were impacting roads within District 11.

> *"Landslide Repair Costs Adding Up as PennDOT Continues to Manage Dozens Across District," November 2, 2018, WTAE TV report, Cheryl Moon-Sirianni is quoted as saying approximately 80 landslides were impacting roads within District 11. The cost to fix all 80 landslides in District 11 would be over 50 million dollars (40 in Allegheny County alone). The Route 30 slide was one of the 80 and took approximately 12 million dollars to repair. Also mentioned the critical work needed for repairing Route 68 landslide impacts. When deciding which landslides to fix, PennDOT relies on the amount of traffic as one of the most important conditions.*

As critical as this problem is for District 11, the landslide problem may be even more significant for District 12 (Figure IIb.1) where the number of impacted roads is considerable (Painter, 2019).

A developing subsidence basin has the potential to upset the limited and temporary equilibrium of many southwestern Pennsylvania colluvium and rock slopes. Slope instabilities can block traffic or fail the very foundation of the highway alignment. In both cases, the safety of the traveling public could be at risk.

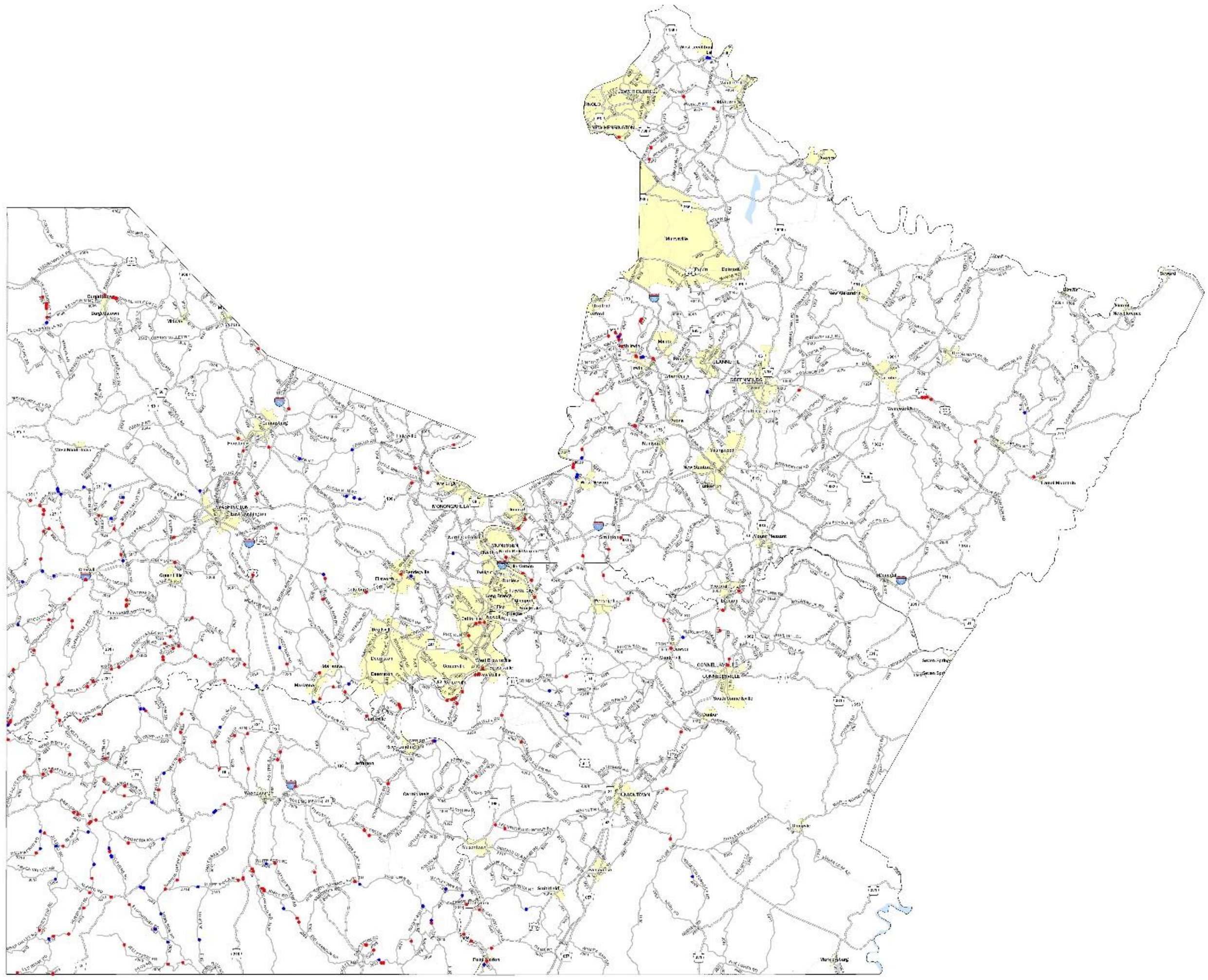

Figure IIb.1 – Landslides identified (Red and blue dots) with PennDOT District 12 (Green, Fayette, Washington, and Westmoreland Counties) as of 13 June 2019

1.0 Types of Slope Instabilities (used interchangeably with Landslides)

The PA Geological Survey website contains an excellent report on landslides in Pennsylvania (Delano and Wilshusen, 2001). In this report, a landslide classification system was proposed with a wide range of possible types (Table IIb.1).

Table IIb.1 – Types of Landslides in Pennsylvania (Delano and Wilshusen,2001)

<table>
<tr><th colspan="2" rowspan="3">Type of movement</th><th colspan="3">Type of material</th></tr>
<tr><th rowspan="2">Bedrock</th><th colspan="2">Engineering soil</th></tr>
<tr><th>Coarse-grained</th><th>Fine-grained</th></tr>
<tr><td colspan="2">Fall</td><td>Rockfall</td><td colspan="2"></td></tr>
<tr><td rowspan="2">Slide</td><td>Translational</td><td>Rockslide</td><td>Debris slide</td><td></td></tr>
<tr><td>Rotational</td><td>Rock slump</td><td colspan="2">Slump</td></tr>
<tr><td rowspan="3">Flow</td><td>Rapid</td><td rowspan="3">Rock creep</td><td>Debris avalanche</td><td>Mudflow</td></tr>
<tr><td></td><td>Debris flow</td><td>Earthflow</td></tr>
<tr><td>Slow</td><td>Talus creep</td><td>Soil creep</td></tr>
</table>

This report also discussed the effect and costs of landslides:

> *"In a 1986 study, more than 700 recent and active landslides in Allegheny County were identified. U.S. Geological Survey (USGS) landslide-inventory maps indicated thousands of landslides in Allegheny and Washington Counties. A 1991 list from the Pennsylvania Department of Transportation (PennDOT) showed that there were 226 problem landslides in Allegheny County, 45 in Beaver County, 77 in Armstrong County, and 26 in Tioga County. A USGS landslide-inventory map showed more than 1,200 recent and 900 old slides on one 7.5-minute quadrangle map in Greene County."*

The 2001 report suggests that many counties in southwestern PA have significant problems with landslides. This is supported by statements on the PA DCNR website on landslides:

> *"The Southwestern Pennsylvania has by far the highest concentration of landslides. Outside that region, high susceptibility areas are mostly smaller and have more varied geology and topography."*

2.0 Existing Inventories of Slope Instabilities Affecting Highway Alignments

Michael Baker International (MBI) has participated in a project to produce web maps of landslides in southwestern PA (Figure IIb.2). The web map, available in a web viewable format, can contain:

- US Geological Survey landslide maps (see example below),
- PennDOT Multi-Modal Project Management System (MPMS) slide projects, and
- PennDOT Road Closure Reporting System (RCRS) data points (landslides are classified as "Debris Covered Roadway" incidents).

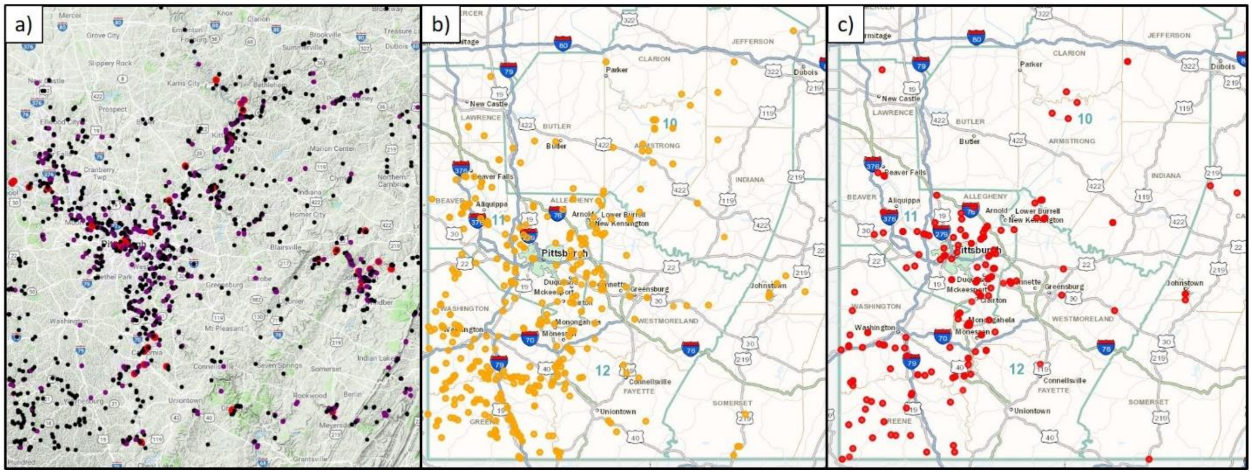

Figure IIb.2 - a) MBI web map showing slope instability information from southwestern Pennsylvania; b) PennDOT Multi-Modal Project Management System (MPMS) slide projects data points; and c) PennDOT Road Closure Reporting System (RCRS) data points, also-known-as PA-511 data.

Figure IIb.3 demonstrates how significant the problem is within the Donora quadrangle (Pomeroy and Davies, 1979) where the I-70 alignment contains numerous slope instabilities. The above work demonstrates that much is already known about slope failure susceptibility.

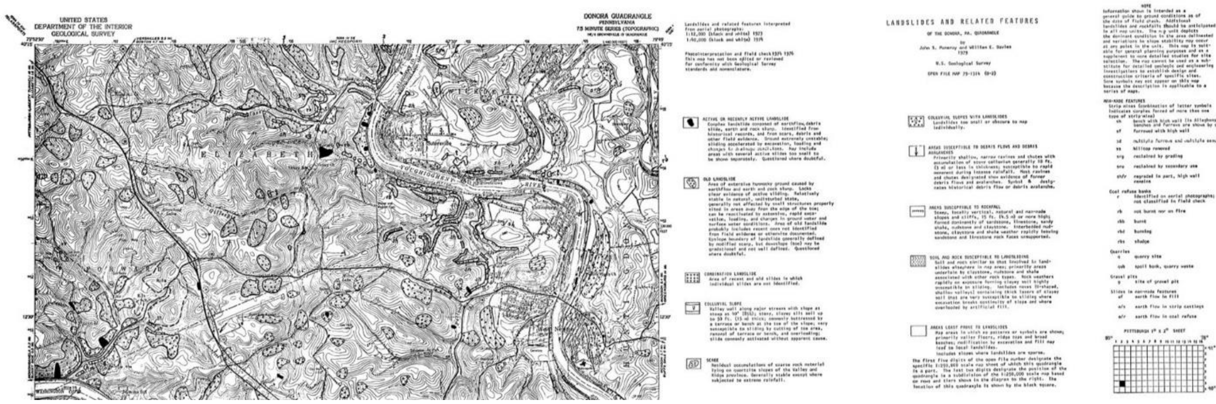

Figure IIb.3 – Portions of the Donora quadrangle map showing the location of slope instabilities identified by the US Geological Survey (Pomeroy and Davies, 1979)

3.0 The 1968-1969 I-79 Slope Failure

Arguably the largest and most prominent slope failure to impact interstate alignments in southwestern Pennsylvania occurred along I-79 just north of where it crosses the Ohio River, nine miles northwest of Pittsburgh (Figure IIb.4). Construction on this section of I-79 began in the autumn of 1968. Massive slope instabilities began to occur soon after construction began and continued into 1969. Hamel and Flint (1972) and Hamel and Adams (1981) published reports that detailed the local soil and rock conditions.

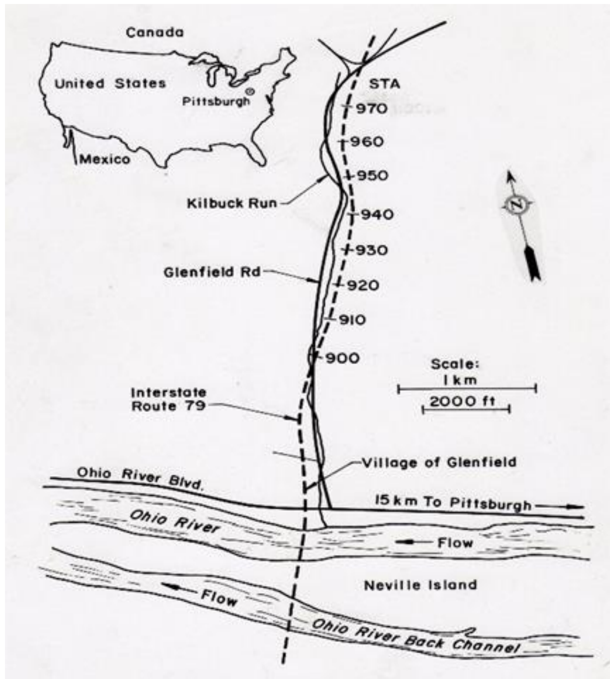

Figure IIb.4 – Location of multiple slope instabilities along I-79 in 1968 and 1969 (the exact station values were not provided)

The Hamel reports indicated that slope instabilities were observed at multiple locations along the highway alignment: 899 to 904, 916, 920 to 922, 926 o 932 and 950 to 955 (Figure IIb.4). A cross-section of one of these slides in shown in Figure IIb.5. Here the bottom-most failure surface was located at the base of a weak rock unit. The colluvium and strata above these planes of weakness moved away from the hillside and into the valley at varying rates. These slope failures added significant cost to the project and delayed the opening of this section of I-79.

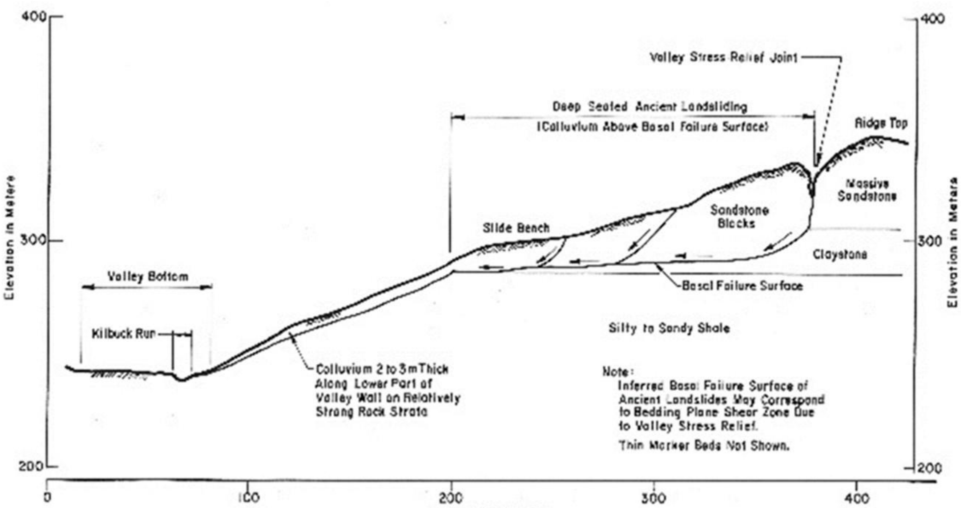

Figure IIb.5 – Slope cross-section Sta 908 (Hamel and Adams, 1981)

4.0 Other Examples of Slope Failures along southwestern Pennsylvania Interstate Alignments

The University has learned that roadway embankment slopes have, on occasion, failed. The University had hoped to example one of these cases in more detail. This could provide realistic examples of how slopes, within an embankment, might fail. However, the difficultly in retrieving these data limited further analysis.

SECTION III – PRE-MINING SITE CONDITIONS

Subsection IIIa – Analysis of As-Built Conditions

1.0 Introduction

The University received three sets of as-built drawing files from PennDOT that cover the 5.7 mile stretch of interstate that overlays the Tunnel Ridge mine property. Though called as-built drawings, the files received would be more accurately described as construction drawings as they display the existing conditions at the time of construction and the proposed highway alignment. These files contained information regarding the areas of cuts and fills between the existing and proposed conditions and the borings that were drilled before construction. To accurately predict the effect that mining would have on the roadway, the existing conditions of the roadway were analyzed.

2.0 Cuts and Fills

Through the analysis of the as-built files provided by PennDOT, the University was able to determine how the roadway was designed and constructed. Due to inherent instabilities of soil when it is placed on a slope, the areas of potential concern along the roadway are large cuts and fills. Figure IIIa.1 below shows the areas of cuts and fills for the roadway throughout the 5.7 mile study area.

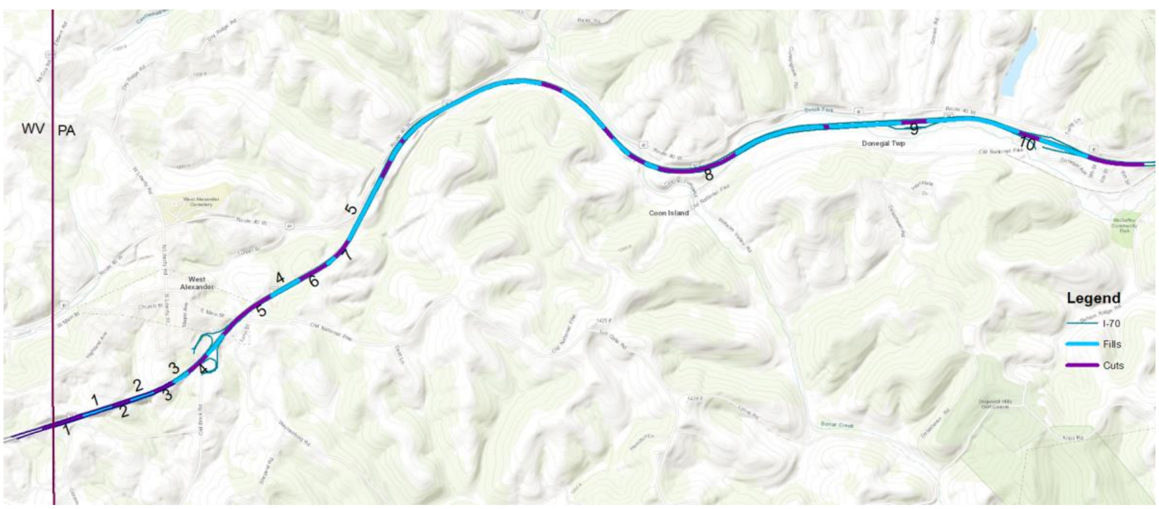

Figure IIIa.1 – Cuts (purple) and Fills (blue) throughout study area with embankments and steep slopes numbered from left to right

Throughout the entire study area, there is approximately 13,448 linear-ft or 2.55 miles of roadway that was constructed in areas of cut. The remainder of the roadway, which is approximately 19,181 linear-feet or 3.63 miles, was constructed in areas of fill. The areas of cut create slopes along the sides of the road and the areas of fill form embankments.

3.0 Test Boring Locations

Through an analysis of the as built drawings, the locations of borings drilled before I-70 was constructed were plotted along the highway alignment. There were 37 borings drilled within the 5.7 mile study area. These borings were mostly shallow, extending down to the first layer of bedrock. These borings were drilled into the native soil, before any construction of the interstate took place. The location of these borings can be seen in Figure IIIa.2.

Figure IIIa.2 – Location of all borings drilled prior to construction of I-70

As Panel 15 will be mined first, additional soil information was collected for this segment of road to create the predictive models. In this contained study area, there are five borings from the original construction phase. An additional eight monitoring wells were drilled along the eastbound highway alignment and an additional 13 boreholes were drilled in the two embankments. Eight of these boreholes were drilled down either side of the center embankment, one borehole was drilled at the edge of the second embankment, and the final four of the boreholes were drilled down the center of the southern side of the second embankment. These boreholes were drilled recently, meaning that they can be used to determine the current properties of the embankments and characteristics of the water table at the time the holes were drilled. The location of these drilled features can be seen below in Figure IIIa.3.

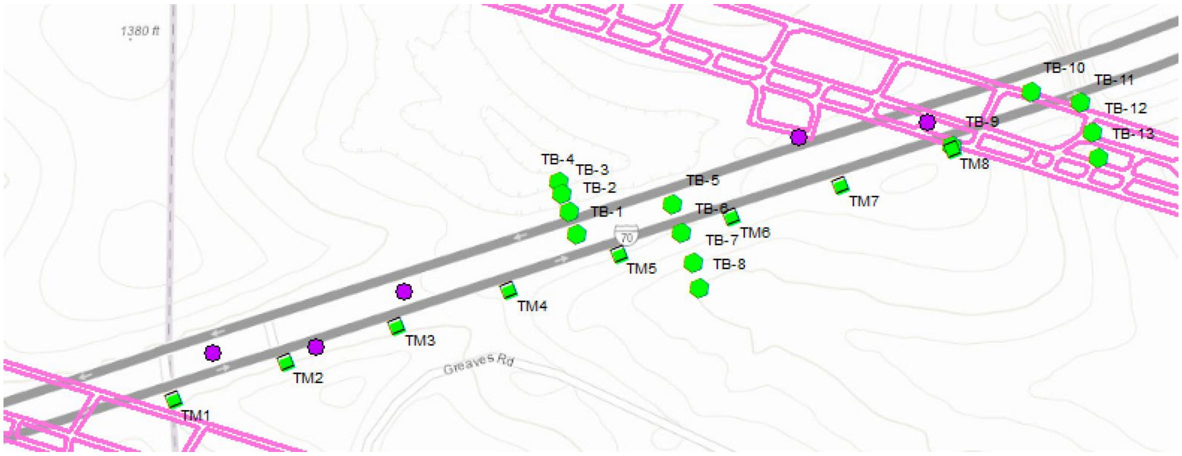

Figure IIIa.3 – Location of borings, boreholes, and monitoring wells along Panel 15 section of I-70

4.0 Embankment Characterization Summary

Along the relevant section of I-70, there are five large embankments. These five embankments include the two embankments located above Panel 15 which will be monitored and observed for future predictions. The embankments range in length from 350 to 650-ft and range in height from 50 to 85-ft. All of the embankments were designed with 2:1 slope. The five (5) embankments are numbered from left to right and are labeled in Figure IIIa.4 below and the characteristics are summarized in Table IIIa.1.

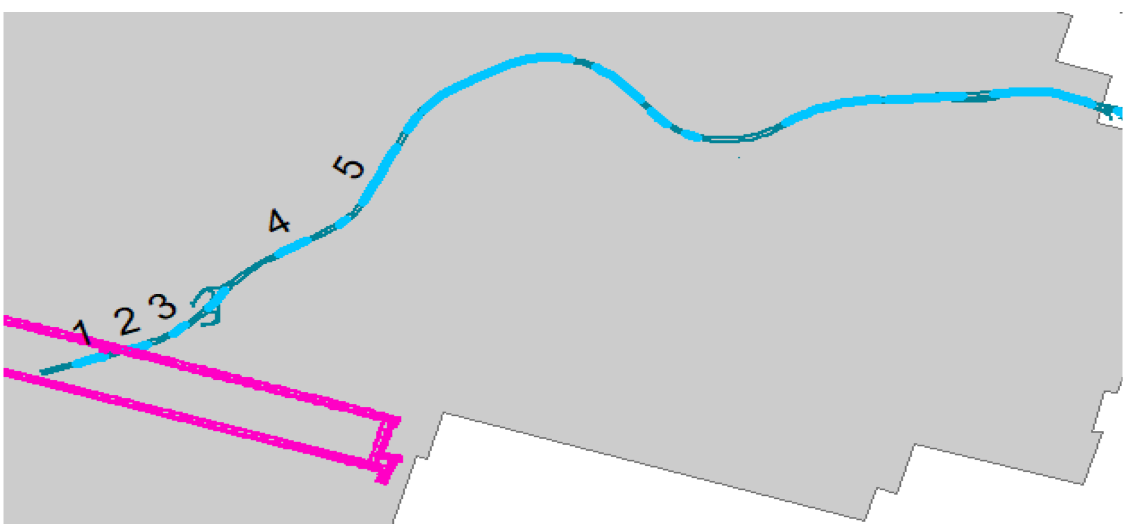

Figure IIIa.4 – Location of areas of fill and five embankments along section of I-70 that may be undermined by Tunnel Ridge Mine

Table IIIa.1 – Embankment Property Summary

Embankment No	Length (ft)	Height (ft)	Slope (H:V)	Depth to water Table (ft)
1	550	72	2:1	28.1' – 38.8' below top of borehole
2	650	86	2:1	~ 43.9' below top of borehole
3	350	58	2:1	0' – 17.0' below top of embankment
4	650	52	2:1	39' – 43.1' below top of embankment
5	650	70	2:1	Above top of embankment

4.1 Embankment #1

The first embankment is approximately 550-ft long and 72-ft tall. It is located above the center of Panel 15. There were eight borings drilled in this embankment to collect soil samples; four borings were drilled on the north side of the road and four were drilled on the south side of the road. A summary of the boring data can be seen from the boring log below in Figure IIIa.5.

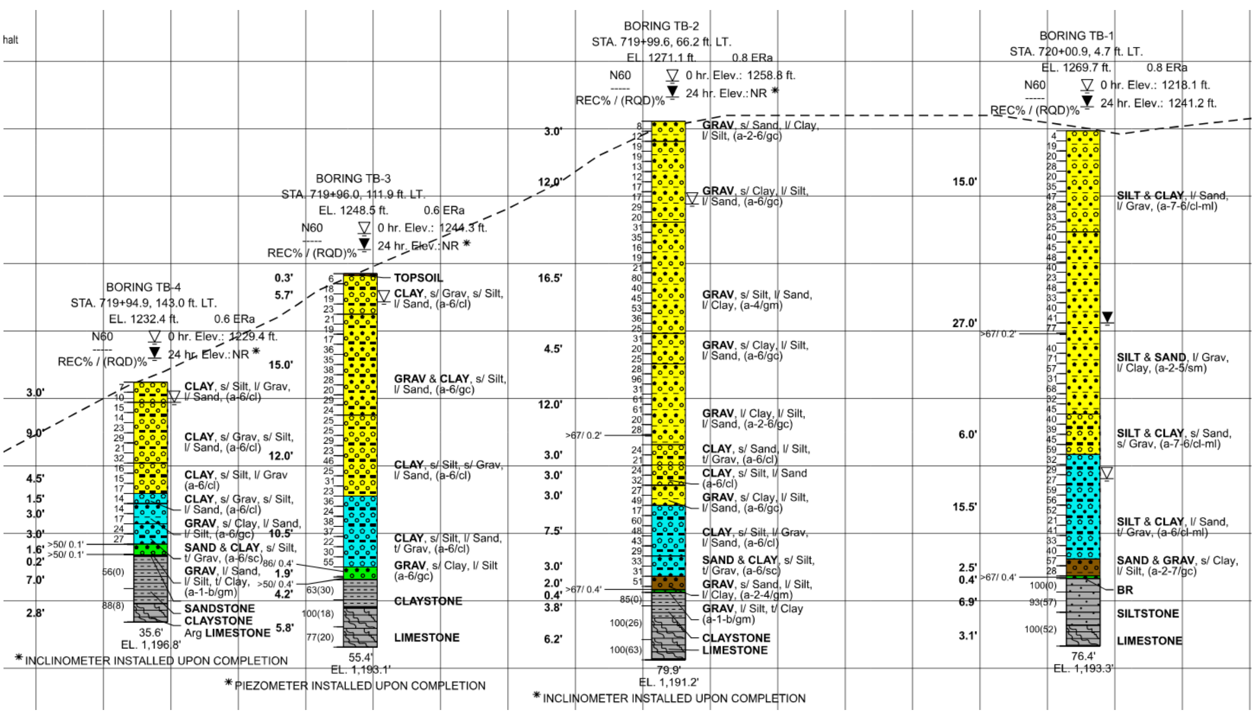

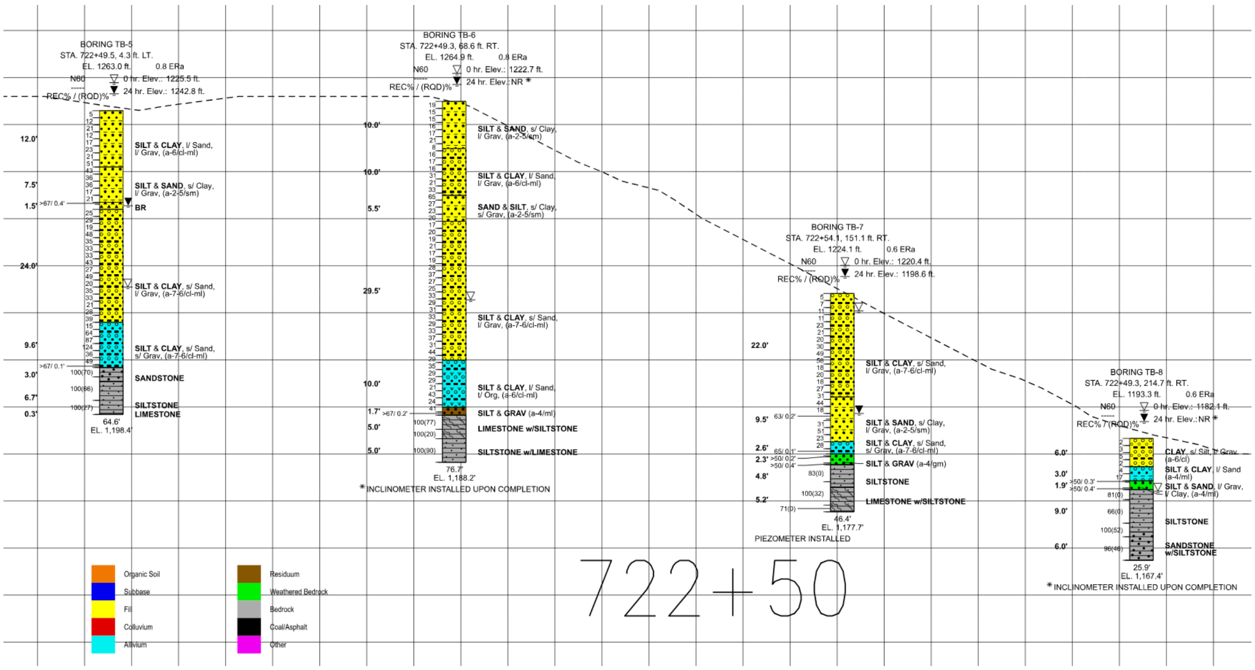

Figure IIIa.5 – Boring log summaries along Embankment #1 showing fill (yellow), alluvium (blue), weathered bedrock (green), residuum (brown), and bedrock (grey) -North side (Top) and South Side (Bottom)

Based on the SPT values from the borings, the north and south sides of the embankments are composed of different strength soils. On the northern side of the roadway, the middle of the embankment has a thick layer of medium to weak silt/clay soils on top of a layer of stronger silt/clay mixed with sand and gravel that sits on top of the sandstone, siltstone, and limestone layers. At the toe of the northern side embankment there is a layer of weak silt/clay soils directly on top of the siltstone and sandstone layers. On the southern side of the roadway, the middle of the embankment has a layer of medium to weak gravel/sand/clay soils on top of a layer of stronger clay mixed with silt and gravel that sits on top of the soft claystone, and limestone layers. There is also evidence in this area of the soil getting weak again before the rock layer, indicating that the alluvium and clay may not have been removed before the embankment was constructed. At the toe on the southern side of the embankment, near TB8, there is a layer of medium to weak clay/silt/gravel soils sitting on a layer of soft claystone and limestone.

From the boring data, on the north side, the water table varies in elevation from 1,241.2-ft at the center of the embankment, 1,258.8 and 1,244.3-ft in the middle of the slope, and 1,229.4-ft at the toe of the embankment. On the south face, the water table varies in elevation from 1,225.5-ft at the center of the embankment, 1,222.7 and 1198.6-ft in the middle of the slope, and 1,182.1-ft at the toe. From the piezometer data, on the north slope, it was determined that the water table fluctuated from 34.5 to 38.8-ft below the top of the embankment, which corresponds to an elevation ranging between 1,209.7 and 1,241.0-ft. On the south slope, it was determined that the water table fluctuated from 28.1 to 34.0-ft below the top of the embankment, which corresponds to an elevation ranging between 1,190.1 and 1,196.0-ft. The fluctuation in the location of the water table is likely due to seasonal effects and variation in rainfall.

In addition to the boring and piezometer data showing water inside the embankment, it is believed that the water may be attributed to a perched water table. During a series of onsite inspections, the University observed saturated soil in this embankment. On the southern side of the embankment it was observed that the soil between TB-7 and TB-8 was saturated and that the water appeared to be draining out of the toe of the slope creating pooling. All these tests and observations indicate that there may be perched water table in the embankment, which may cause stability issues as the formation is undermined.

4.2 Embankment #2

The next embankment is approximately 650-ft long and 86-ft tall. It is located above one of the gate roads of Panel 15. There were four borings drilled in this embankment to collect soil samples. A summary of the boring data can be seen from the boring log below in Figure IIIa.6.

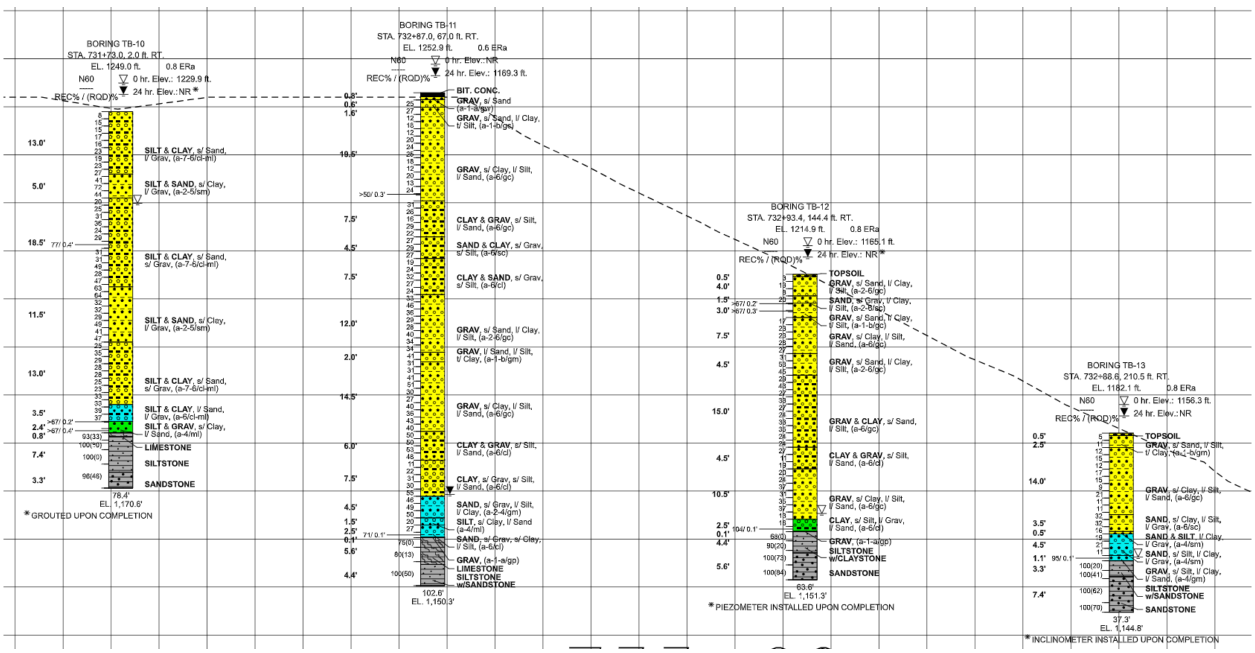

Figure IIIa.6 – Boring log summary for southern side of Embankment #2 showing fill (yellow), alluvium (blue), weathered bedrock (green), residuum (brown), and bedrock (grey)

Based on the SPT values from the borings, the southern side of the second embankment is also composed of many different soil types. In the center of the embankment, there is a layer of weak silt and clay on top of a medium strong layer of silt and sand followed by a layer of medium strength silt, sand, and clay all resting on strong limestone, siltstone, and sandstone. There is also evidence in this area of the soil getting weak again before the rock layer, indicating that the native material may not have been removed before the embankment was constructed. Down the slope and at the toe of the embankment, the primary material is a medium strength gravel soil mixed with sand and clay sitting on a strong siltstone and sandstone layer.

From the boring data, it was determined that the water table varies from 1,230.3 to 1,169.3-ft at the crest and is 1,156.3-ft at the toe. Based on this data, it appears that the water table follows the path of the surface elevations as it decreased from the top to the toe of the embankment. From the piezometer data, it was determined that the water table at the slope was 43.9-ft below the surface of the embankment and at an elevation of 1,171-ft, compared to 1,169.6-ft at the slope from boring data.

4.3 Embankment #3

This embankment is approximately 350-ft long and 58-ft tall. It is located above one of the panels that may be mined in the future. Since this panel will not be undermined in the immediate future, there is not boring data representing the embankment after construction. There were no borings drilled to collect soil samples for the construction of this embankment; however, there were two borings drilled nearby. Through this testing, it was determined that the native soil in this location was composed of a number of soil types including shaley clay and weathered shale. Due to the proximity to the embankment, the material underneath this embankment is likely similar to this boring data. Based on the previous embankments, it can be assumed that the embankment was constructed with minimal removal of this natural material. A summary of the boring data can be seen from the boring log below in Figure IIIa.7.

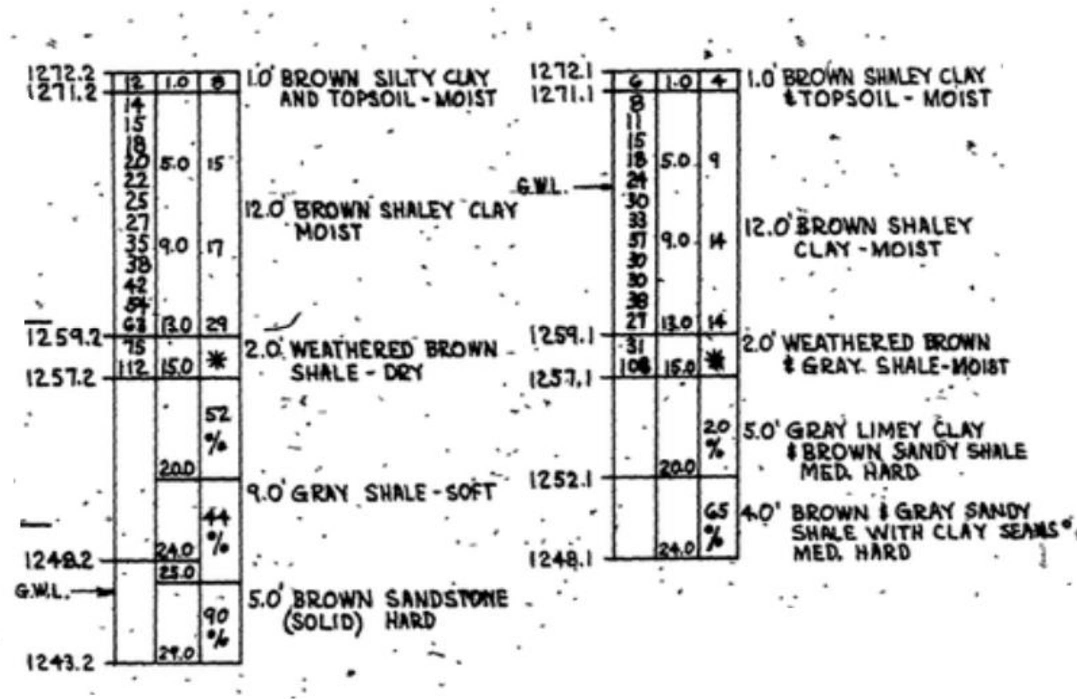

Figure IIIa.7 – Boring log summary test holes near Embankment #3 - Hole 6 (R) and Hole 7 (L)

Based on the SPT values from the borings, native soil is composed of different soil types. There is a layer of weaker silty clay topsoil followed by a thicker layer of medium strength shaley clay on top of stronger weathered shale. Underneath these layers of soil is medium to soft shale and a stronger sandstone. From the boring data, it was determined that the water table once sat at an elevation between 1,266.1-ft (Hole 7) and 1,247.2-ft (Hole 6). This elevation would place the groundwater table between the top of the embankment and 17-ft below the top of the embankment.

4.4 Embankment #4

This embankment is approximately 650-ft long and 52-ft tall. It is located above one the panels that may be mined in the future. Since this panel will not be undermined in the immediate future, there is not boring data representing the embankment after construction. There were two borings drilled to collect soil samples for the construction of this embankment. Through this testing, it was determined that the native soil in the location of this embankment was composed of a number of soil types including sandy clay and weathered shale. Based on the previous embankments, it can be assumed that the embankment was constructed with minimal removal of this natural material. A summary of the boring data can be seen from the boring log below in Figure IIIa.8.

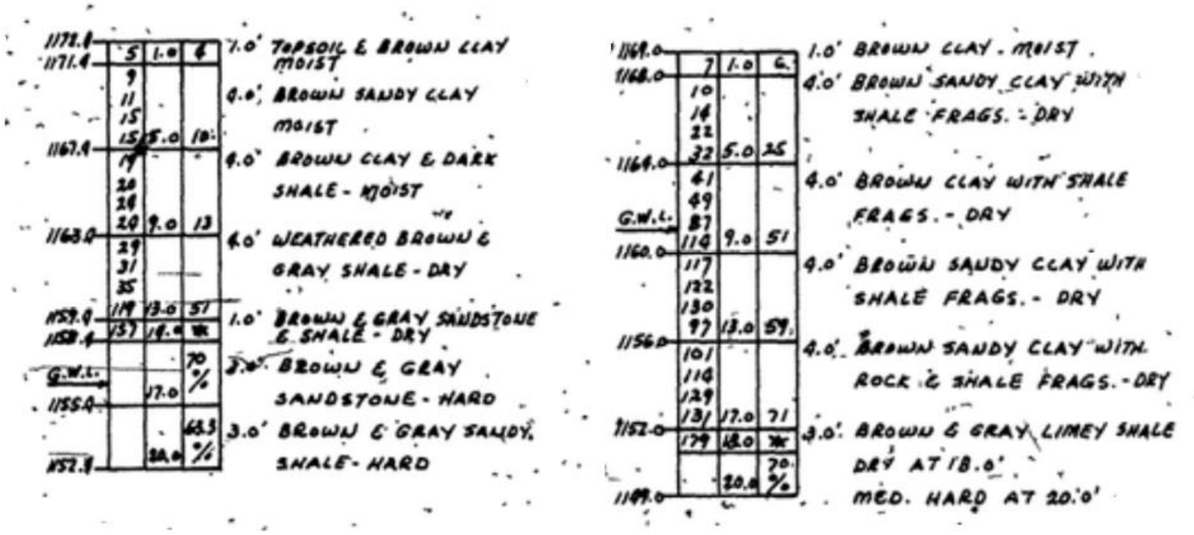

Figure IIIa.8 – Boring log summary for Embankment #4 - Hole 16 (L) and Hole 18 (R)

Based on the SPT values from the borings, native soil is composed of different soil types. There is a layer of weaker clay followed by a layer of medium strength shaley/sandy clay on top of stronger weathered shale. Underneath these layers of soil is medium hard sandy/limey shale. From the boring data, it was determined that the water table once sat at an elevation between 1156.9-ft (Hole 16) and 1161.0-ft (Hole 18). This elevation would place the groundwater table between 39 and 43.1-ft below the top of the embankment.

4.5 Embankment #5

This embankment is approximately 650-ft long and 70-ft tall. Prior to this study there was not boring data representing the embankment. There were no borings drilled to collect soil samples for the construction of this embankment; however, there was one boring drilled nearby. Through this testing, it was determined that the native soil in this location was composed of a number of soil types including clay with shale fragments and rocks such as sandstone and limestone. Due to the proximity to the embankment, the material underneath this embankment is likely similar to this boring data. Based on the previous embankments, it can be assumed that the embankment was constructed with minimal removal of this natural material. A summary of the boring data can be seen from the boring log below in Figure IIIa.9.

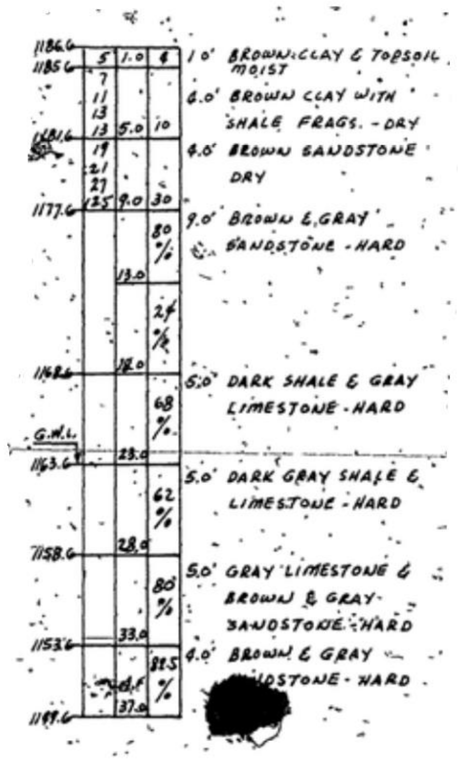

Figure IIIa.9 – Boring log summary test hole near Embankment #5 - Hole 15

Based on the SPT values from the borings, native soil is composed of different soil types. There is a layer of weaker clay followed by a layer of medium weak strength clay with shale fragments on top of strong sandstone. Underneath these layers of soil is hard shale and limestone on top of a hard sandstone. From the boring data, it was determined that the water table once sat at an elevation of 1,164.6-ft. This elevation would place the groundwater table well above the elevation of the top of the embankment, which sits at a maximum elevation of 1,140-ft.

5.0 Cut Slope Characterization Summary

Along the relevant section of I-70, there are ten steep cut slopes. These ten slopes include two slopes located above Panel 15 which will be monitored and observed for future predictions. The slopes range in length from 450 to 1500-ft and range in height from 22 to 102-ft. The slopes were cut with slopes at a steepness of 2:1, 1.5:1, or 1:1. The ten slopes are numbered from left to right and are labeled in Figure IIIa.10 and a summary of the slope properties can be seen in Table IIIa.2 below.

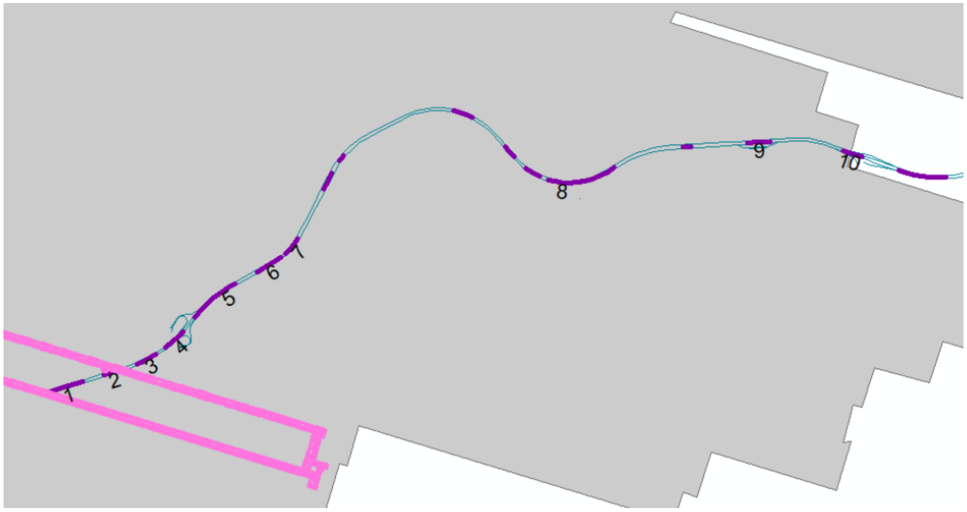

Figure IIIa.10 – Location of areas of cut and ten steep slopes along section of I-70 that may be undermined by Tunnel Ridge Mine

Table IIIa.3 – Detailed Cut Slope Property Summary

Cut Slope No.	Length, ft	Height, ft	Slope (H:V)	No. of Borings Drilled	Slope Material Properties
1	1000	58	1:1	3	Weathered, broken, and soft rocks
2	410	22	2:1	2	Moist sandy clay and weathered rocks
3	475	28	2:1	3	Shaley clay and weathered rock
4	500	26	2:1	0	NA
5	1500	48	1.5:1	2	Weathered and medium hard shales
6	850	103	1:1	4	Solid, hard limestone and shale
7	450	72	1:1	3	Solid, hard limestone and sandstone
8	1200	64	1:1	4	Hard shale, sandstone, and limestone
9	500	34	2:1	3	Hard, solid sandstone
10	725	28	2:1	0	NA

The cut slopes are generally comprised of limestone, sandstone, and shale rocks. The material comprising the slopes vary in strength, being primarily comprised of weathered rock, soft rock, and hard rock. Despite this variability, the slopes are stable under present conditions; however, it is impossible to predict how the slopes will react to the high stresses and strains induced by the undermining process.

5.1 Slope #1

The first slope is approximately 1000-ft long and 58-ft tall. There is a flat section located on both sides of this slope, which breaks the slope into two sections. The steep sections of this slope are at a 1:1 slope. It is located above the center of Panel 15. There were three borings drilled in this area to collect soil samples. These samples were collected prior to the construction of the roadway, meaning that they reflect the native soils that were removed. A summary of the boring data can be seen from the boring logs below in Figure IIIa.11.

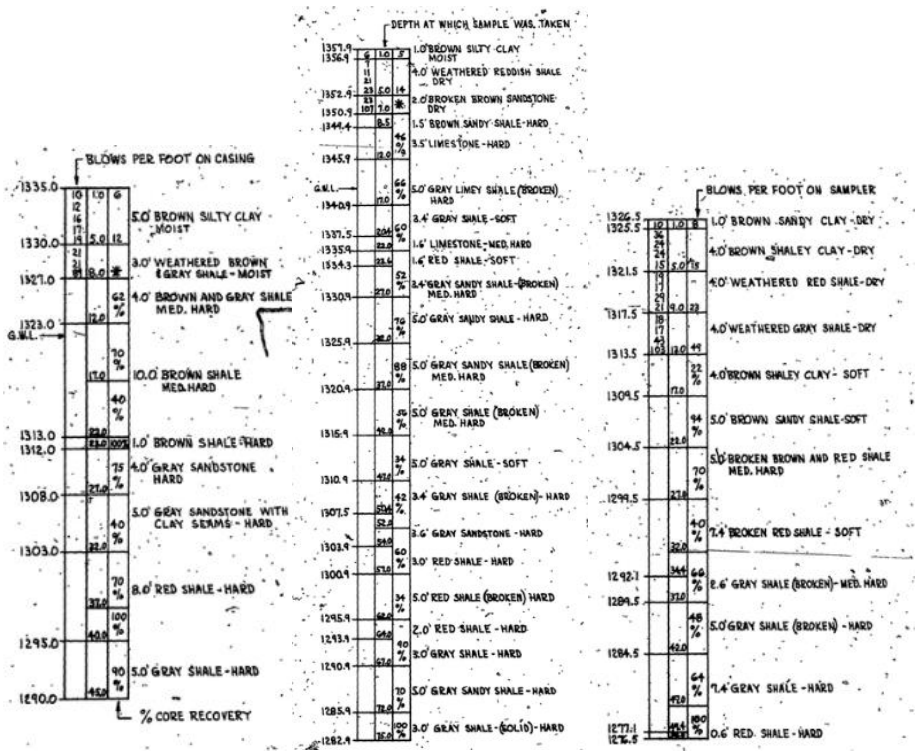

Figure IIIa.11 – Test holes near Slope #1 - Hole 1 (L), Hole 1A (M), and Hole 1B (R)

These boring logs demonstrate that the native soil in this location was comprised primarily of a thin layer of silty, sandy clay on top of weathered shale and limestone. Each boring was drilled until it hit solid, hard shale rock. They vary in depth from 45-ft to 75-ft deep. With the roadway at an elevation of approximately 1296-ft, the slopes consist mostly of weathered, broken, and soft rocks.

5.2 Slope #2

The next slope is approximately 410-ft long and 22-ft tall. The steep sections of this slope are at a 2:1 slope. It is located above the edge of Panel 15. There were two borings drilled in this area to collect soil samples. These samples were collected prior to the construction of the roadway, meaning that they reflect the native soils that were removed. A summary of the boring data can be seen from the boring logs below in Figure IIIa.12.

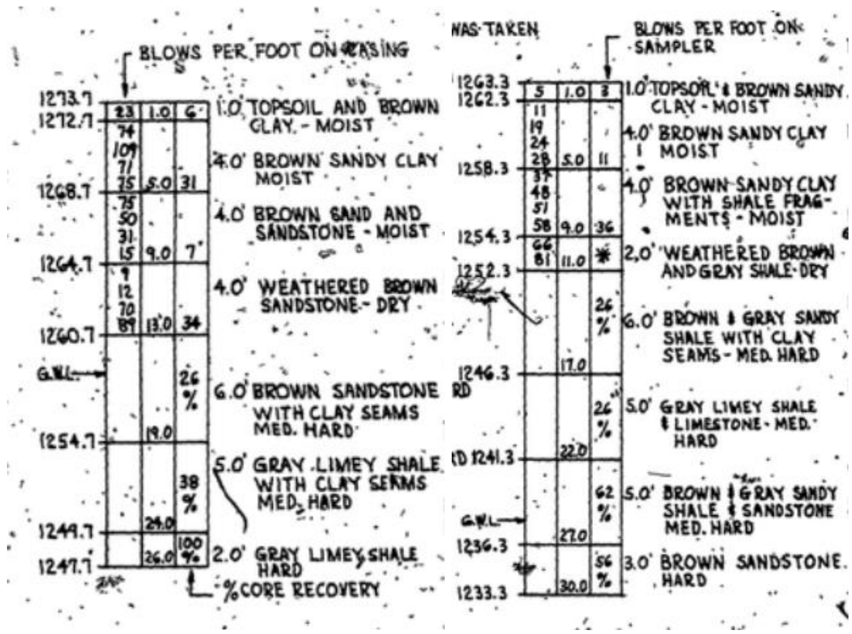

Figure IIIa.12 – Test holes near Slope #2 - Hole 2 (L) and Hole 4 (R)

These boring logs demonstrate that the native soil in this location was comprised primarily of layers of topsoil, sandy clay, weathered sandstones and shales, and solid shale and sandstone. Each boring was drilled until it hit solid, hard shale rock. They vary in depth from 26 to 30-ft deep. With the roadway at an elevation of approximately 1254-ft, the slopes consist mostly of moist sandy clay and weathered rocks.

5.3 <u>Slope #3</u>

The next slope is approximately 475-ft long and 28-ft tall. The steep sections of this slope are at a 2:1 slope. There were three borings drilled in this area to collect soil samples. These samples were collected prior to the construction of the roadway, meaning that they reflect the native soils that were removed. A summary of the boring data can be seen from the boring logs below in Figure IIIa.13.

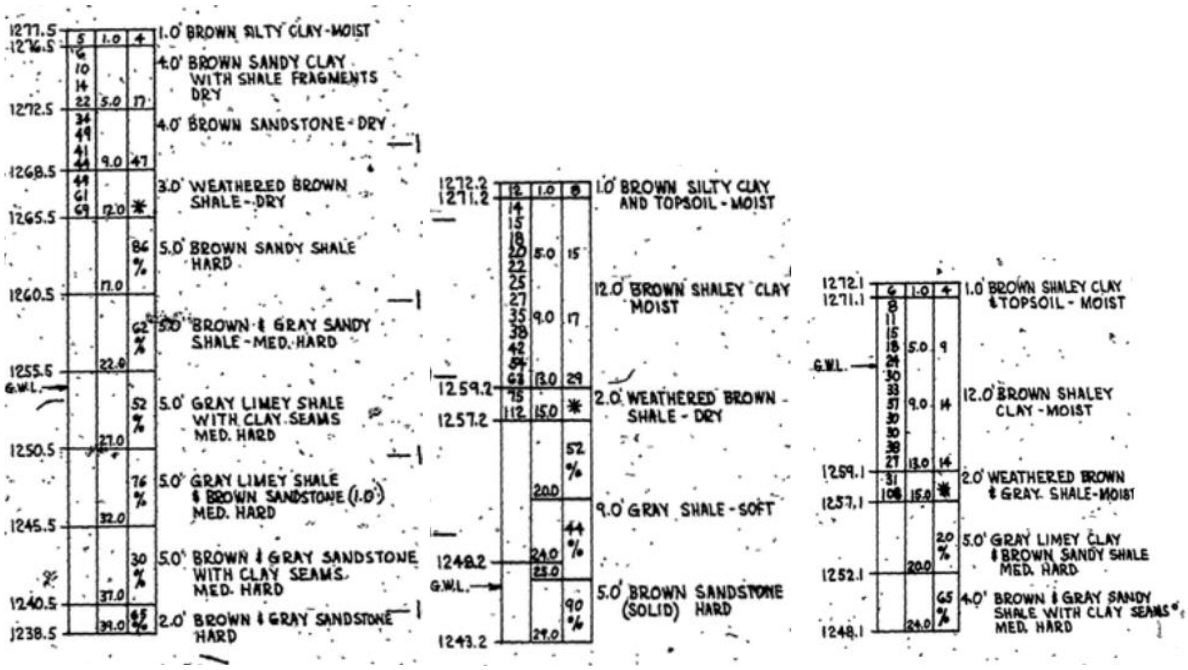

Figure IIIa.13 – Test holes near Slope #3 - Hole 5 (L), Hole 6 (M), and Hole 7 (R)

These boring logs demonstrate that the native soil in this location was comprised primarily of silty clay, shaley clay, weathered shale, and hard rocks. Each boring was drilled until it hit solid, hard rock. They vary in depth from 24 to 39-ft deep. With the roadway at an elevation of approximately 1260-ft, the slopes consist mostly of shaley clay and weathered rock.

5.4 Slope #4

The next slope is approximately 500-ft long and 26-ft tall. The steep sections of this slope are at a 2:1 slope. There were no borings drilled in this area before the interstate was constructed.

5.5 Slope #5

The next slope is approximately 1500-ft long and 48-ft tall. The steep sections of this slope are at a 1.5:1 slope. There were two borings drilled in this area to collect soil samples. These samples were collected prior to the construction of the roadway, meaning that they reflect the native soils that were removed. A summary of the boring data can be seen from the boring logs below in Figure IIIa.14.

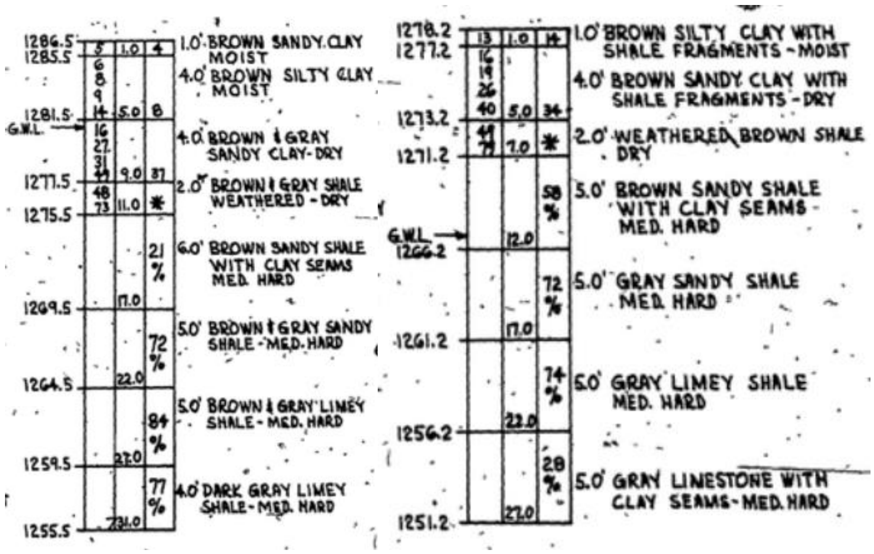

Figure IIIa.14 – Test holes near Slope #5 - Hole 8 (L) and Hole 9 (R)

These boring logs demonstrate that the native soil in this location was comprised primarily of sandy clay, weathered shale, sandy shale, and limey shale. Each boring was drilled until it hit medium hard rock. They vary in depth from 27 to 31-ft deep. With the roadway at an elevation of approximately 1250-ft, the slopes consist mostly of weathered and medium hard shales.

5.6 Slope #6

The next slope is approximately 850-ft long and 102-ft tall. There is a flat section located on both sides of this slope, which breaks the slope into two sections. The steep sections of this slope are at a 1:1 slope. There were four borings drilled in this area to collect soil samples. These samples were collected prior to the construction of the roadway, meaning that they reflect the native soils that were removed. A summary of the boring data can be seen from the boring logs below in Figure IIIa.15.

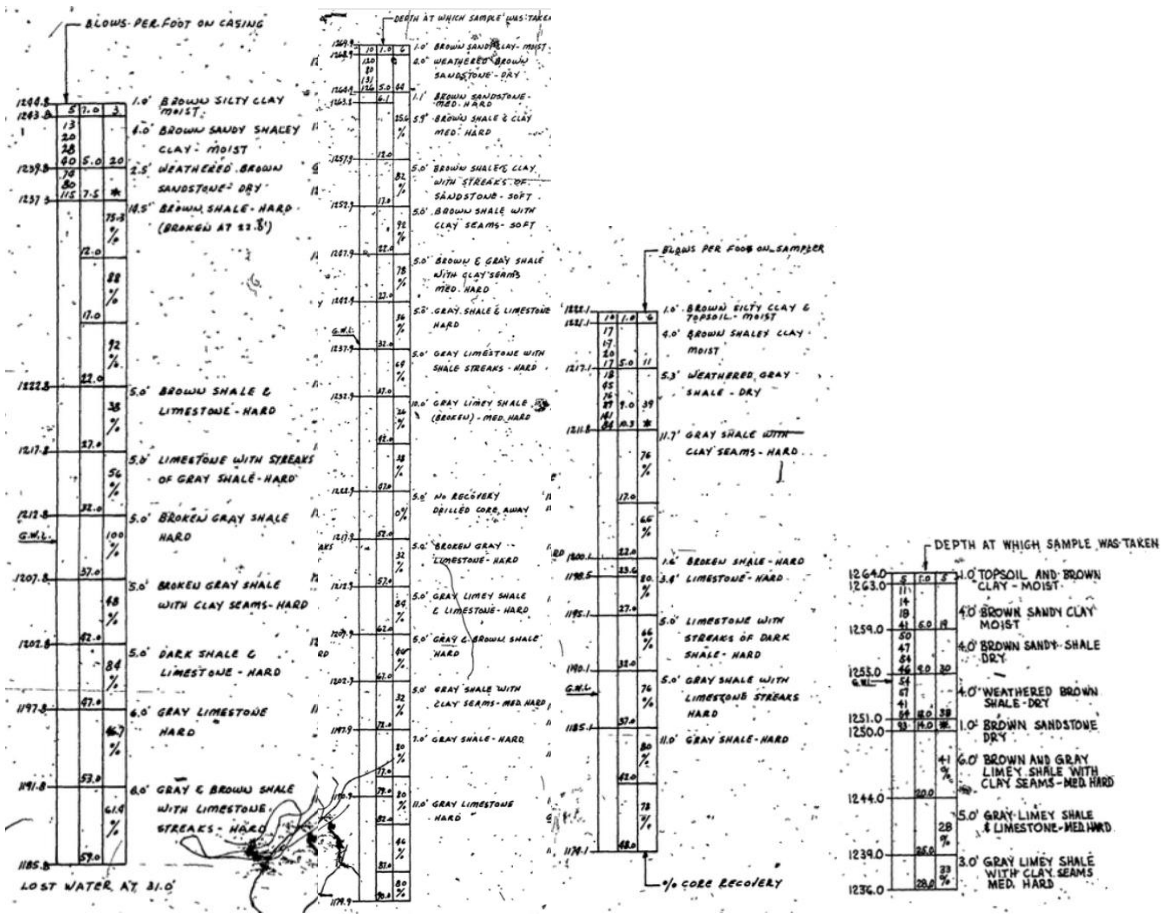

Figure IIIa.15 – Test holes near Slope #6 - from left to right Hole 10, 11, 12, and 3

These boring logs demonstrate that the native soil in this location was comprised primarily of clays, weathered shale, weathered sandstone, and various hard rocks. They vary in depth from 28 to 90-ft deep. With the roadway at an elevation of approximately 1172-ft, the slopes consist mostly of solid, hard limestone and shale.

5.7 <u>Slope #7</u>

The next slope is approximately 450-ft long and 72-ft tall. There is a flat section located on both sides of this slope, which breaks the slope into two sections. The steep sections of this slope are at a 1:1 slope. There were three borings drilled in this area to collect soil samples. These samples were collected prior to the construction of the roadway, meaning that they reflect the native soils that were removed. A summary of the boring data can be seen from the boring logs below in Figure IIIa.16.

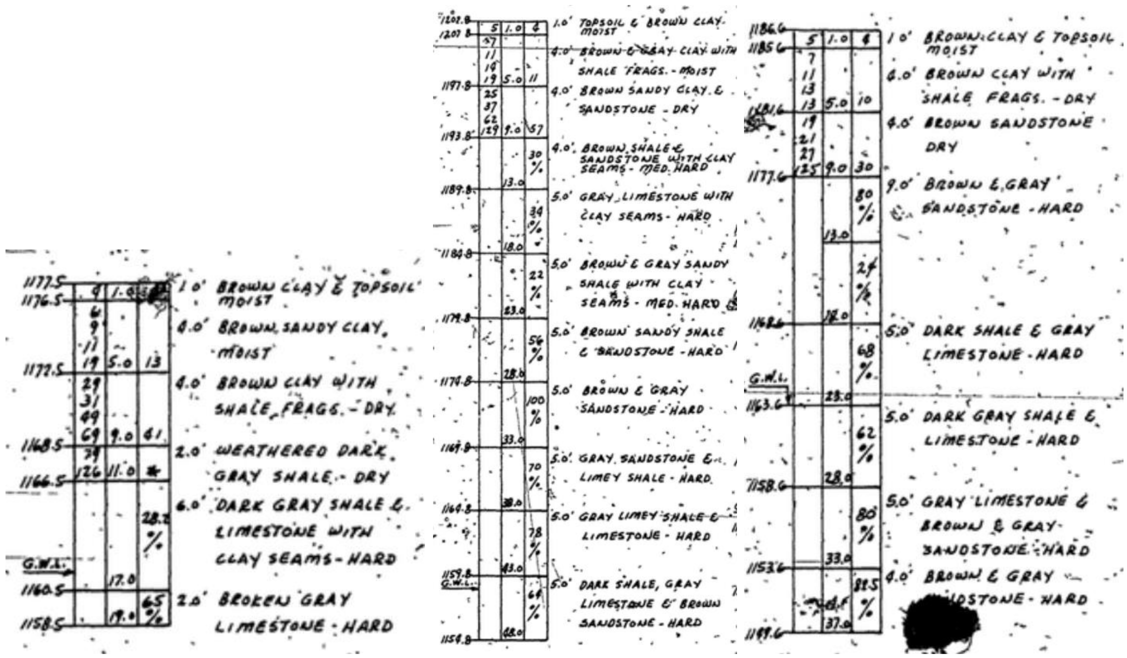

Figure IIIa.16 – Test holes near Slope #7 - Hole 13 (L), Hole 14 (M), and Hole 15 (R)

These boring logs demonstrate that the native soil in this location was comprised primarily of clays, and hard limestones and sandstones. They vary in depth from 19 to 48-ft deep. With the roadway at an elevation of approximately 1150-ft, the slopes consist mostly of solid, hard limestone and sandstone.

5.8 Slope #8

The next slope is approximately 1200-ft long and 64-ft tall. The steep sections of this slope are at a 1:1 slope. There were four borings drilled in this area to collect soil samples. These samples were collected prior to the construction of the roadway, meaning that they reflect the native soils that were removed. A summary of the boring data can be seen from the boring logs below in Figure IIIa.17.

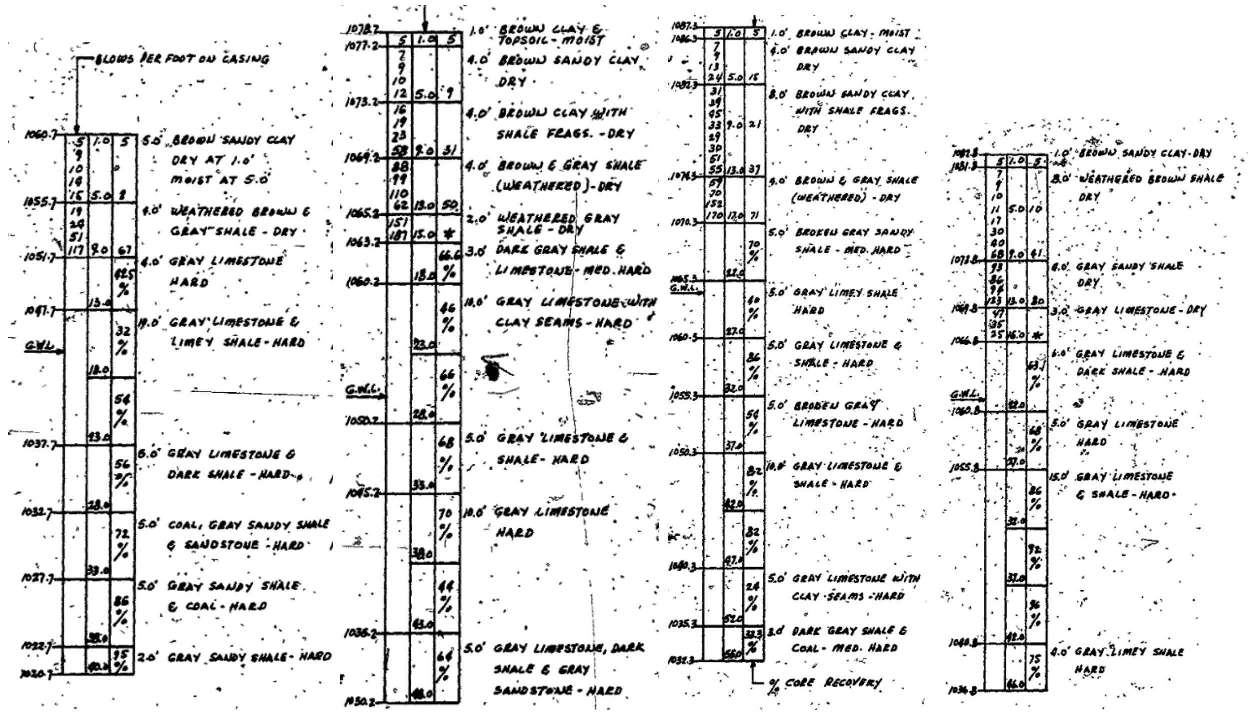

Figure IIIa.17 – Test holes near Slope #8 - from left to right Hole 7, 8, 9, 10

These boring logs demonstrate that the native soil in this location was comprised primarily of sandy clay, weathered shale, limestone, sandstone, and shale. They vary in depth from 46 to 56-ft deep. With the roadway at an elevation of approximately 1,030-ft, the slopes consist mostly of hard shale, sandstone, and limestone.

5.9 Slope #9

The next slope is approximately 500-ft long and 34-ft tall. The steep sections of this slope are at a 2:1 slope. There were three borings drilled in this area to collect soil samples. These samples were collected prior to the construction of the roadway, meaning that they reflect the native soils that were removed. A summary of the boring data can be seen below in Figure IIIa.18.

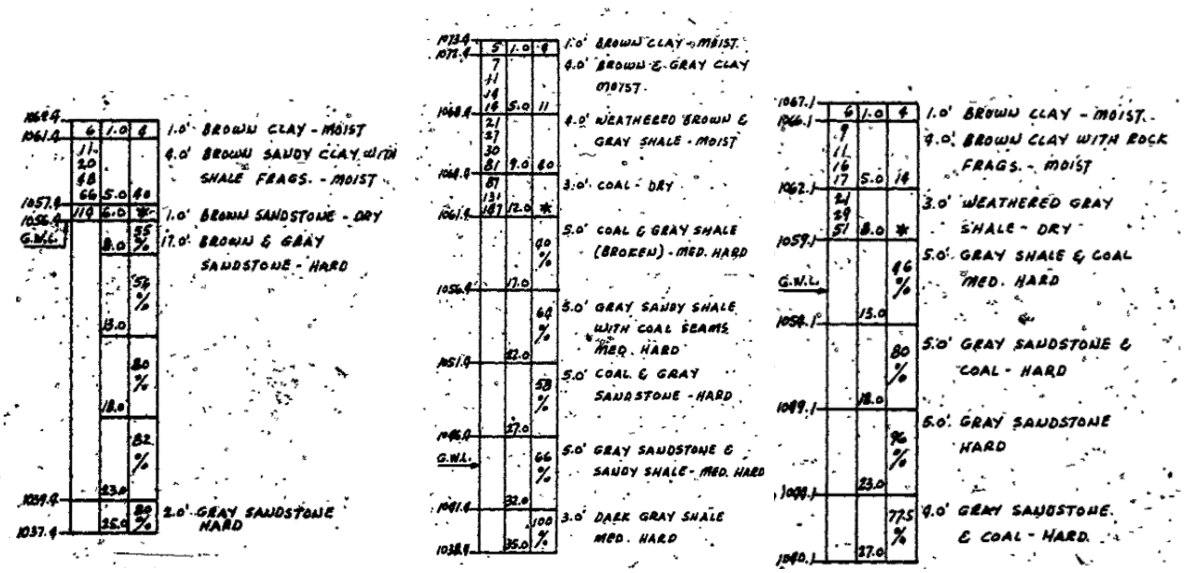

Figure IIIa.18 – Test holes near Slope #9 - Hole 11 (L), Hole 12 (M), and Hole 13 (R)

These boring logs demonstrate that the native soil in this location was comprised primarily of moist clays, weathered shale, shale, and sandstone. They vary in depth from 25 to 35-ft deep. With the roadway at an elevation of approximately 1,044-ft, the slopes consist mostly of hard, solid sandstone.

5.10 Slope #10

The next slope is approximately 725-ft long and 28-ft tall. The steep sections of this slope are at a 2:1 slope. There were no borings drilled in this area before the interstate was constructed.

6.0 Construction Methods

After reviewing the as-built plans, the University discovered some concerns regarding the construction of the embankments. Traditionally, when an embankment is constructed, the native soil is removed, new material is notched into existing rock, and drains are installed in the slope. Since there are no details in the plans illustrating the construction of the embankments, the University must assume that they were not constructed properly. There is no evidence of notching between the new soil and the existing rock. There is evidence that the bottoms of the embankments are not only not benched, but they are also not horizontal; this means that the interface between the fill and the placed material is sloping, forming a slipping plane for embankment. From analyzing the boring data and the embankment profiles, it was observed that there is likely natural, loose soil between the fill material and rock layers.

There is also no indication of drains in the embankments in the as-built plans. However, through site visits, it was determined that there is a single drain in the study area. The drain is located in the center island and drains to a rock lined strip at the edge of the southern side of embankment 1. From the surface it appears that the water is not discharging to the top of this discharge stripe, but rather to the bottom where there is pooling and oversaturated soil, which would indicate that it is not operating as intended. This failing drain could contribute to the excess of water at the bottom of the southern side of the embankment.

The combination of undrained water, alluvium underneath the embankment, and no benching system may influence how the embankments behave when experiencing the subsidence and may cause instabilities as the route is undermined.

7.0 Summary

The as-built files provided to the University contained information regarding the areas of cuts and fills between the existing and proposed conditions and the borings that were drilled before construction. From these files it was determined that ~45-pct of the 5.7 mile alignment within the study area was constructed in areas of cut, while the other 55-pct was constructed in areas of fill. There were 37 borings drilled throughout the study area and along the alignment, which characterize the material properties of the native material. An additional 13 borings were drilled in the two embankments that will be influenced by the mining of Panel 15. These 13 borings characterize the fill material placed to build these embankments, as well as the characteristics of the water table.

The review of as-built files as well as current alignment conditions resulted in the identification and characterization of five embankments within the study area. Two of these embankments are located within the influence of Panel 15 and the other three are likely to be influenced by future mining. The embankments are primarily comprised of granular fill material. The slopes of these embankments are currently mostly stable, aside from the occasional surface scarp caused by oversaturation, but it is impossible to predict how the embankments will react to undermining.

The review continued to include an analysis of the cut slopes. There are a total of 10 cut slopes within the extent of the study area. Borings were taken in the native soil prior to construction and were used to characterize these cut slopes. These slopes are primarily comprised of strong, hard rock but also contained weathered and soft rock. The slopes are currently stable, but it is hard to predict how the slopes will react to undermining.

Through a detailed review of the as-built files provided by PennDOT, the University considered the construction methods utilized while building the embankments. The files provided contained very little information regarding the construction of the embankments, so it cannot be confirmed that modern stability methods were implemented. Modern stability methods for this type of embankment in southwestern Pennsylvania would include 1) the removal of colluvium at the base of the embankment, 2) notching the fill into the bedrock slope, and 3) installing a drainage system at the base of the fill.

However, in the embankments constructed along I-70, there is no indication that the colluvium soil layer was removed nor that the fill was benched, or notched, into bedrock. In fact, there is some evidence that the native colluvium was not removed before the fill material was placed. It has also been reported that large boulders were discovered at the base of Embankment #1's south slope. It can be assumed, but cannot be confirmed, that the boulders were added to the toe of the slope to enhance the overall stability of the embankment.

Subsection IIIb – Evaluation of the Soil and Rock Laboratory Tests

1.0 Introduction

Mr. Pat Brown from Earth Incorporated has provided the laboratory results on soil and rock samples taken from boreholes (TB-1 to TB-13) made at the two embankments (EM#1 and EM#2) located in the study section of I-70 located above the Panel 15 forming part of the longwall mine underneath (Figure IIIb.1). The laboratory results also report tests that were conducted in three soil samples taken from the surface of Embankment #1 (samples HS-1, HS-2 and HS-3) as well as rock testing from selected boreholes.

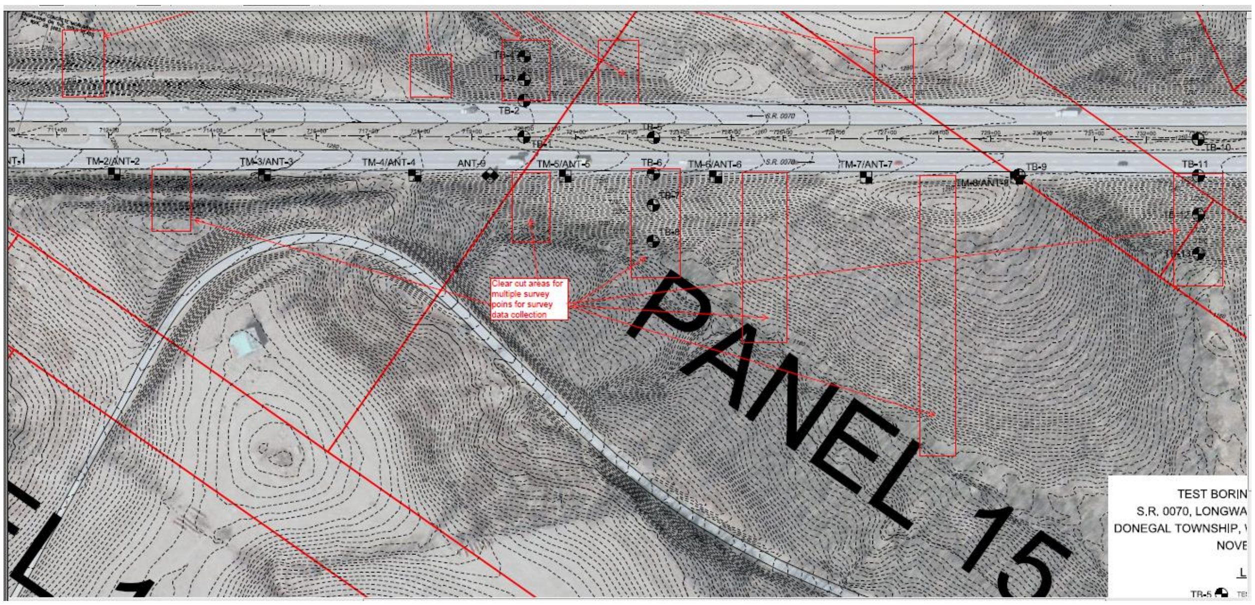

Figure IIIb.1 – Location of the boreholes TB-1 to TB-13 in Embankments #1 and #2

2.0 Soil Tests Performed

The testing on the soils samples taken from boreholes TB-1 to TB-13 as well as on soil samples HS-1, HS-2 and HS-3 were conducted to evaluate: USC and AASHTO soil classifications, Atterberg limits, grain size distribution curves, natural moisture content, optimum moisture content, dry unit weight, penetrometer tests to obtain the unconfined compression of soils, direct and Confined Undrained (CU) tri-axial testing to obtain the effective shear strength parameters (effective cohesion intercept, c, and effective friction angle, ϕ). A summary of the requested soil tests is shown in Table IIIb.1. A summary of the test results is shown in Table IIIb.2.

Table IIIb.1 – Laboratory Tests Required

Earth, Inc. Laboratory Test Requisition Form

Project #: 1813 | Project Name: S.R. 0070 Longwall Mining Tunnel Ridge Mine – Panel 15 | Project Engineer: Patrick Brown

Date: 11/26/2018, Updated 12/21/18 | Due Date: | ASTM/AASHTO: ASTM

Station	Boring No.	Sample Interval (ft.)	Sample Type	Sample Origin/ Rock Description	Moisture Content	Sieve Analysis	Hydrometer Analysis	Atterberg Limits	Standard Proctor	Remolded Direct Shear	Triaxial Shear - CU	Unconfined Compression	Point Load	Other/Special Instructions
720+00	TB-1	6.0 – 11.0	Shelby Tubes (ST-1 & ST-2)	Fill	X	X	X	X			X			CU - 3 Points. σ_3 = 5.5, 11.0, 16.5 psi
		21.0 – 23.6	Shelby Tubes (ST-3 & ST-4)	Fill	X	X	X	X			X			CU - 3 Points. σ_3 = 18.0, 36.0, 54.0 psi
		66.4 – 73.3	Rock Core	Siltstone									X	
	TB-2	15.0 – 31.5	Jars (S-11 to S-21)	Fill	X	X	X	X		X				CD - 3 Points. σ_1 = 2000, 4000, 8000 psf
		37.5 – 46.5	Jars (S-26 to S-31)	Fill	X	X	X	X						
		57.0 – 64.5	Jars (S-39 to S-43)	Alluvium	X	X	X	X						
		75.4 – 75.9	Rock Core	Limestone								X		
	TB-3	9.0 – 18.0	Jars (S-7 to S-12)	Fill	X	X	X	X						
		21.0 – 33.0	Jars (S-15 to S-22)	Fill	X	X	X	X		X				CD - 3 Points. σ_1 = 3000, 6000, 12,000 psf
		33.0 – 43.5	Jars (S-23 to S-29)	Alluvium	X	X	X	X		X				CD - 3 Points. σ_1 = 4000, 8000, 16,000 psf
		45.4 – 49.6	Rock Core	Claystone									X	
		51.7 – 52.4	Rock Core	Limestone								X		

Station	Boring No.	Sample Interval (ft.)	Sample Type	Sample Origin/ Rock Description	Moisture Content	Sieve Analysis	Hydrometer Analysis	Atterberg Limits	Standard Proctor	Remolded Direct Shear	Triaxial Shear - CU	Unconfined Compression	Point Load	Other/Special Instructions
720+00	TB-4	3.0 – 12.0	Jars (S-3 to S-8)	Fill	X	X	X	X						
		25.8 – 32.8	Rock Core	Claystone									X	
722+42	HS-1*	0.0 – 3.0	Bag (B-1)	Fill	X	X	X	X	X		X			Remolded CU - 3 Points. σ_3 = 2, 4, 8 psi Sample remolded to 95% Max. Dry Density
722+50	TB-5	24.2 – 26.0	Shelby Tube (ST-4 & ST-6)	Fill	X	X	X	X			X			CU - 3 Points. σ_3 = 18.5, 37.0, 55.5 psi
		55.5 – 56.0	Rock Core	Medium Grained Sandstone								X		
	TB-6	10.5 – 19.5	Jars (S-8 to S-13)	Fill	X	X	X	X						
		30.0 – 45.0	Jars (S-21 to S-30)	Fill	X	X	X	X		X				CD - 3 Points. σ_1 = 4000, 8000, 16,000 psf
		55.5 – 64.5	Jars (S-38 to S-43)	Alluvium	X	X	X	X						
		69.0 – 69.7	Rock Core	Limestone interbedded with Siltstone								X		
		75.2 – 76.2	Rock Core	Siltstone interbedded with Limestone								X		
	TB-7	3.0 – 18.0	Jars (S-3 to S-12)	Fill	X	X	X	X		X				CD - 3 Points. σ_1 = 1000, 2000, 4000 psf
		22.5 – 31.5	Jars (S-16 to S-21)	Fill	X	X	X	X						
		36.4 – 41.2	Rock Core	Siltstone									X	
	TB-8	6.5 – 8.5	Shelby Tube (ST-1)	Alluvium	X	X	X	X			X			CU - 3 Points. σ_3 = 6, 12, 24 psi
		10.9 – 19.9	Rock Core	Siltstone									X	

Station	Boring No.	Sample Interval (ft.)	Sample Type	Sample Origin/ Rock Description	Moisture Content	Sieve Analysis	Hydrometer Analysis	Atterberg Limits	Standard Proctor	Remolded Direct Shear	Triaxial Shear - CU	Unconfined Compression	Point Load	Other/Special Instructions
722+50	HS-2*	0.0 – 2.0	Bag (B-1)	Fill	X	X	X	X	X		X			Remolded CU - 3 Points. σ_3 = 4, 8, 16 psi Sample remolded to 95% Max. Dry Density
733+00	TB-10	18.0 – 36.0	Jars (S-13 to S-24)	Fill	X	X	X	X		X				CD - 3 Points. σ_1 = 2500, 5000, 10,000 psf
		67.7 – 75.1	Rock Core	Siltstone									X	
	TB-11	9.0 – 18.0	Jars (S-6 to S-11)	Fill	X	X	X	X						
		34.5 – 42.0	Jars (S-23 to S-27)	Fill	X	X	X	X						
		96.4 – 96.9	Rock Core	Limestone								X		
		102.0 – 102.4	Rock Core	Siltstone interbedded with Sandstone								X		
	TB-12	9.0 – 16.5	Jars (S-7 to S-14)	Fill	X	X	X	X						
		21.0 – 36.0	Jars (S-15 to S-24)	Fill	X	X	X	X		X				CD - 3 Points. σ_1 = 3000, 6000, 12,000 psf
		53.6 – 58.0	Rock Core	Siltstone interbedded with Claystone									X	
		61.2 – 62.2	Rock Core	Sandstone								X		
	TB-13	3.0 – 16.5	Jars (S-3 to S-11)	Fill	X	X	X	X		X				CD - 3 Points. σ_1 = 1000, 2000, 4000 psf
		26.6 – 29.9	Rock Core	Siltstone interbedded with Sandstone									X	
		34.0 – 34.4	Rock Core	Silty, Fine Grained Sandstone										Sample broke during preparation process; test could not be performed.
	HS-3*	0.0 – 2.0	Bag (B-1)	Fill	X	X	X	X	X		X			Remolded CU - 3 Points. σ_3 = 4, 8, 16 psi Sample remolded to 95% Max. Dry Density

*Hand dug sample in fill embankment slope.

Table IIIb.2 – Soils laboratory test

1/10/2019

SUMMARY OF LABORATORY SOIL TESTING RESULTS

S.R. 0070 LONGWALL MINING
TUNNEL RIDGE MINE – PANEL 15
WASHINGTON COUNTY, PA

Boring No.	Sample Depth (feet)	Type of Sample	Sample Origin	Classification		USCS Gradation			Atterberg Limits			Natural Moisture Content[1] (%)	Standard Proctor Test		Natural Dry Density (pcf)	Natural Moisture Content[2] (%)	Direct Shear Effective Stress		CU Triaxial Shear Effective Stress	
				USCS	AASHTO	% Rock Frags. or Gravel	% Sand	% Fines	LL	PL	PI		Maximum Dry Density (pcf)	Optimum Moisture Content (%)			Cohesion (psf)	Friction Angle (degrees)	Cohesion (psf)	Friction Angle (degrees)
TB-1	6.0 - 11.0	Shelby Tubes (ST-1 & ST-2)	Fill	CL	A-6(11)	17.7	15.1	67.2	38	19	19	14.2	-	-	115.1	12.8	-	-	28.8	33.5
TB-1	21.0 - 23.6	Shelby Tubes (ST-3 & ST-4)	Fill	CL	A-6(6)	6.5	42.5	51.0	39	20	19	11.6	-	-	98.5	8.6	-	-	633.6	25.6
TB-2	15.0 - 31.5	Jars (S-11 to S-21)	Fill	GC	A-2-6(1)	43.0	31.4	25.6	36	19	17	3.2	-	-	117.6	8.5	417.6	29.4	-	-
TB-2	37.5 - 46.5	Jars (S-26 to S-31)	Fill	GC	A-2-6(1)	40.8	28.7	30.5	34	19	15	5.3	-	-	-	-	-	-	-	-
TB-2	57.0 - 64.5	Jars (S-39 to S-43)	Alluvium	CL	A-6(8)	12.5	16.5	71.0	33	19	14	15.4	-	-	-	-	-	-	-	-
TB-3	9.0 - 18.0	Jars (S-7 to S-12)	Fill	GC	A-2-6(1)	43.6	23.3	33.1	35	20	15	11.5	-	-	-	-	-	-	-	-
TB-3	21.0 - 33.0	Jars (S-15 to S-22)	Fill	CL	A-7-6(11)	18.0	21.6	60.4	41	18	23	20.6	-	-	103.2	18.4	316.8	27.2	-	-
TB-3	33.0 - 43.5	Jars (S-23 to S-29)	Alluvium	CL	A-6(8)	3.5	29.1	67.4	33	18	15	17.8	-	-	102.2	20.0	792.0	24.9	-	-
TB-4	3.0 - 12.0	Jars (S-3 to S-8)	Fill	GC	A-7-6(3)	44.3	20.1	35.6	46	20	26	17.4	-	-	-	-	-	-	-	-
HS-1*	0.0 - 3.0	Bag (B-1)	Fill	CL	A-7-6(12)	8.2	24.2	67.6	42	22	20	34.2	110.3	15.9	-	-	-	-	57.6	23.8
TB-5	24.2 - 26.0	Shelby Tubes (ST-4 & ST-6)	Fill	CL	A-7-6(12)	33.2	9.9	56.9	48	22	26	20.5	-	-	118.9	12.2	-	-	72.0	30.2
TB-6	10.5 - 19.5	Jars (S-8 to S-13)	Fill	GC	A-6(2)	35.4	26.3	38.3	34	19	15	10.2	-	-	-	-	-	-	-	-
TB-6	30.0 - 45.0	Jars (S-21 to S-30)	Fill	GC	A-2-7(2)	48.9	22.0	29.1	41	20	21	9.7	-	-	128.7	5.9	734.4	25.1	-	-

[1]Moisture content from classification testing.
[2]Moisture content from direct shear or triaxial testing.
*Hand dug sample in fill embankment slope.

Sheet 1 of 2

1/10/2019

SUMMARY OF LABORATORY SOIL TESTING RESULTS

S.R. 0070 LONGWALL MINING
TUNNEL RIDGE MINE – PANEL 15
WASHINGTON COUNTY, PA

Boring No.	Sample Depth (feet)	Type of Sample	Sample Origin	Classification		USCS Gradation			Atterberg Limits			Natural Moisture Content[1] (%)	Standard Proctor Test		Natural Dry Density (pcf)	Natural Moisture Content[2] (%)	Direct Shear Effective Stress		CU Triaxial Shear Effective Stress	
				USCS	AASHTO	% Rock Frags. or Gravel	% Sand	% Fines	LL	PL	PI		Maximum Dry Density (pcf)	Optimum Moisture Content (%)			Cohesion (psf)	Friction Angle (degrees)	Cohesion (psf)	Friction Angle (degrees)
TB-6	55.5 - 64.5	Jars (S-38 to S-43)	Alluvium	CL	A-7-6(10)	25.2	16.7	58.1	43	21	22	24.4	-	-	-	-	-	-	-	-
TB-7	3.0 - 18.0	Jars (S-3 to S-12)	Fill	GC	A-6(4)	38.2	16.9	44.9	38	20	18	10.6	-	-	111.8	13.6	446.4	24.4	-	-
TB-7	22.5 - 31.5	Jars (S-16 to S-21)	Fill	GC	A-2-6(0)	41.1	33.5	25.4	29	18	11	11.6	-	-	-	-	-	-	-	-
TB-8	6.5 - 8.5	Shelby Tube (ST-1)	Alluvium	MH	A-7-5(21)	5.2	20.6	74.2	58	31	27	37.7	-	-	89.2	37.7	-	-	316.8	23.2
HS-2*	0.0 - 2.0	Bag (B-1)	Fill	CH	A-7-6(11)	13.3	34.7	52.0	56	29	27	10.7	110.8	15.4	-	-	-	-	115.2	29.8
TB-10	18.0 - 36.0	Jars (S-13 to S-24)	Fill	SC	A-7-6(5)	27.3	27.6	45.1	42	21	21	14.5	-	-	110.4	13.1	633.6	25.1	-	-
TB-11	9.0 - 18.0	Jars (S-6 to S-11)	Fill	GC	A-6(4)	37.8	16.9	45.3	39	22	17	14.8	-	-	-	-	-	-	-	-
TB-11	34.5 - 42.0	Jars (S-23 to S-27)	Fill	CL	A-6(15)	9.5	12.1	78.4	40	20	20	16.3	-	-	-	-	-	-	-	-
TB-12	9.0 - 16.5	Jars (S-7 to S-14)	Fill	GC	A-2-6(1)	40.5	27.8	31.7	32	18	14	11.2	-	-	-	-	-	-	-	-
TB-12	21.0 - 36.0	Jars (S-15 to S-24)	Fill	GC	A-2-6(1)	47.1	23.8	29.1	36	21	15	10.9	-	-	118.3	11.7	792.0	26.1	-	-
TB-13	3.0 - 16.5	Jars (S-3 to S-11)	Fill	GC	A-2-6(1)	40.9	28.6	30.5	33	18	15	13.2	-	-	120.0	12.6	648.0	26.6	-	-
HS-3*	0.0 - 2.0	Bag (B-1)	Fill	CL	A-7-6(9)	26.6	21.0	52.4	47	25	22	14.9	115.8	13.7	-	-	-	-	14.4	31.7

[1]Moisture content from classification testing.
[2]Moisture content from direct shear or triaxial testing.
*Hand dug sample in fill embankment slope.

Sheet 2 of 2

From the CU-tri-axial tests, plots are provided that relate the value of the deviator stress ($\Delta\sigma = \sigma_1 - \sigma_3$) with the axial strain (ε) in the samples subjected to tri-axial compression (Figures IIIb.2 and IIIb.3). From these plots the values of the Young's Modulus of Elasticity, E, can be obtained. These plots indicated that the soil samples behaved as either an elastic-plastic material before the samples failed under shear (Figure IIIb.3). Also, some of the soils forming the embankments behaved under tri-axial compression conditions as a strain hardening material. These findings are important for the modelling of the embankments using the Finite Element approach.

The Young's modulus of elasticity, E, can be obtained from the following relationship (Briaud, 2001):

$$E = \frac{\sigma_1 - 2\mu\sigma_3}{\epsilon_f} \qquad \text{[Eq. IIIb.1]}$$

Where σ_1 is the major principal stress, μ is the Poisson's ratio, σ_3 is the minor principal stress, and ϵ_f is the strain at failure. These parameters can be obtained from Table IIIb.1 and Figures IIIb.2 and IIIb.3. The value of μ varies between 0 and 0.5. For saturated soils, μ is equal to 0.5.

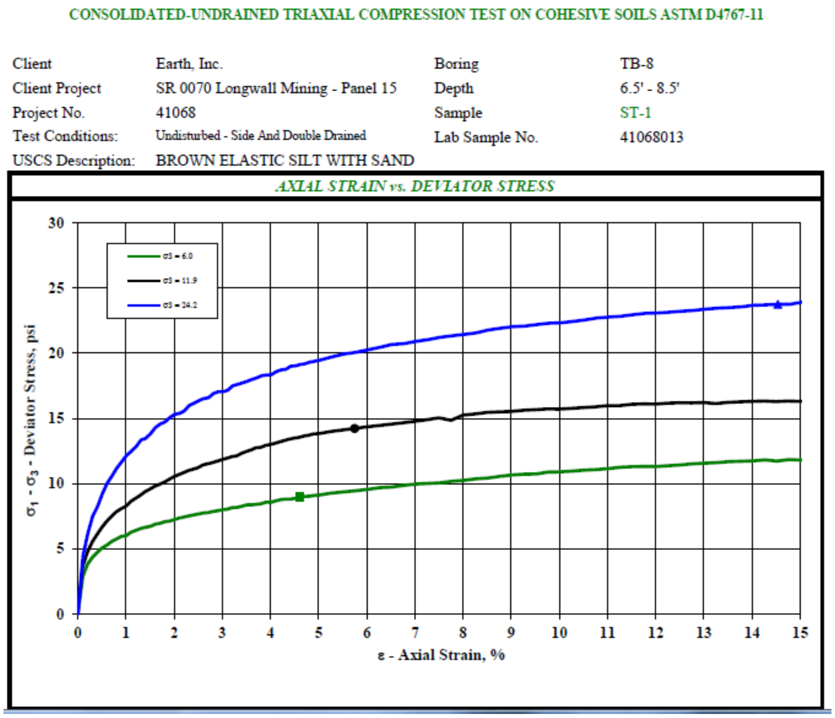

Figure IIIb.2 – Stress-strain plot from a CU triaxial test on soil sample from borehole TB-8

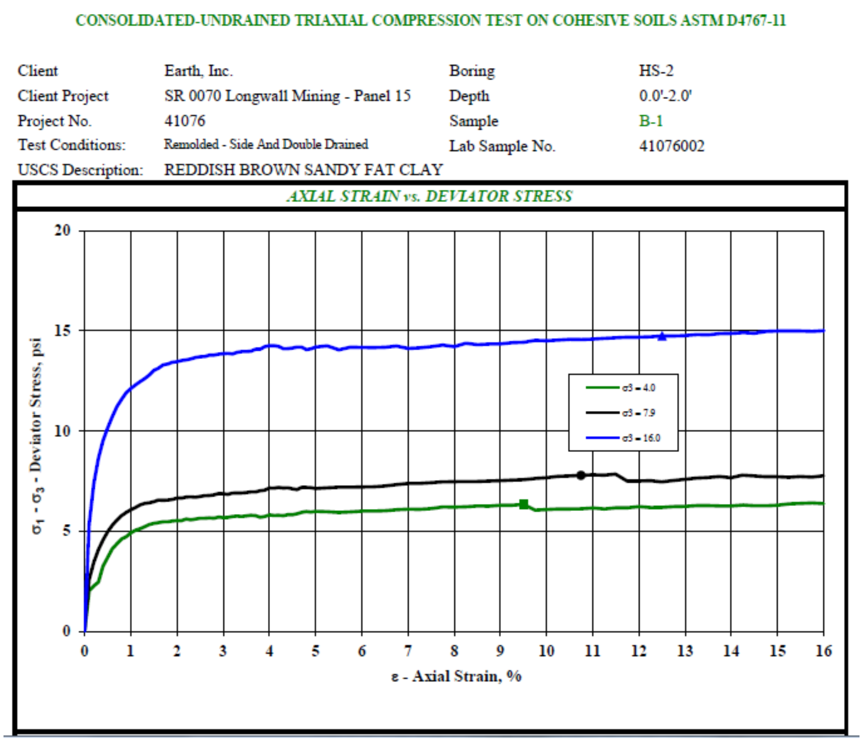

Figure IIIb.3 – Stress-strain relationships for sample H-2 from surface of Embankment #1

Penetrometer tests were also carried out on a limited number of samples. The penetrometer test gives the unconfined compressive strength (q_u) of the soil samples. Results of the penetrometer tests are shown in Table IIIb.3.

Table IIIb.3 – Penetrometer test results to obtain the unconfined compressive strength, q_u, of soils

Borehole Number	**Depth, ft**	**Unconfined compressive strength, q_u, tsf**
TB-1	0 – 1.5	0.5
TB-4	0 – 1.5	1.5
TB-4	1.5 - 3	2.0

3.0 Rock Tests Performed

The rock testing conducted on rock samples obtained from the bottom of the boreholes TB-1 to TB-13 included: Rock Description, Measurements of the Rock Quality Designation (RQD) values to measure the quality of the rock, Point Load Tests and Unconfined Compression Tests. The results of the rock tests are shown in Table IIIb.4.

Table IIIb.4 – Rock testing results

SUMMARY OF ROCK STRENGTH TESTING RESULTS

S.R. 0070 LONGWALL MINING
TUNNEL RIDGE MINE – PANEL 15
WASHINGTON COUNTY, PA

Boring No.	Sample Depth (feet)	Core Run Number	Rock Description	RQD by Run (%)	Type of Test[1]	Unconfined Compression Strength	
						(psi)	(tsf)
TB-1	66.4 - 73.3	R-1/R-2/R-3	Soft to Medium Hard Siltstone	0/57/52	P.L.	320	23
TB-2	75.4 - 75.9	R-2	Hard Limestone	26	U.C.	21,546	1,551
TB-3	45.4 - 49.6	R-1/R-2	Very Soft Claystone	30/18	P.L.	293	21
TB-3	51.7 - 52.4	R-2	Hard Limestone with Soft Claystone Interbeds	18	U.C.	40,826	2,939
TB-4	25.8 – 32.8	R-1/R-2	Very Soft Claystone	0/8	P.L.	162	12
TB-5	55.5 - 56.0	R-1	Medium Hard to Hard, Medium Grained Sandstone	70	U.C.	10,072	725
TB-6	69.0 - 69.7	R-1	Soft to Hard Limestone interbedded with Siltstone	77	U.C.	25,318	1,823
TB-6	75.2 - 76.2	R-3	Soft to Medium Hard Siltstone interbedded with Limestone	90	U.C.	16,836	1,212
TB-7	36.4 - 41.2	R-1/R-2	Soft to Medium Hard Siltstone	0/32	P.L.	1,673	120
TB-8	10.9 - 19.9	R-1/R-2/R-3	Very Soft to Medium Hard Siltstone with Clay Layers	0/0/52	P.L.	9,283	668
TB-10	67.7 - 75.1	R-1/R-2/R-3/ R-4	Very Soft to Soft Siltstone	33/80/0/ 46	P.L.	206	15
TB-11	96.4 - 96.9	R-2	Medium Hard Limestone	13	U.C.	11,248	810
TB-11	102.0 - 102.4	R-3	Medium Hard Siltstone interbedded with Sandstone	50	U.C.	12,962	933

Sheet 1 of 2

SUMMARY OF ROCK STRENGTH TESTING RESULTS

S.R. 0070 LONGWALL MINING
TUNNEL RIDGE MINE – PANEL 15
WASHINGTON COUNTY, PA

Boring No.	Sample Depth (feet)	Core Run Number	Rock Description	RQD by Run (%)	Type of Test[1]	Unconfined Compression Strength	
						(psi)	(tsf)
TB-12	53.6 - 58.0	R-1/R-2/R-3	Soft to Medium Hard Siltstone interbedded with Claystone	0/20/73	P.L.	3,617	260
TB-12	61.2 - 62.2	R-4	Medium Hard Sandstone	84	U.C.	14,164	1,020
TB-13	26.6 - 29.9	R-1/R-2	Soft to Medium Hard Siltstone interbedded with Sandstone	20/41	P.L.	4,222	304

[1] U.C. = Unconfined Compression Test; P.L. = Point Load Test

From the results of Table IIIb.4, values of the cohesion, c, and friction angle of the rock, ϕ, can be obtained and used for the stability analysis of the Embankments #1 and #2. Rahn (1996) has provided the values of ϕ for various sedimentary rocks. With the values of qu and ϕ the cohesion of the rocks can be estimated using the following relationship (Brady and Brown, 1985),

$$q_u = \frac{2c\cos\emptyset}{1-sin\emptyset} \quad \text{[Eq. IIIb.2]}$$

Also, the values of c and ϕ can be obtained from the results of the CU tri-axial compression tests as previously shown in Figures IIIb.2 and IIIb.3.

4.0 Analysis of the Results

The Embankments #1 and #2 are composed mainly of soils of low plasticity (CL = clay of low plasticity and ML = silt of low plasticity and mixtures of silty clay with gravel) (Figure IIIb.4). The values of the effective cohesion intercept, c, are low and range in values between 28.8 and 633.6-psf. The value of the effective angle of internal friction, ϕ, range in value between 23.2 and 33.5-deg. These shear strength parameters were obtained from CU tri-axial tests measuring pore water pressures at failure in the samples. The values of the dry unit weight, γ, of the materials forming part of Embankments #1 and # 2 do not change much. The values of γ varies between 98.5 and 128.7-pcf. Because of the low value of the cohesion intercept, slope failures in embankments with materials with low cohesion will likely be of the shallow type (Edil and Vallejo, 1980).

Analysis of the samples taken from the boreholes indicated that the CL and ML soils have high percentage of gravels dispersed in these soils. These gravels will increase the strength of the CL and ML soils. Gravel acts to reinforce the soil structure producing higher value of the friction angle, ϕ (Vallejo and Lobo-Guerrero, 2005). Thus, the presence of the gravel in the soils may enhance the stability of the embankments.

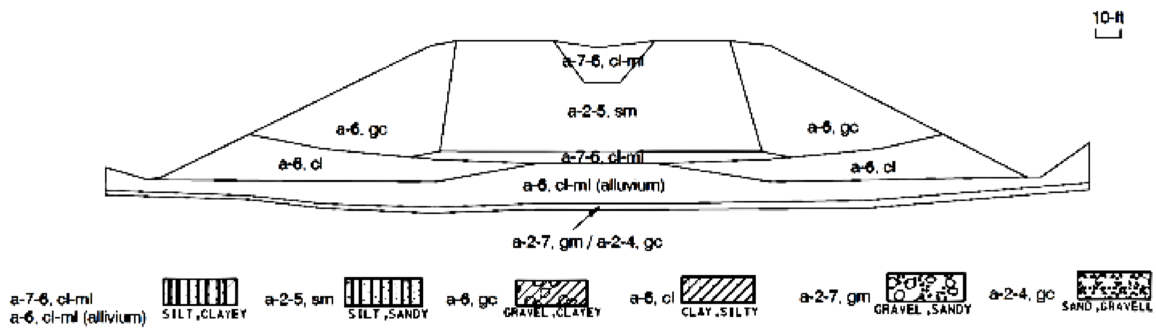

(b) 720+00 (looking from WV to PA)

Figure IIIb.4 – Cross section at 720+00 of Embankment #1 looking from West Virginia to Pennsylvania

Also, an analysis of Figures IIIb.2, IIIb.3 and IIIb.4 indicates that some of the soils within the embankments display strain hardening behavior. A soil with a strain hardening behavior, as shown in Figures IIIb.2 and IIIb.4, becomes stronger with a compressive or shear strains (Newmark, 1960).

According to Iannacchione and Vallejo (2000) and Vallejo and Lobo-Guerrero (2005), the presence of gravel in a soil-rock mixture causes the mixture to develop a higher shear resistance when subjected to direct shear conditions. Figure IIIb.5 shows a plot of the values of the cohesion intercept, c, and friction angle, ϕ, of soil-rock mixtures with different percentages of gravel in the mixtures. This figure indicates that when the mixture is subjected to shear, an increase in the percentage of the gravel in the mixture causes an increase in the friction angle and slight decrease in the cohesion intercept.

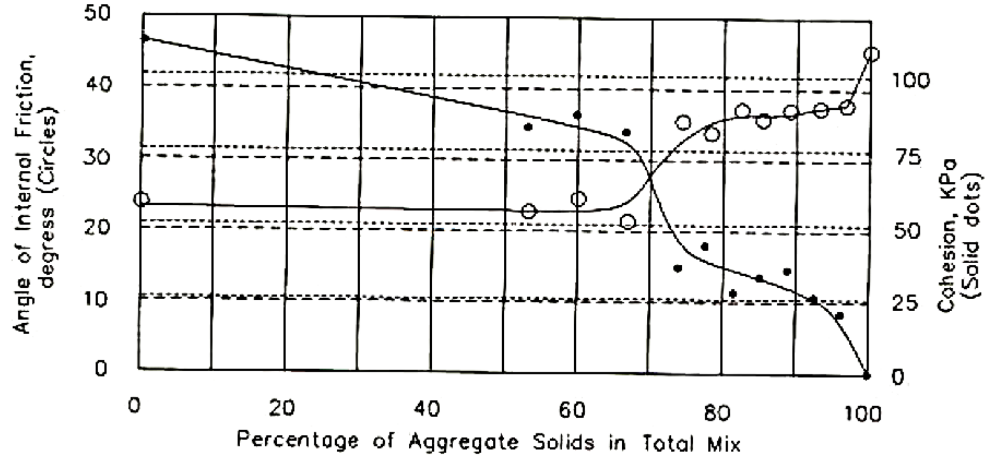

Figure IIIb.5 – Values of the cohesion intercept, c, and friction angle, ϕ as a function of the percentage of aggregates in the soil-rock mixture (Iannacchione and Vallejo, 2000)

Lastly, longwall mining induced extension and compression of the embankment fill may cause consolidation. This consolidation could cause the gravel particles to become closer to each other in the shear zone. The closer the gravel particles become within the shear zone, the greater the shearing resistance of the soil-rock mixture.

SECTION IV – PREDICTIVE MODELS

Subsection IVa – Analysis of SDPS Model for Panel 15

1.0 Introduction

An initial analysis of Panel 15 in the Tunnel Ridge Mine was developed using the Surface Deformation Predication System (SDPS) modeling software to consider the effects of undermining on I-70. This analysis considered both the final and dynamic subsidence basin that may impact the highway and the embankments. Based on the mine maps received from the Tunnel Ridge Mine, the panel has a width of approximately 1,200-ft and a length of approximately 14,500-ft.

The following assumptions were made for this analysis:

- Extraction thickness = 7.25-ft
- Supercritical Subsidence Factor = 64.2-pct
- Average overburden thickness is 675-ft
- Average percentage of hard rock is approximately 25-pct (typical for Pittsburgh Coalbed Longwall Mine)
- All pillars will remain rigid, minimizing vertical subsidence over the gate roads
- Surface is at a constant elevation
- The longwall face progresses at an average rate of 115-ft/day

2.0 Background on Subsidence Basin Formation

Longwall mining generates subsidence basins that propagate to the surface inducing stresses and strains. The panel characteristics, including width (W), length (L), and overburden (h), influence the formation of a subsidence basin. Figure IVa.1 shows some of these properties involved with defining a subsidence basin. A subsidence basin will form when the ratio of panel extraction width to the overburden depth exceeds 0.25. Based on the nature of longwall panels in Pennsylvania, the formation of subsidence basins can be expected for all extracted panels (Iannacchione et al., 2011).

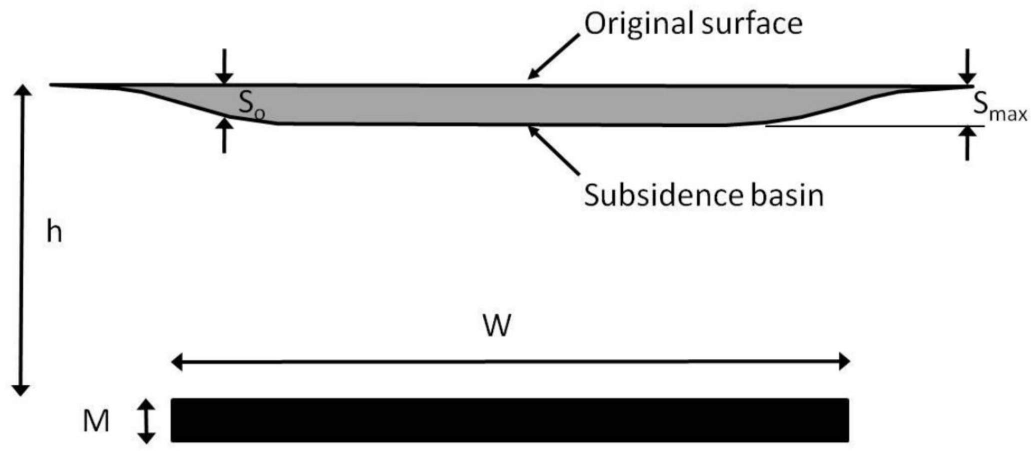

Figure IVa.1 – Properties that impact the formation of a subsidence basin (Iannacchione et al., 2011)

As subsidence basins propagate to the surface, subsidence affects the strata differently throughout the overburden. There are four generally accepted zones of movement: the caved zone, fractured zone, continuous bending (deformation) zone, and soil zone (Figure IVa.2) (Peng et al., 1992). The caved zone is the area immediately above the extraction area that breaks up and fills the void. The fractured zone is immediately above the caved zone and is characterized by strata breakage, loss of continuity, and increased permeability. The amount of fracturing within this zone decreases from bottom to top. Immediately above the fractured zone is the deformation zone, which is characterized strata bending. While there may be some small fissures in this zone, the strata continuity is not disrupted. Finally, the soil layer is the surface layer consisting of soil and weathered rocks. Some cracks may open in this layer as the face passes but cracks are likely to close once subsidence concludes (Peng et al., 1992).

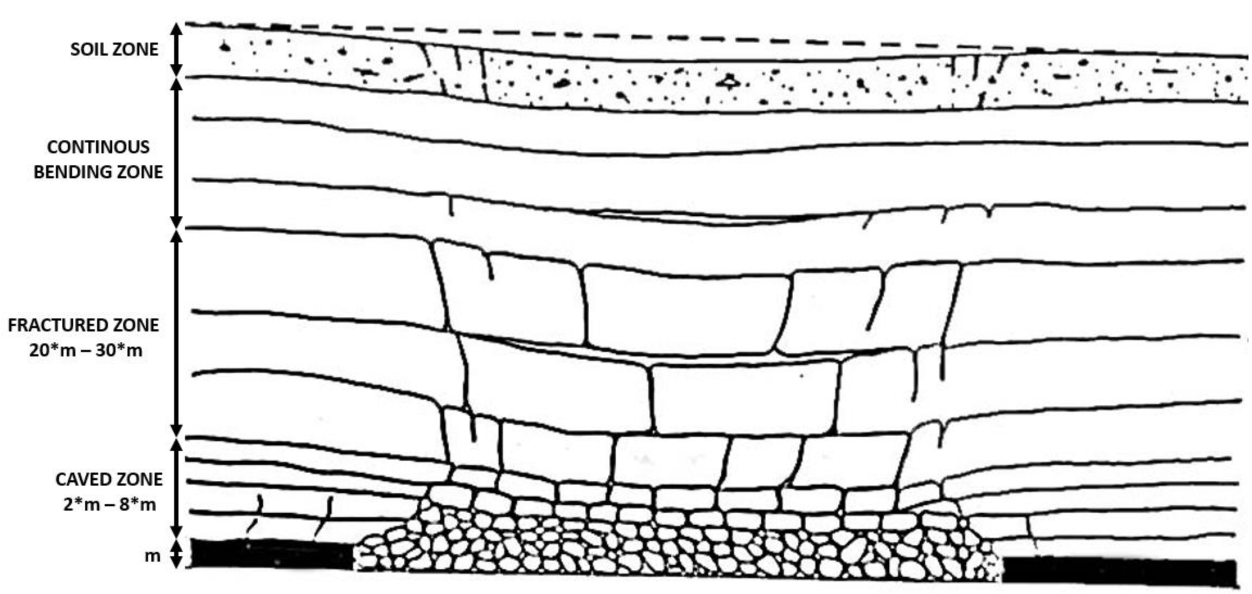

Figure IVa.2 – Four zones of strata movement above longwall mining (Peng et al., 1992)

Subsidence basins are characterized as supercritical, critical, or subcritical based on the ratio of width to overburden. A width to overburden ratio greater than 1.2 typically produces a supercritical basin, while a ratio less than 1.2 typically produces a subcritical basin (Karmis et al., 1981). A supercritical basin has a flat bottom that reaches maximum vertical subsidence predicted for the given characteristics; contrarily, a subcritical basin slopes to a point with a peak subsidence of less than the maximum vertical subsidence predicted. Most modern longwall panels fall into the supercritical category. Tunnel Ridge's Panel 15 being considered in this study, has a width to overburden ratio of 1.78, classifying it too as a supercritical basin.

2.1 Final Subsidence Basin Formation

For a horizontal coal seam, every point of a subsidence basin moves towards the center of the basin. As a result, the movements caused by longwall mining include vertical subsidence and horizontal displacement. The subsidence basin can also be characterized by slope, curvature, horizontal strain, twisting, and shear strain (Peng et al., 1992). These indices are defined by first and second derivates of the surface movement in the x and y planes.

There are a variety of factors that influence the magnitude and shape of the final deformations caused by a subsidence basin. Surface subsidence and strata movements are a result of both mining activities and geologic conditions. The following factors can have an influence on the final subsidence basin (Peng et al., 1992):

- Strength and hardness of overburden strata
- Width of mined opening
- Overburden depth
- Extraction height
- Proximity of nearest longwall panel
- Topography

In general, the maximum subsidence will be smaller when the strata is strong and hard than if it was soft and weak. The maximum subsidence is also smaller when the extraction height is lower. In the Pittsburgh coalbed, extraction height is relatively consistent, averaging 7-ft in height. Topography may also impact the movement on the surface due to subsidence. The stability of steep slopes within a surface basin may be impacted by subsidence causing landslides in slip-prone areas (Peng et al., 1992). The influence of overburden and panel width can be seen Figure IVa.3.

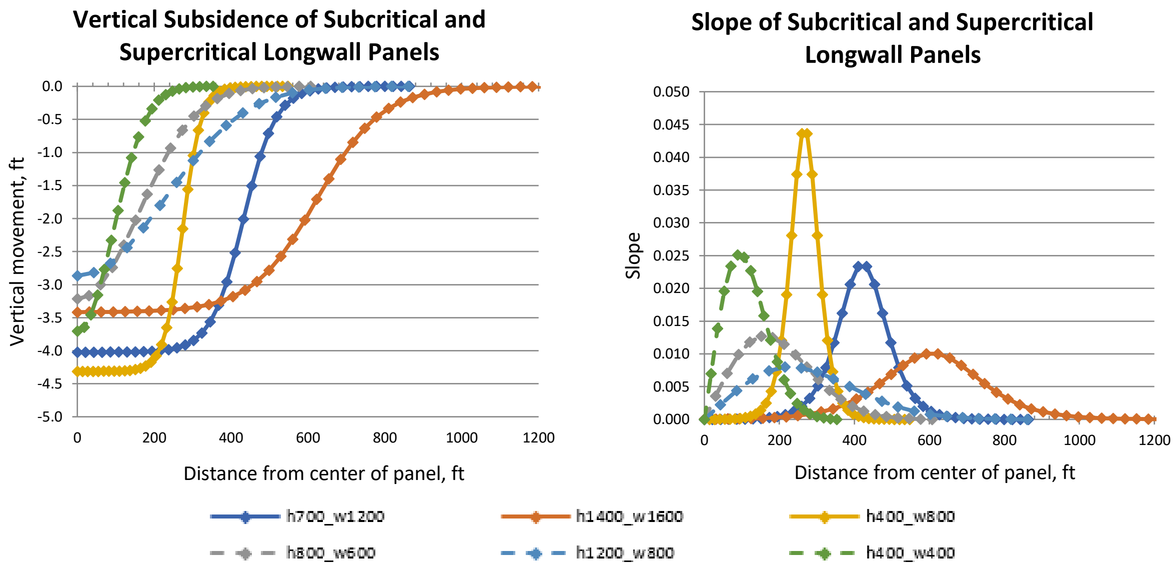

Figure IVa.3 – Profile function models of longwall panel vertical subsidence (left) and slope (right) for supercritical (solid lines) and subcritical (dashed lines) panels (Adelsohn and Iannacchione, 2019)

As can be seen in Figure IVa.3, overburden and panel width influence the amount of vertical subsidence, the width of the basin, and slope of the basin sides. In general, shallower panels produce more vertical subsidence, while deeper panels produce less vertical subsidence. The width of the panel is directly proportional to the width of the final subsidence basin and the radius of influence, r. The narrow, shallow panels also tend to produce greater slopes, which is a surrogate to horizontal deformation, and the supercritical panels tend to produce higher slopes than their subcritical equivalents.

2.2 Dynamic Subsidence Basin Formation

As longwall mining occurs over time, the subsidence basin forms as a gradual dynamic wave. The dynamic subsidence wave subjects the ground first to tension and then compression (Figure IVa.4) (Peng et al., 1992). This gradual change causes the surface to experience horizontal stresses and strains within the radius of influence, r, before and after the inflection point. These stresses and strains occur at different magnitudes and locations than represented by the final subsidence event.

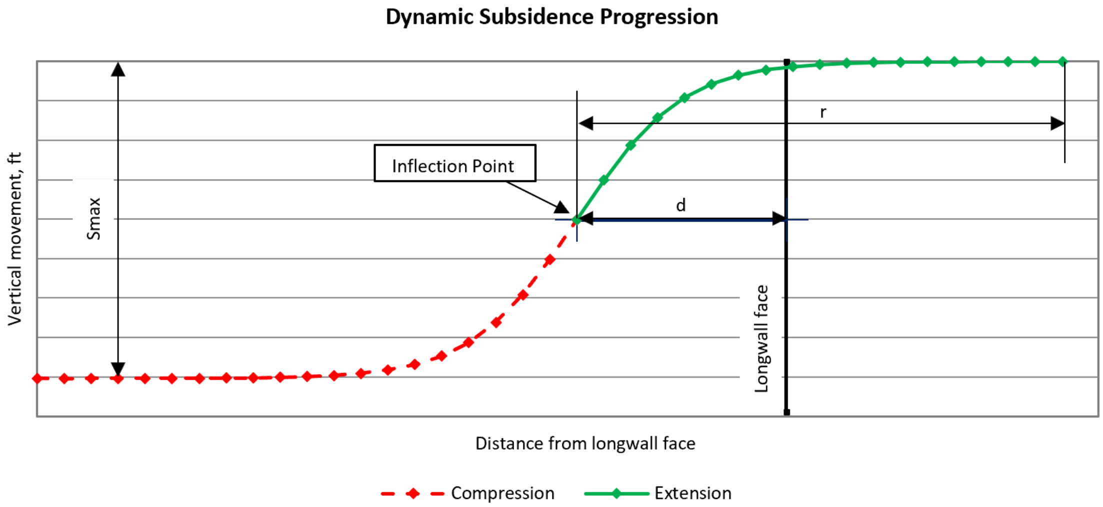

Figure IVa.4 – Relationship between vertical subsidence and tension/compression deformations cause by a dynamic subsidence wave

When the longwall face is a sufficient distance away from the set-up entry, the center of the basin reaches the maximum possible subsidence values. The subsidence profile continues to progress forward in a regular rate until the face reaches the end of the panel. When the face stops, the profile continues to subside and stabilize until it reaches the final subsidence profile. As the face is advancing, it is estimated that subsidence reaches 97-pct of final subsidence when the face is a distance of 1.2 times the overburden height away from the point (Peng et al., 1992).

2.3 <u>Subsidence Prediction Methods</u>

There are a number of different methods that can be utilized to predict subsidence due to longwall mining. These methods can be classified into empirical, semi-empirical, and numerical methods. For this analysis, only the empirical and semi-empirical methods are considered. These methods include graphical methods, profile function methods, and influence function methods.

The graphical method is derived from an extensive field database. These databases have been collected over many years of mining in one area. Formulas are developed based on the data collected in these regions, which can be applied to future mines. A disadvantage of this method is that it is developed in a specific context (overburden geology, mine dimensions, extraction thickness, etc.) and cannot be accurately applied in other contexts (Saeidi et al., 2012).

The profile function methods are analytical models that utilize mathematical equations to model subsidence. These mathematical functions have been obtained by fitting curves to match the predicted profile with previously observed conditions. The two most common profile functions are the negative exponential function and the hyperbolic tangent function (Saeidi et al., 2012).

The influence function methods are based on the superposition principle and consider displacements induced by subsidence at a given point is caused by the sum of all surface subsidence due to the extraction of an infinite number of elements in the seam horizon. This method has advantages over the other methods because it can be applied to any type of mine geometry and can analyze both vertical and horizontal ground movements induced by subsidence simultaneously (Saeidi et al., 2012).

The more complex analysis of Panel 15 was performed with SDPS. The SDPS program utilizes the influence function method.

3.0 Final Subsidence Predictive Model Using Empirical Methods

Empirical relationships were employed to characterize the subsidence basin of Panel 15 in the Pittsburgh Coalbed. The department of mining engineering at West Virginia University collected approximately 40 case studies from longwall mines in the Pittsburgh Coalbed to develop these relationships. For supercritical panels, the maximum vertical subsidence, inflection point location, and influence radius are provided below:

$$a = 0.6760821 * 0.9997678^{h} = 0.6760821 * 0.9997678^{675} = 0.578 \quad \text{[Eq. IVb.1]}$$

$$S_{max} = a * m = 0.578 * 7.25 \rightarrow \boldsymbol{S_{max} = 4.19\ ft} \quad \text{[Eq. IVb.2]}$$

$$d = 0.45439 * h * e^{-0.000914*h} = 0.45439 * 675 * e^{-0.000914*675} \rightarrow \boldsymbol{d = 165.5\ ft} \quad \text{[Eq. IVb.3]}$$

$$r = \frac{h}{\tan(\beta)} = \frac{675}{\tan(67)} \rightarrow \boldsymbol{r = 286.5\ ft} \quad \text{[Eq. IVb.4]}$$

With the aid of these empirical relationships and the profile function method, a generalized picture of the final subsidence basin can be constructed (Figure IVa.5).

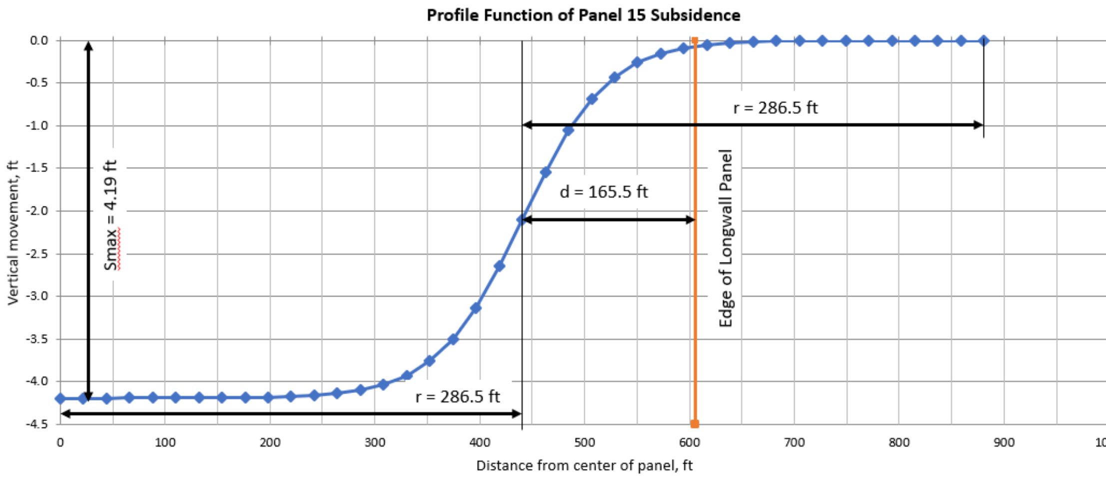

Figure IVa.5 – Generalized final subsidence basin sketched utilizing the profile function method and empirical relationships derived from Pittsburgh Coalbed data

4.0 Final Subsidence Predictive Model Using SDPS

The SDPS program can predict deformation, slope, and strain over the extent of a longwall mining operation and displays these values using graphs. The models can be generated for the entire panel and displayed as a 3D graph or can be generated for points and displayed as a 2D cross-sectional graph. Using the SDPS final predictive model, the vertical subsidence, slope, horizontal displacement, and horizontal strain that could affect the ground surface as a result of mining panel 15 were predicted. A 3D model of the final subsidence basin that may be generated for panel 15 can be seen below in Figure IVa.6.

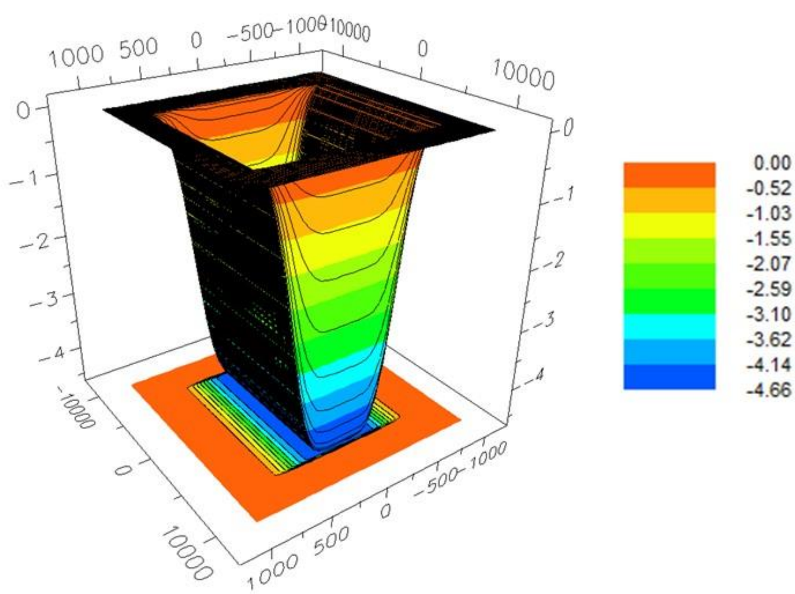

Figure IVa.6 – 3D model of vertical subsidence over the extent of Panel 15

To refine the analysis, the model and calculations were generated for the specific highway alignment of I-70 that was undermined. The highway crosses the middle of the panel at an angle, as shown below in Figure IVa.7.

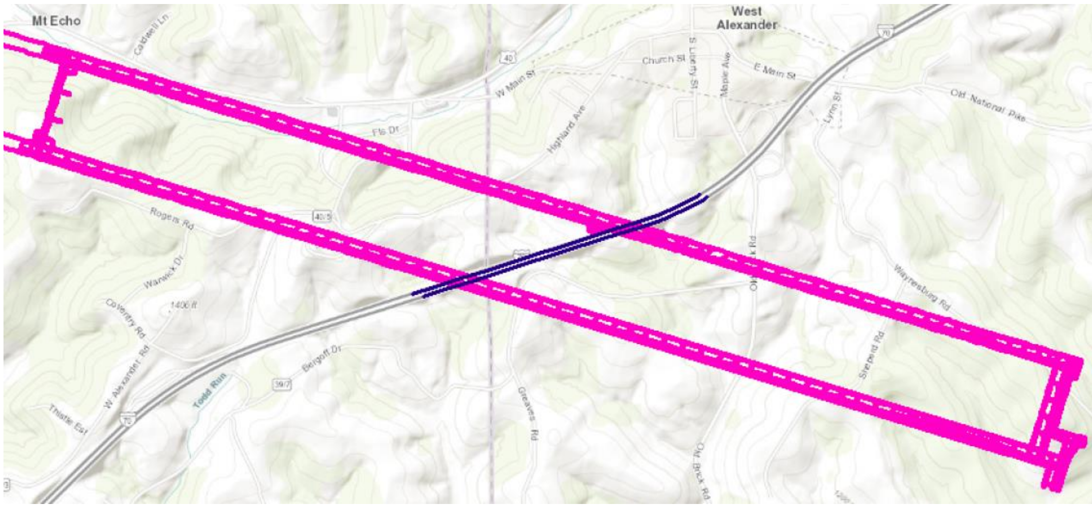

Figure IVa.7 – Orientation of I-70 alignment crossing Panel 15

Additional graphs visually representing the vertical subsidence, slope, horizontal strain, and horizontal displacement were generated along this alignment and are displayed from the center of the panel to the edge of influence. These graphs can be seen below in Figures IVa.8 through IVa.11.

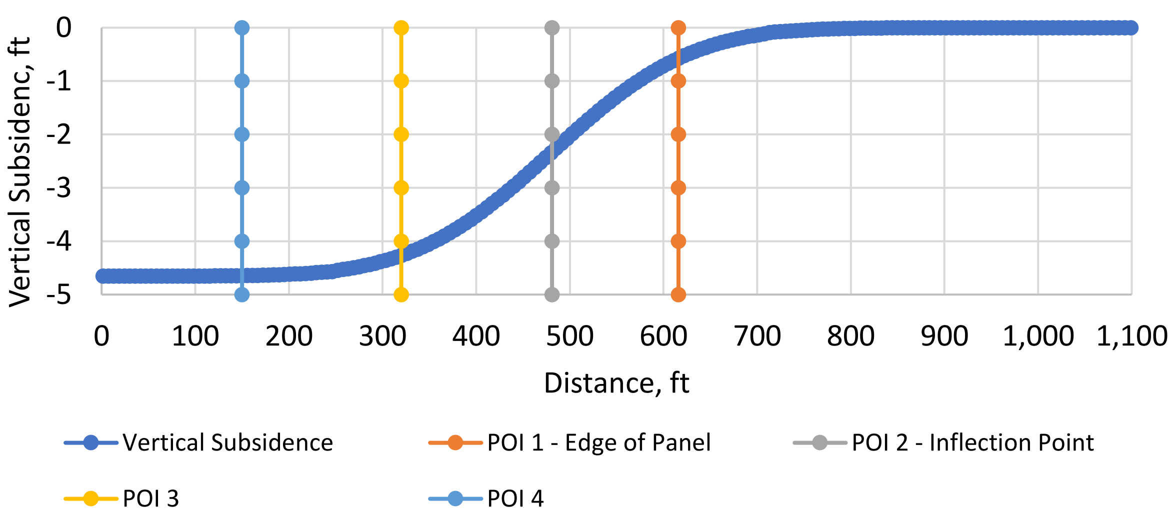

Figure IVa.8 – Model of vertical subsidence on I-70 alignment from undermining eastern half of Panel 15

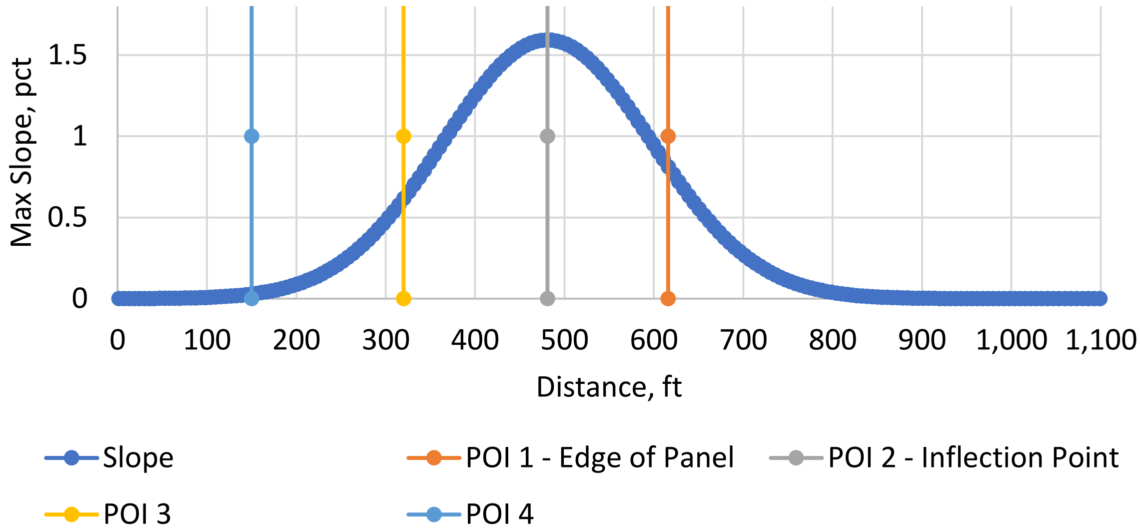

Figure IVa.9 – Model of maximum slope on I-70 alignment from undermining eastern half of Panel 15

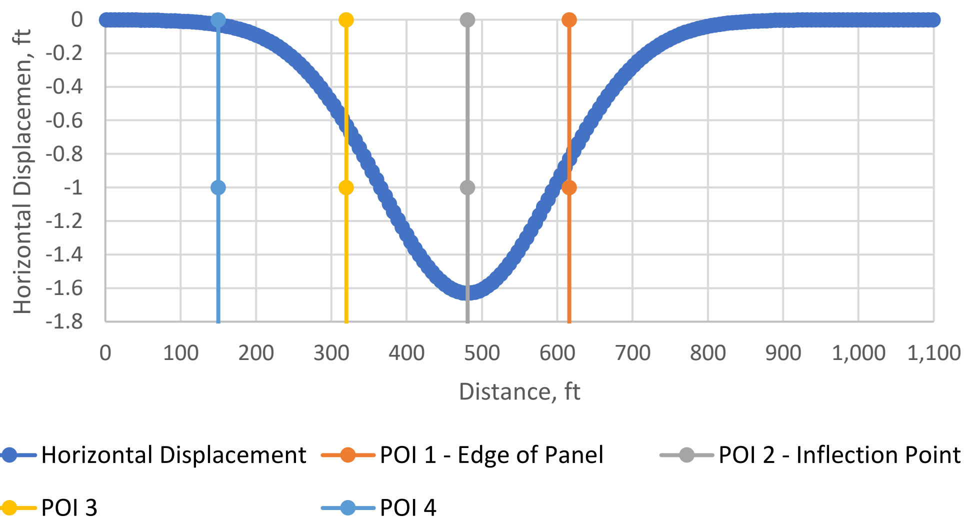

Figure IVa.10 – Model of horizontal displacement on I-70 alignment from undermining eastern half of Panel 15

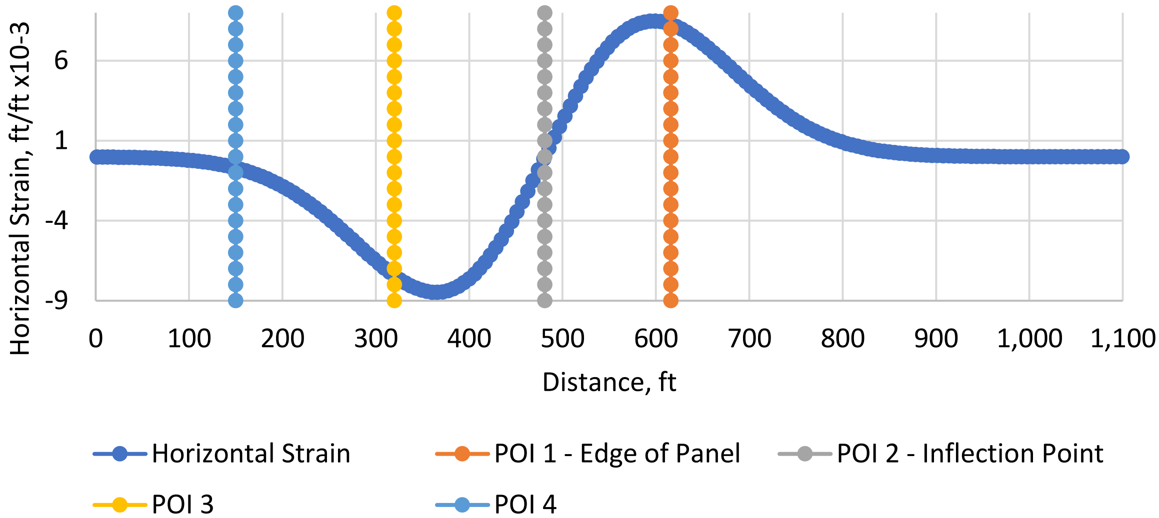

Figure IVa.11 – Model of horizontal strain on I-70 alignment from undermining eastern half of Panel 15

To better understand the relationship between the position and magnitude of each of these quantities, four points of interest (POIs) were considered along the alignment. These POIs were considered at 150, 320, 481 and 616-ft from the center of the panel; the POI at 481-ft corresponds with the inflection point of the subsidence basin and the POI at 616-ft corresponds with the edge of the panel. A summary of the values from these points can be seen in Table IVa.1.

Table IVa.1 – Predicted values of displacement, strain, and slope on highway alignment due to undermining of Panel 15 at specific points of interest

	Distance from Center of Panel, ft	**Predicted Values**			
		Vertical Subsidence, ft	**Max Slope, pct**	**Max Horizontal Strain, $1x10^{-3}$**	**Horizontal Displacement, ft**
POI 1 - Edge of Panel	616	-0.57	0.81	8.27	-0.83
POI 2 - Inflection Point	481	-2.33	1.59	0	-1.63
POI 3	320	-4.26	0.62	-7.46	-0.63
POI 4	150	-4.65	0.03	-0.70	-0.03
Minimum		-4.66	-1.59	-8.48	-1.63
Maximum		0	1.59	8.48	1.63

5.0 Dynamic Subsidence Predictive Model

The SDPS program has a function to model a dynamic subsidence wave caused by longwall mining; however, this function was found to be unreliable under certain conditions in the model. To combat this issue, the University used the final subsidence basin to project a dynamic wave.

The theoretical dynamic subsidence wave behaves like the edge of the final subsidence basin being projected forward as a function of time, as can be seen in Figure IVa.12.

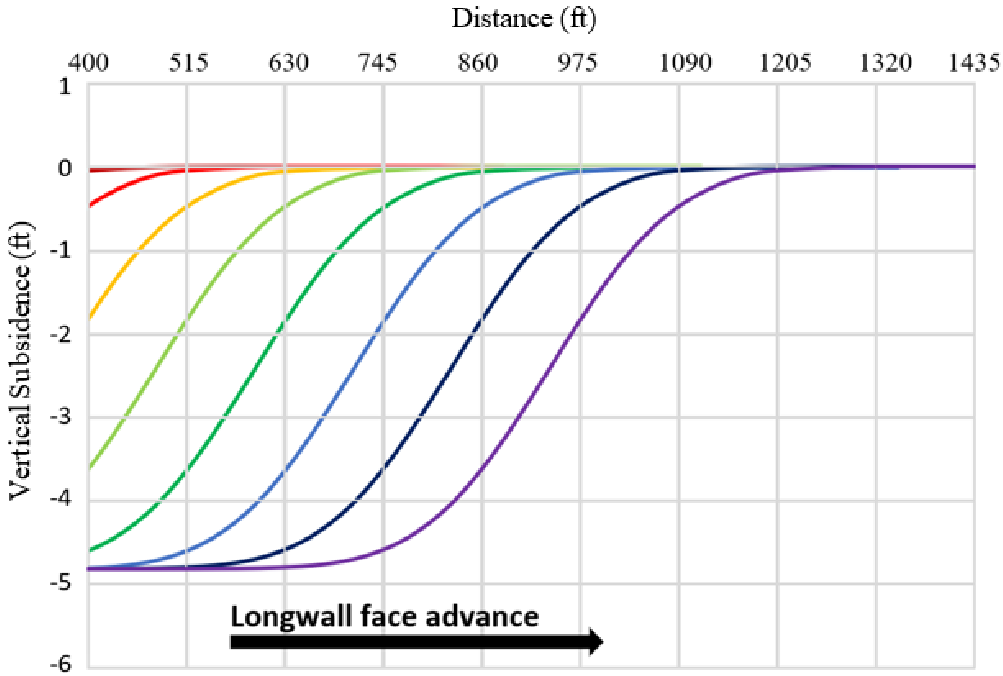

Figure IVa.12 – Longwall subsidence basin progression over time

The subsidence profiles were generated using the final subsidence basin created for Panel 15 using SDPS. The subsidence basin was advanced forward in 115-ft increments to mirror the daily longwall face progression. As can be seen in this figure, a point does not experience maximum subsidence immediately after the face passes. Based on this analysis, it takes six subsidence basin progressions for a point at its original elevation to reach maximum subsidence; this equates to six days of mining, or a longwall face advance of about 690-ft.

Since the highway crosses the longwall panel at an angle and the amount of subsidence on the surface varies across the width of a longwall panel, the profiles shown in Figure IVa.12 are insufficient to get a full picture of the dynamic effect on the road. As a result, a 3D model of the subsidence basin extent shown in Figure IVa.12 was generated. A contour map of the extent can be seen in Figure IVa.13. Like the 2D profile shown above, this 3D representation can be progressed as a function of time to model dynamic subsidence.

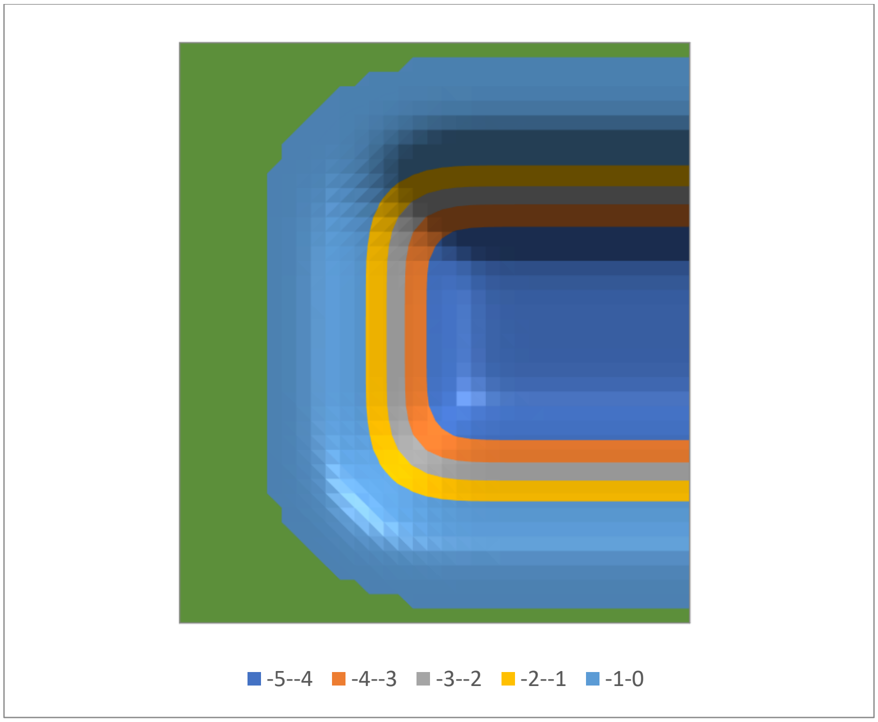

Figure IVa.13 – Contour map of edge of 3D subsidence basin in feet

Modeling the horizontal displacement caused by the moving longwall face is a bit more complicated. Since horizontal displacement is directional, it must be considered in the x and y directions separately, where the x axis is along the panel's width and the y axis is along the panel's length. Figures IVa.14a and IVa.14b show the x and y horizontal displacement, respectively.

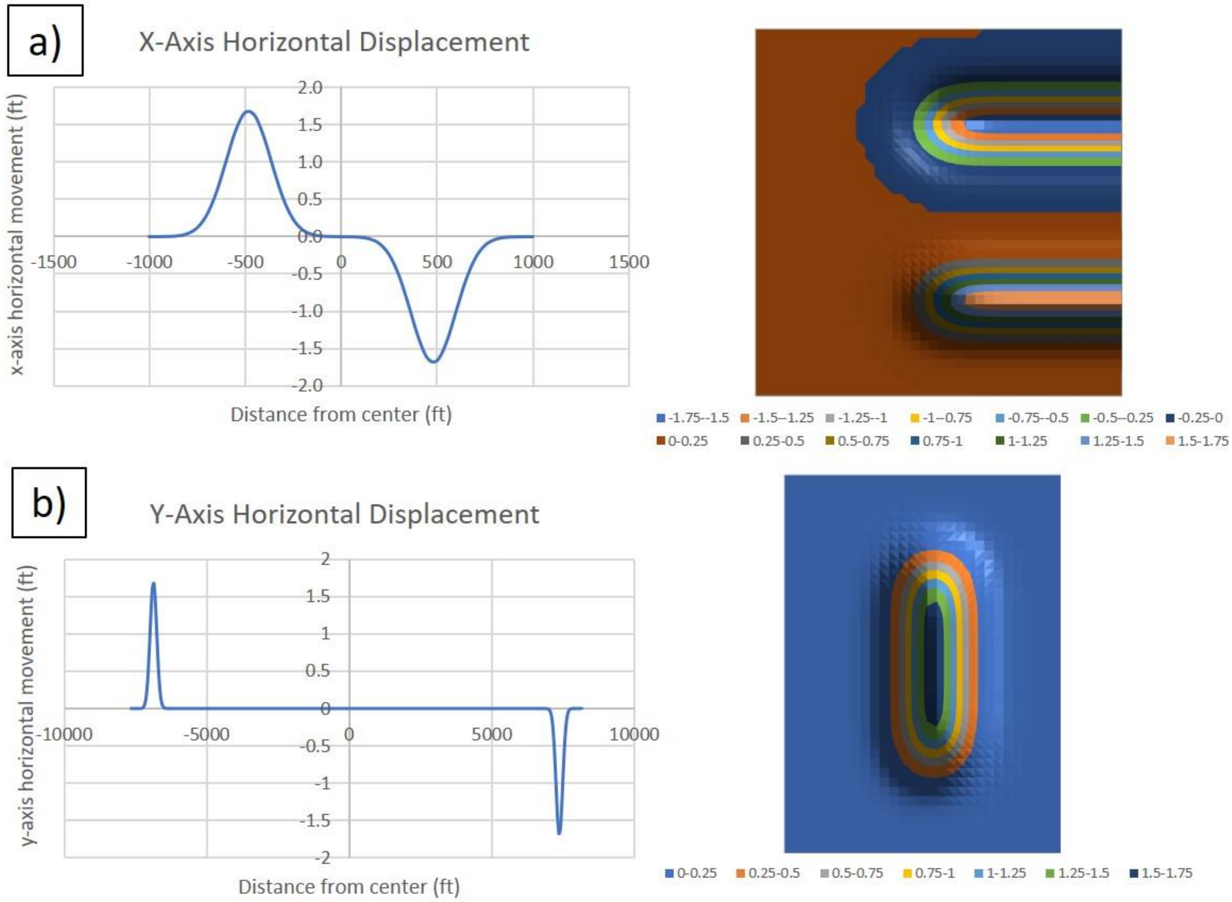

Figure IVa.14 – a) Horizontal displacement along x-axis shown as profile (left) and contours (right) and b) Horizontal displacement along y-axis shown as profile (left) and contours (right)

As can be seen in Figures IVa.13 and IVa.14, the horizontal movement caused by subsidence is significant, exceeding 1.5-ft of movement in some locations. Therefore, it is imperative that the horizontal movement be considered as well when analyzing the impact of the dynamic subsidence wave on the road and embankments. This horizontal displacement can be treated similarly to the vertical subsidence, meaning that the edge of the horizontal displacement contour maps can also be progressed as a function of time to model dynamic subsidence. It is important to note that the x and y orientations associated with the SDPS data do not correspond with the north-south-east-west coordinate system; this means that the SDPS data needs to be transformed before it can be applied to the road and embankments.

6.0 Summary

Predictive models were utilized to estimate parameters of the subsidence basin generated by the mining of Tunnel Ridge's Panel 15. Through use of the graphical method, a maximum subsidence of 4.19-ft was predicted and the radius of influence was expected to extend approximately 121-ft beyond the edge of the panel / gate road entries. Contrarily, when modeled with the influence function method by way of SDPS, the maximum subsidence predicted was 4.65-ft and was expected to extend approximately 150-ft beyond the edge of the longwall panel. The differences between these two models show the inherent uncertainty of predictive models and emphasize that the models will need to be calibrated to the specific behavior of Panel 15 once it is undermined.

Subsection IVb – A 3D Model Representative of the Initial Study Area Embankment Conditions Prior to Undermining

1.0 Introduction

Longwall Panel 15 was extracted in early 2019 (Figure IVb.1) passing under a segment of I-70 between the West Virginia/Pennsylvania border and West Alexander interchange. Two embankments on this segment will be analyzed for the prediction of the behaviors of other embankments impacted by longwall mining in the future.

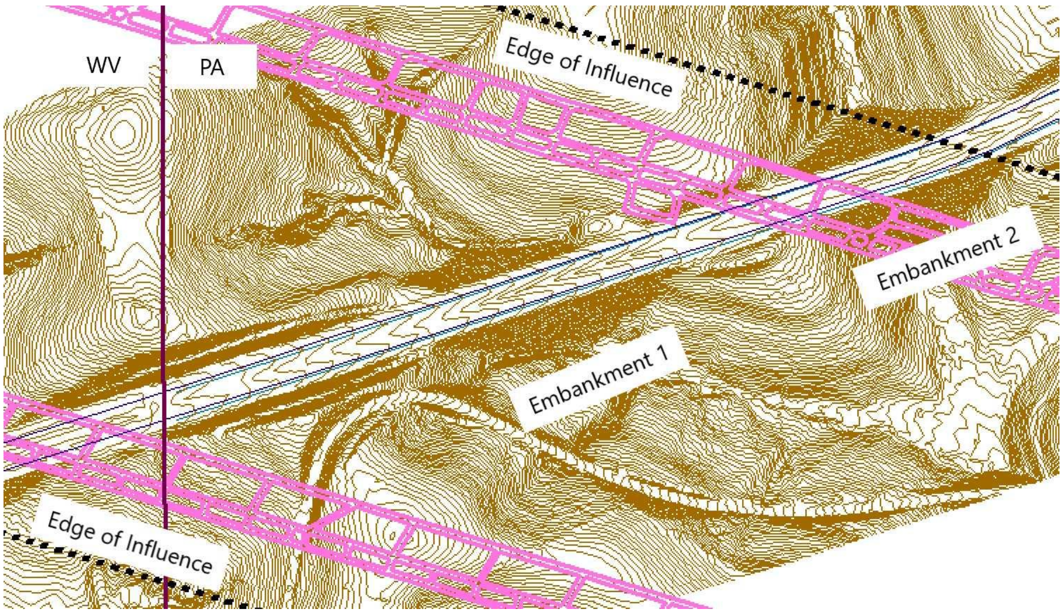

Figure IVb.1 – Overview of the Panel 15 and two embankments on I-70

The content of this subtask is to conduct the stress-strain field as well as the slope stability analysis of Embankment #1 before impacted by longwall mining. A three-dimensional Finite Element model of the Embankment #1 was constructed and tested to simulate the behavior of the embankment under gravity loading. Shear Strength Reduction Method (SRM) has been validated to obtain a factor of safety for Embankment #1 and to investigate the most likely location and characteristics of rupture surfaces within the embankment. The soil profile was obtained from test borings and plotted on cross sections. Material properties, including the shear strength parameters, were obtained from laboratory test results supplied by PennDOT contractors.

2.0 Embankment Contours in 3D

2.1 <u>Determination of the Embankment #1 Outline</u>

From the elevation data found in the topography of Embankment #1 (Figure IVb.2a), the profile of the embankment can be determined. The topography contour lines parallel to the highway represents the slope surface of the embankment going down from the pavement edge to the toe.

The elevations of toes of the embankment were 1,220 and 1,190-ft on the north and south respectively according to the contour lines. Another characteristic of contour lines to detect the outline of embankment is that the contour will vary in the direction when reaching the edge of the slope. The points can be identified on each contour line, which differentiate the embankment from the other parts of ground, and connected to find the outline of the embankment in overview, as shown in Figure IVb.2b.

Based on this obtained geometry, twelve control faces were selected to reflect the major geometry of the embankment. Figure IVb.2c indicates the horizontal locations of these control faces as well as the relationship between their locations and the topography. A coordinate system was constructed in AutoCAD in order to obtain the accurate coordinates of each point.

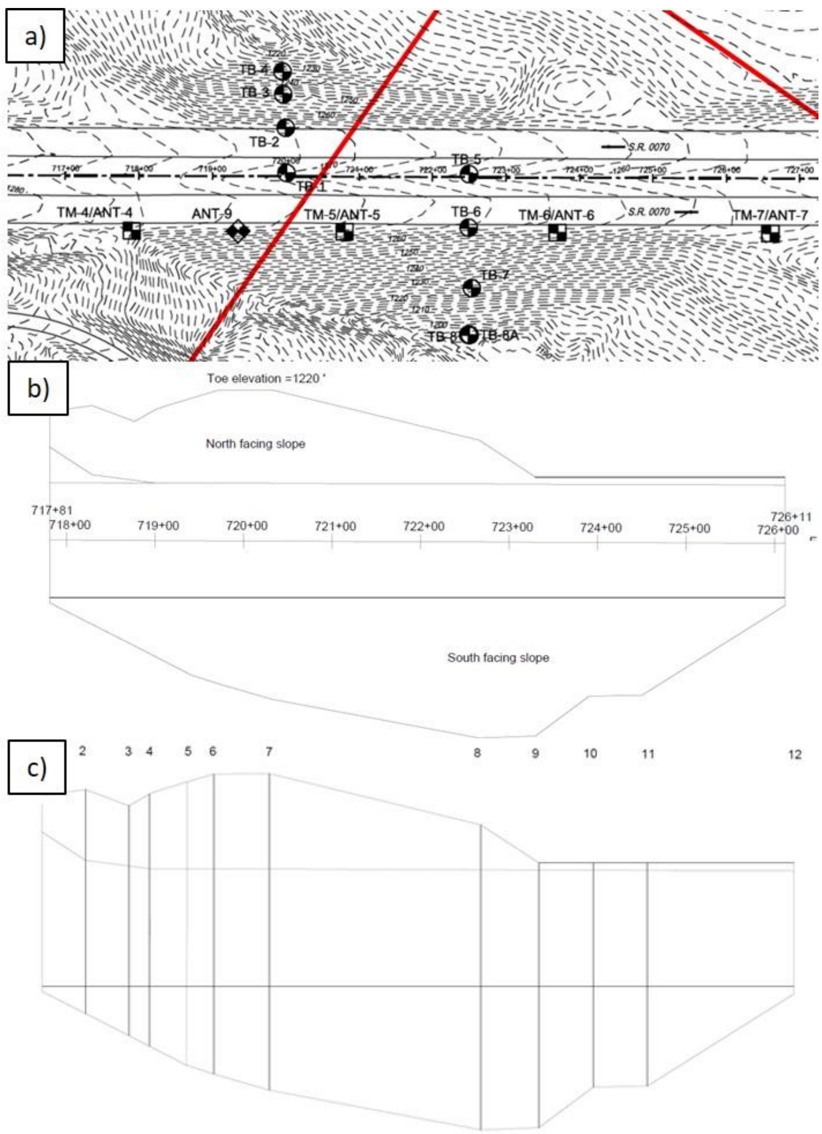

Figure IVb.2 – Determination of the overview geometry of Embankment #1: a) topographic map of Embankment #1, b) obtained geometry, and c) twelve control faces

2.2 Determination of Point Elevation

After determining the horizontal coordinates of each point in the control faces, next step was to determine the vertical coordinate (elevation) of each point. These points are divided into three groups, 24 points on the pavement, 12 points on the south slope, 12 points on the north slope, shown in Figure IVb.3a. The constructed twelve control faces in ABAQUS are shown in Figure IVb.3b. The University first determined the elevation of the points on the top and then used the magnitude of slope to determine the elevation of toes. The magnitudes of slope of highway, north slope and south slope were calculated as

$$slope_{pavement} = \frac{change\ in\ elevation}{total\ length} = \frac{1276 - 1258}{830.67} = 0.022$$
$$slope_{north\ slope} = \frac{change\ in\ elevation}{total\ length} = \frac{54}{105.21} = 0.513 \qquad \text{[Eq. IVb.1]}$$
$$slope_{south\ slope} = \frac{change\ in\ elevation}{total\ length} = \frac{72}{158.61} = 0.454$$

The resulted coordinates were imported in ABAQUS to construct twelve control faces.

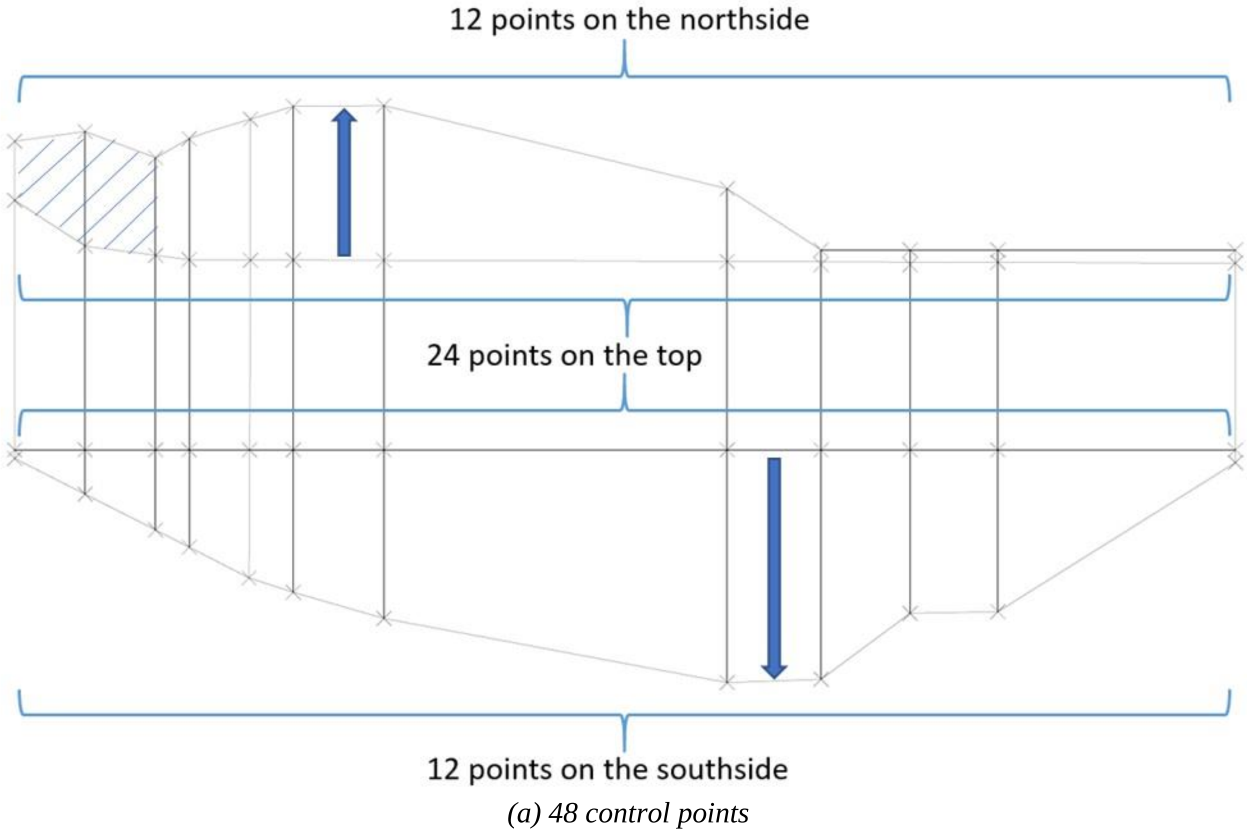

(a) 48 control points

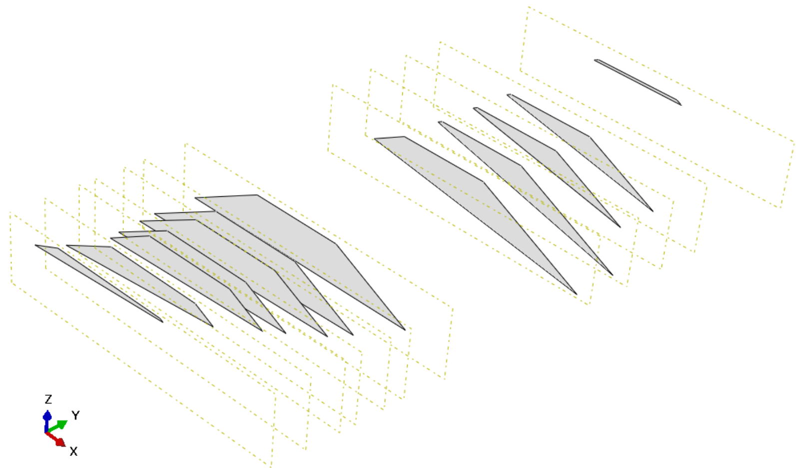

(b) Constructing 12 uniform control faces after importing coordinates of 48 points in ABAQUS

Figure IVb.3 – Forty-eight points and twelve cross sections to control the geometry of the uniform 3D model of Embankment #1

2.3 Determination of the Interior Profiles for Different Layers of Soil

To create an accurate model, it was necessary to divide the embankment fill into distinct layers with representative material properties. In order to do this, the University started from two known cross sections and then obtain a generalized cross section for the construction of the 3D layered model.

2.3.1 *Layered Model in 2D*

Two cross sections of Embankment #1 containing the profiles and types of soil were constructed at 720+00 and 720+50 (Figure IVb.4) based on the boring test results shown in Figure IVb.4a and IVb.4b, respectively. The main body of the embankment is composed of three parts, fill, alluvium, and a mixture of soil and rock fragments on the bottom. The fill, which is the major part of the embankment, mainly consists of sandy silt forming the upper part and clayey silt forming the lower part. It was noticed that the soil type of the lower part of the embankment is same as that of the alluvium on top of the bed rock, which means that there was high possibility that the embankment was constructed using the local soil at least in the lower part.

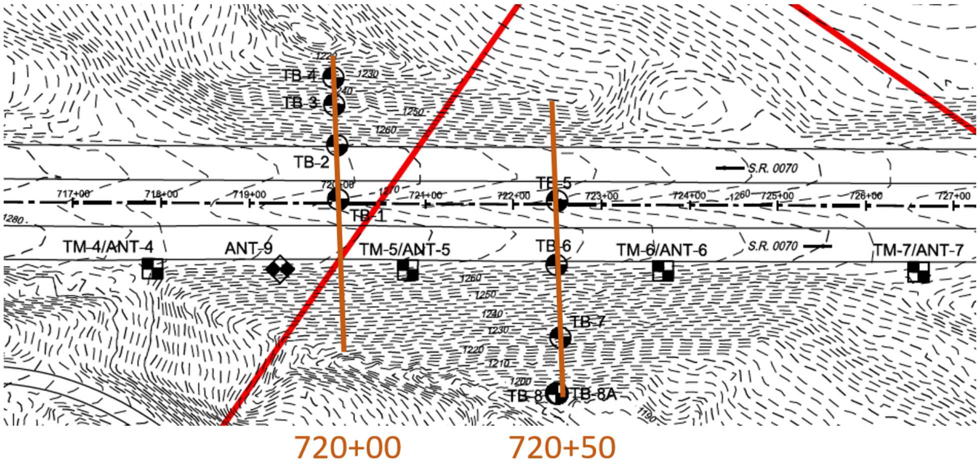

Figure IVb.4 – Locations of two cross sections at 720+00 and 720+50

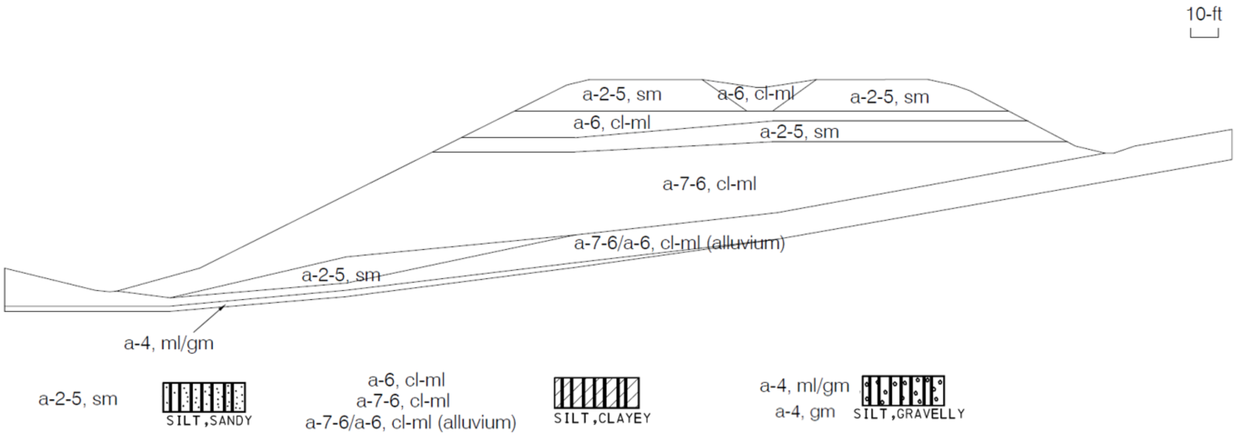

(a) 720+50 (looking from PA to WV)

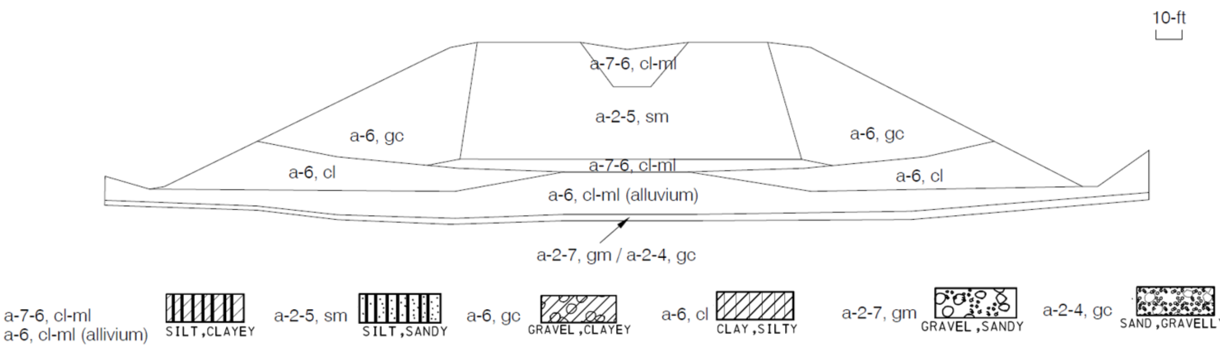

(b) 720+00 (looking from WV to PA)

Figure IVb.5 – Geometry of layered Embankment #1 in two dimensions at cross section (a) 720+50 and (b) 720+00

2.3.2 Simplified Layered Model in 3D and Implemented in the Finite Element Method

The 3D configuration of the embankment was based on these two cross sections, which contain all of the information known about the soil profile of Embankment #1. A simplified layered model is proposed in this section based on the generalization of these two cross sections. This simplified layered model made it possible to mesh in three-dimensional Finite Element model. Otherwise, with the sophisticated shape, the distorted face produced difficulty in constructing the 3D model.

Two facts can be extracted from the 2D cross sections in terms of the original ground surface. First, the embankment was constructed within a valley. Second, from the cross section 720+50, east portion of Embankment #1 was constructed on an inclined bed rock while from the 720+00, the west part was on a place which was horizontal compared to the east part. This indicates the original ground surface underneath the pavement was not horizontal along the transversal axis of highway neither especially in the east parts.

Based on the two facts of the original ground surface, the embankment can be divided into two parts in the perspective of construction procedure. The valley was first filled with soil in the lower part which was similar to alluvium (maybe taken from nearby cuts) to make the ground surface horizontal along the transversal direction. This can be seen in known cross sections 720+00 and 720+50. Then, the upper part was filled by sandy silt and gravelly silt according to two known cross sections.

Soil properties at two known cross-sections were used to construct a simplified 3D layered model. The complicated layers were generalized by summarizing the similarities of these two cross sections, making some simplifications. Figure IVb.6 and IVb.7 indicate the process of determining the generalized cross section from the two complicated layered cross sections. This configuration can be then applied on the other control faces to build up the 3D model (Figure IVb..8).

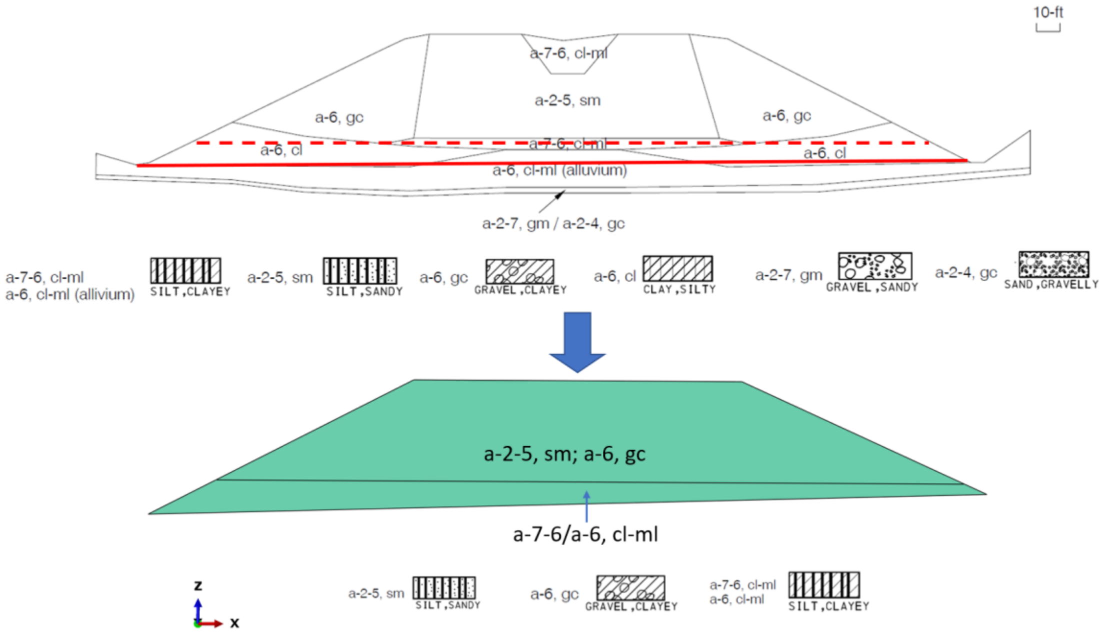

Figure IVb.6 – Simplified cross section in 3D model obtained from the sophisticated 2D model at 720+00

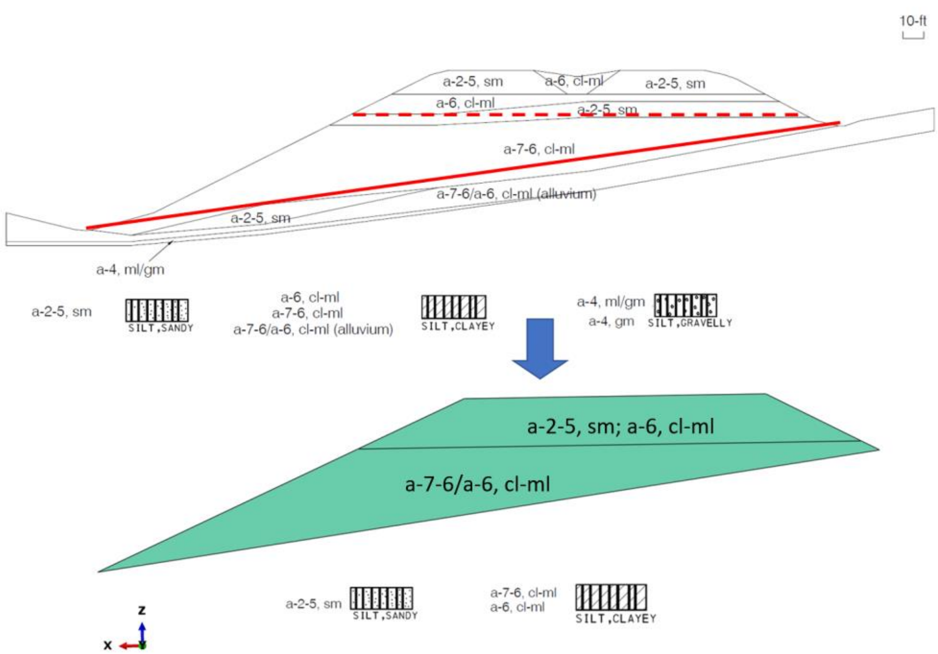

Figure IVb.7 – Simplified cross section in 3D model obtained from the sophisticated 2D model at 720+50

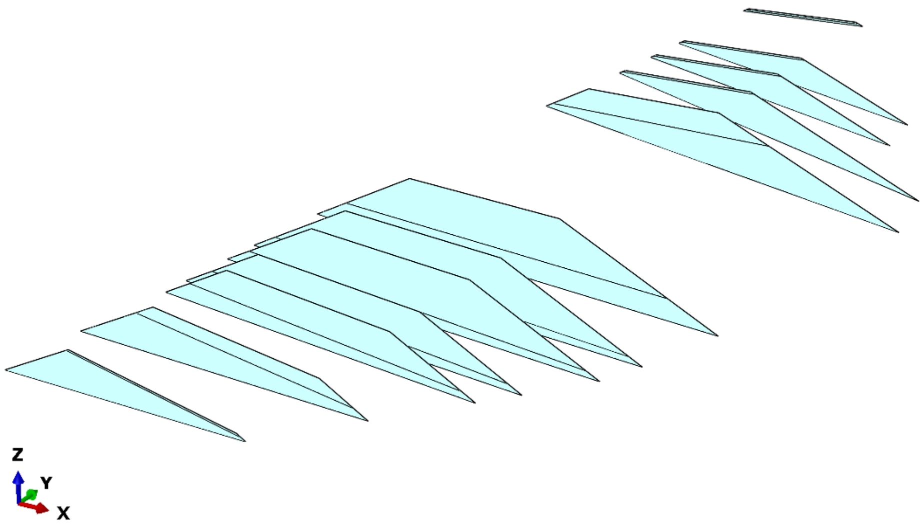

Figure IVb.8 – All twelve control faces in constructing the three-dimensional layered model

Summarized from the two cross sections (based on the second fact above), there are basically two parts to fill the valley and construct the embankment. First, clayey silt (a-7-6) was placed on the bottom to construct a platform that is horizontal in the transversal direction in each cross section. Then sandy silt (a-2-5) and lateral gravelly silt (a-4) was arranged on the top of the platform to construct a longitudinally horizontal bed for the highway alignments. The layered 3D model of the embankment consisted of these two portions (Figure IVb.9). The elevation of the platform in each cross section was determined by the average measurement from the two known cross sections, that is, 4-ft above the higher toe of each cross section.

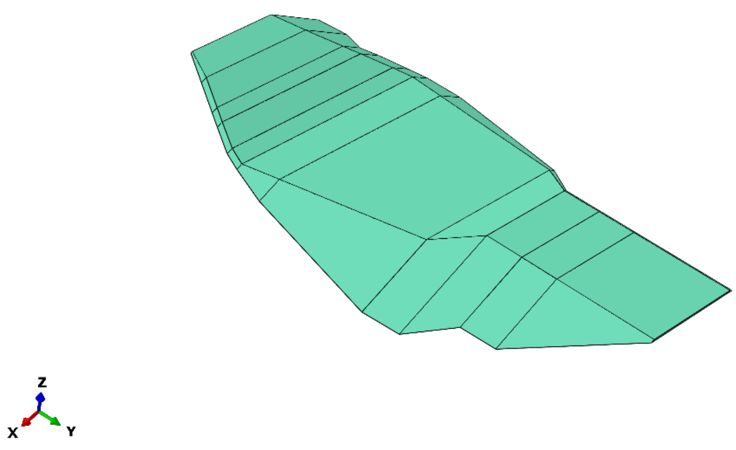

(a) lower part of Embankment #1, clayey silt

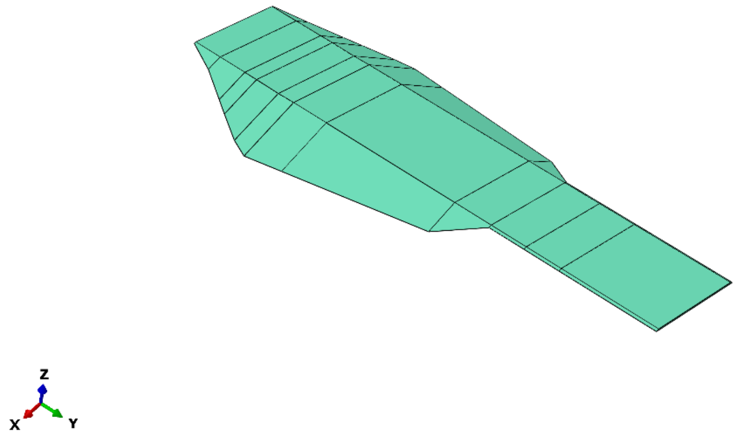

(b) upper part of Embankment #1, combination of clayey gravel and sandy silt

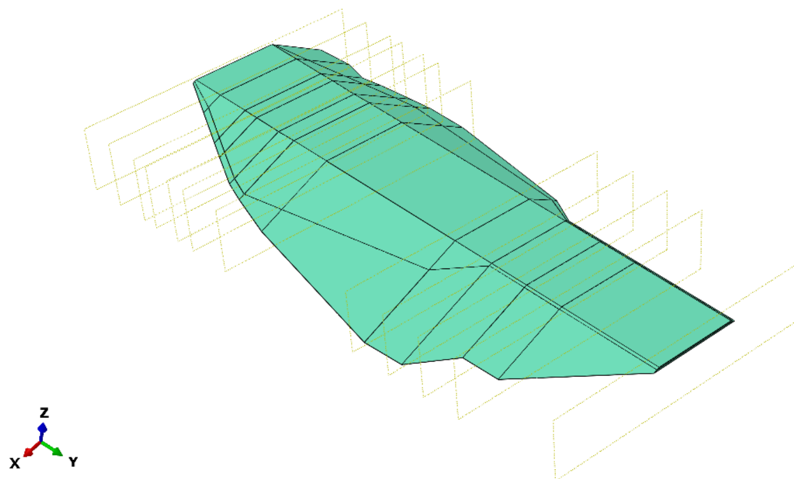

(c) combined layered three-dimensional Embankment #1

Figure IVb.9 – Configuration of three-dimensional Embankment #1 with two layers

The general configuration of the cross section of the embankment made it possible for the layered 3D model implemented in the FEM and will be helpful for the modeling of other embankments on the highway. The overviews of the final layered embankment in three dimensions, and the topography are summarized in Figure IVb.IVb.10.

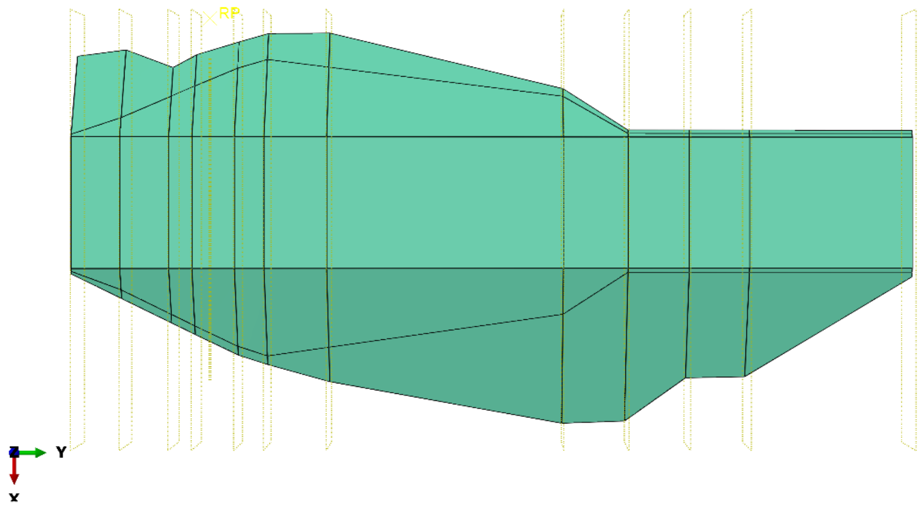

(a) Overview of the layered 3-D model

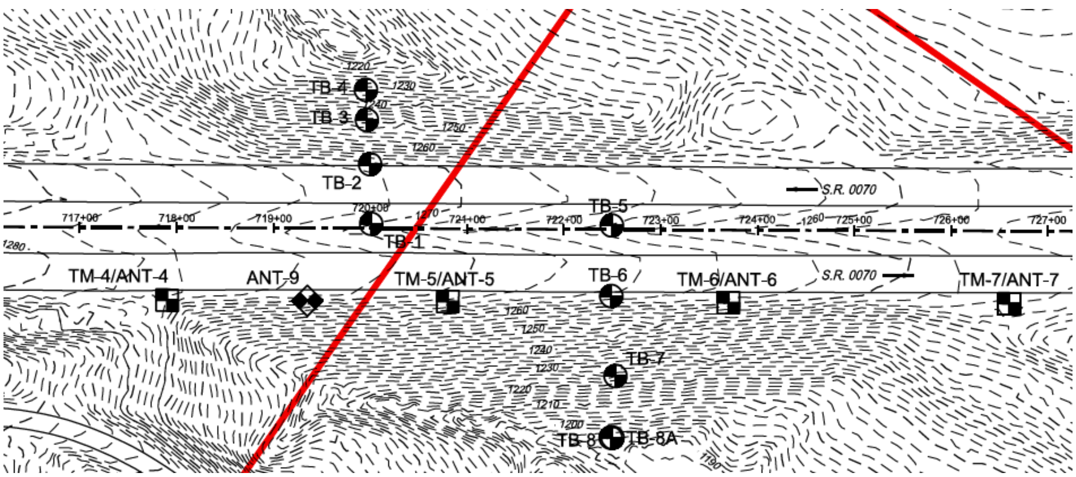

(b) Topography of Embankment #1

Figure IVb.10 – Exhibition of the overview of the (a) layered 3-D model; (b) topography of Embankment #1

3.0 Material Properties

The material properties of soil are obtained from the Consolidated undrained (CU) triaxial tests conducted on Shelby tube soil samples. Figure IVb.11a, b, and c show the locations of these tests. The results of CU triaxial test are summarized in Table IVb.1IVb.1.

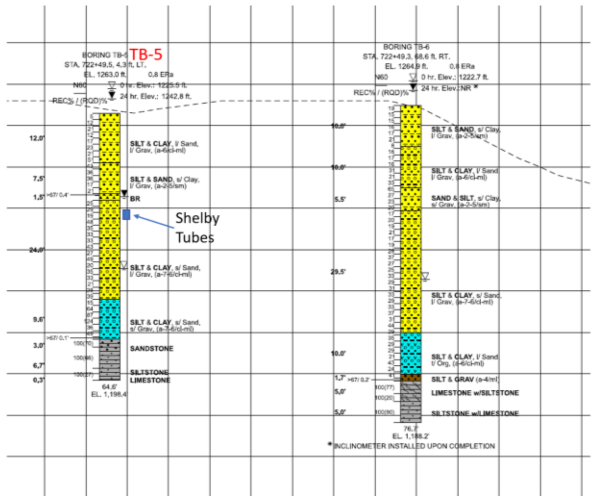

(a) TB-5 @ 720+50

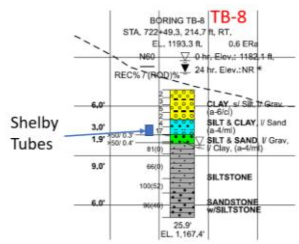

(b) TB-8 @ 720+50

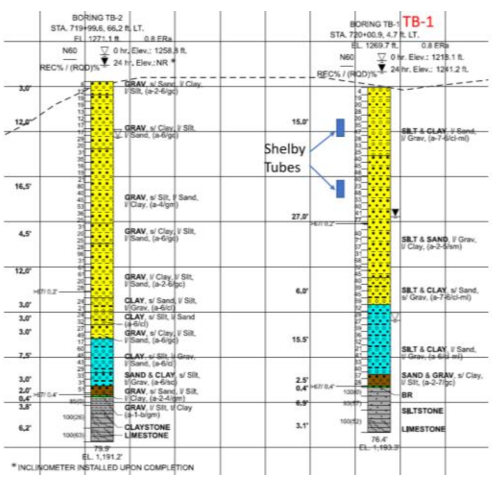

(c) TB-1 @ 720+00

Figure IVb.11 – Locations of Shelby tubes at (a)TB-5, (b)TB-8, and (c)TB-1

Figure IVb.12 indicates that the typical constitutive law of soil in the embankment is elasto-plastic with subtle strain-hardening trend. Data provided in Table IVb.1 indicates the material properties for four representative soil samples utilized in constructing the original embankment. It should be noted that these four samples are located at the top or in the middle depth of the fill or the alluvium (colluvium) located at the base of the Embankment #1. Some differences exist between the layers forming the embankment with respect to their shear strength parameters. These differences will be taken into account when conducting the slope stability analysis.

Table IVb.1 – Summary of laboratory CU triaxial test results from Shelby tubes

	depth(ft)	USCS	AASHTO	γ, pct	ω, pct	ϕ, pct	c, psf
TB1	6.0-11.0	CL	a-6 Fill	115.1	12.8	33.5	28.8
TB1	21-23.6	CL	a-2-5 Fill	98.5	8.6	25.6	633.6
TB5	24.2-26	CL	a-7-6 Fill	118.9	12.2	30.2	72.0
TB8	6.5-8.5	MH	a-7-5 Alluvium	89.2	37.7	23.2	316.8

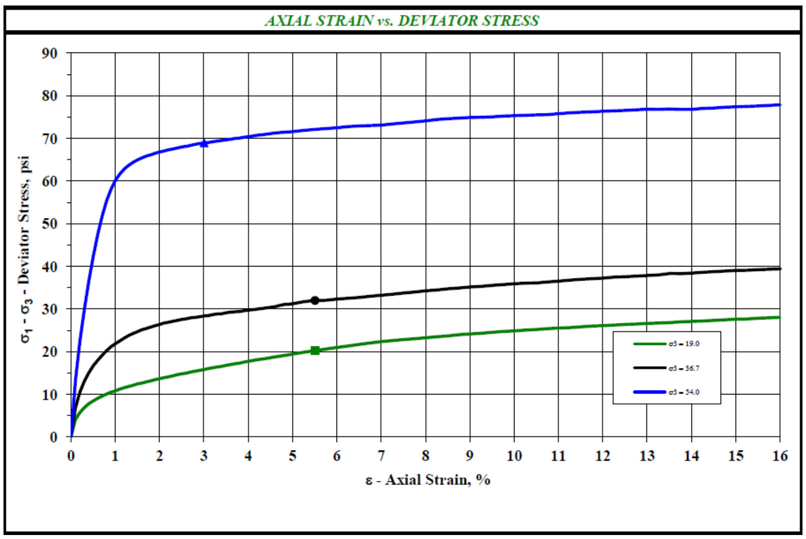

Figure IVb.12 – Stress strain relationship of soil sample in Embankment #1 from laboratory results

The young's modulus is calculated as (Briaud, 2001)

$$E = \frac{\sigma_1 - 2\mu\sigma_3}{\epsilon_f} \qquad \text{[Eq. IV.2]}$$

The bulk unit weight of the soil is obtained considering the average water content of 19.46% obtained from the lab results at TB-1 to TB-8. The results are shown in the following equation as (Wu, 1970)

$$\begin{aligned} \overline{\gamma_{bulk}} &= \overline{\gamma_{dry}}(1 + \overline{w}) \\ &= 95.17(1 + 19.46\%) \\ &= 113.7 - \text{pcf} \end{aligned} \qquad \text{[Eq. IV.3]}$$

The first sample in TB1 represents a soil that can be classified as a-6 in AASHTO classification system and is located at shallow depth. The second sample represents a soil with higher cohesion and lower friction angle which classified by AASHTO as sandy silt (a-2-5). There is a large difference in the shear parameters between of these two materials (Table IVb.1IVb.1).

The other two samples were located at cross section 720+50. One was located in the middle depth of the layer which made up the major part of this cross section, a-7-6 in AASHTO and existed as clayey silt, which is considered to be representative in this kind of material. The last Shelby tube sample was located at the middle level of alluvium. It was indicated that alluvium has rather high cohesion but low friction angle.

The Shelby tube soil samples can represent most types of soil included in the two known cross sections. However, none of them were prepared for testing the gravelly soil located at the lateral parts of Embankment #1 at cross section 720+00 (Figure IVb.13).

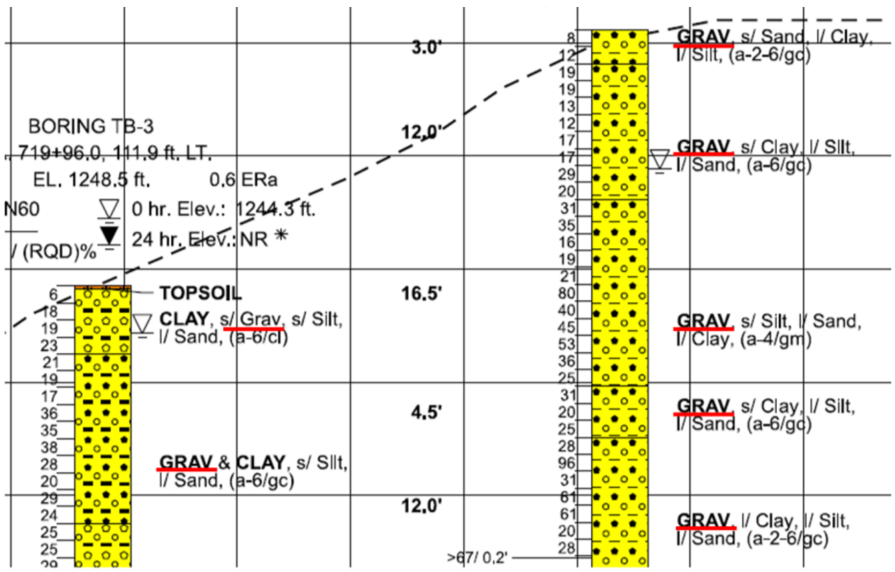

Figure IVb.13 – Clayey/Silty gravel in the lateral region of embankment at cross section 720+00

According to Iannacchione and Vallejo (2000), such mixture of soil and rock fragments induced increases in friction angle and decrease in cohesion when the ratio of rock fragments in the mixture rises. The material properties of the material in this portion can be determined from the shear strength data for a sandy clay - gravel mixture (Figure IVb.IVb.14). The friction angle increased from 34 to 36-deg as the gravel concentration ratio rises from 20 to 40-pct. This variation can be utilized to determine the friction angle of the clayey gravel in the lateral parts.

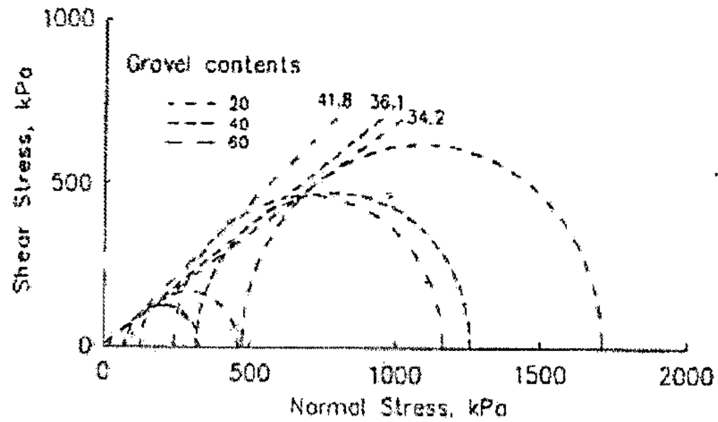

Figure IVb.14 – Variation of shear strength of sandy clay gravels with changes of rock ratios. Graph from Iannacchione and Vallejo, 2000. (Data from Donaghe and Torrey, 1979)

As has already been stated, the friction angle of silt and clay in Shelby tube TB1 at a depth of 6 to 10-ft was 34-deg from laboratory results. The shear parameters of gravel soil were determined based on this material using the variation of friction angle (Figure IVb.IVb.14). The gravel ratio in these two types of material increased from 18 to 42-pct (from laboratory tests), which is almost exactly identical to the gravel content growth (20 to 40-pct) in Figure IVb.IVb.14. The resulting shear strength parameters for different soil types are summarized in Table IVb.2. In the resulting 3D model, the material properties of the upper layer are taken as the average of the corresponding parts in the regions, shown in Table IVb.3.

Table IVb.2 – Summary of soil properties in different layers in cross sections

Layer name	**Soil name**	**AASHTO**	**Approximate Depth, ft**	**C, psf**	**ϕ, deg**
Fill:	Clayey silt	a-6	0-10	100	34
	Clayey silt	a-6	10-20	120	34
Upper	Gravelly clay	a-6	0-40	80	36
	Sandy silt	a-2-5	20-30	634	25.6
	Sandy silt	a-2-5	30-40	734	25.6
Lower	Clayey silt	a-7-6	30-60	180	36
Alluvium	Clayey silt	a-7-6/a-6	55-65	317	28
Gravel	Silty gravel	a-4	65-70	200	37

Table IVb.3 – Summary of soil properties in the simplified three-dimensional model

Layer name	Soil name	AASHTO	Approximate Depth, ft	C, psf	Φ, deg	E, psf
Upper	Sandy silt/ Clayey Silt/ Gravelly clay	a-2-5/a-6	0-40	377	30	1,315,784
Lower	Clayey silt	a-7-6	30-60	180	36	1,106,929

4.0 Shear Strength Reduction Method (SRM)

4.1 Introduction to SRM

Shear strength reduction method (SRM) has been widely utilized in the slope stability analysis, initially developed by Zienkiewicz et al., 1975. Further improvements of the method were provided by other researchers (Matsui and San, 1992; Dawson et al.,1999; Griffiths and Lane, 1999; Zheng et al., 2005).

In the conventional slope stability analysis using limit equilibrium method (LEM), the critical slip surface was needed to be determined. The factor of safety in the conventional method is defined as the ratio of shear strength to the inducing shear stress along the potential slip surface. When using the finite element method (FEM), there is no need to define the slip surface in advance and the stress-strain relationship of soil in the slope is considered. However, it is difficult to trace the failure slip surface in a slope based on certain stress failure criterion and it is difficult to derive an equivalent factor of safety. This has been solved using SRM technique. Griffith and Lane have suggested that the widespread use of SRM should be seriously taken into consideration as a powerful alternate method to the traditional limit equilibrium method.

Centrifuge tests have indicated that the plastic shear strain zone in unstable slopes coincided with the rupture surface (Roscoe, 1970). In other words, the development of plastic shear strain reflected the potential failure and the stability of the slope was dependent on the shear strength of the soil in the slope. The SRM can be applied to see in which part of the slope the plastic strain will develop and how the slope fails.

On one hand, the SRM associated with FEM has the following advantages: a) The final result of shear strain will show the critical failure surface in the slope under gravity and with strength reduction; b) The interslice shear force assumption is not needed in this method; c) it is applicable to many complicated cases and can give the stresses and movements that the traditional LEM cannot provide. On the other hand, the method has disadvantage of the long time needed to set up the computer model and perform the analysis. However, as the development of commercial computer software, this is no longer a problem.

In the SMR, in order to obtain the factor of safety (FS) equivalent to LEM, the strength reduction factor is utilized (Ho, 2017). The factor is employed to reduce the cohesion (c) and tanϕ until the slope fails. The original shear strength parameters are divided with this factor to obtain the reduced shear strength parameters c_r and ϕ_r as

$$c_r = \frac{c}{SRF}, \tan \phi_r = \frac{\tan \phi}{SRF} \qquad \text{[Eq. IVb.4]}$$

where c and ϕ are the shear strength parameters, cohesion and friction angle, R the shear strength reduction factor.

The critical shear strength reduction ratio is the shear strength reduction ratio when the slope fails with the reduced strength parameters. The critical value of the ratio is approximately consistent with the factor of safety using Bishop's limit equilibrium method. The failure pattern can be traced from the shear strain development.

4.2 Validation Test of SRM

A typical slope stability test of a uniform soil slope has been utilized for the verification test of the shear strength reduction method. The results were compared to the closed form solution given by Dawson, 1999. The soil density was taken as 1,250-psf. The cohesion is 258-psf. Friction angle is 20-deg. The factor of safety (FS) of this slope is equal to one using the limit equilibrium method. Three element strategies are compared in this validation test, triangular, quadrilateral, and quadrilateral – dominated, shown in Figure IVb.15.

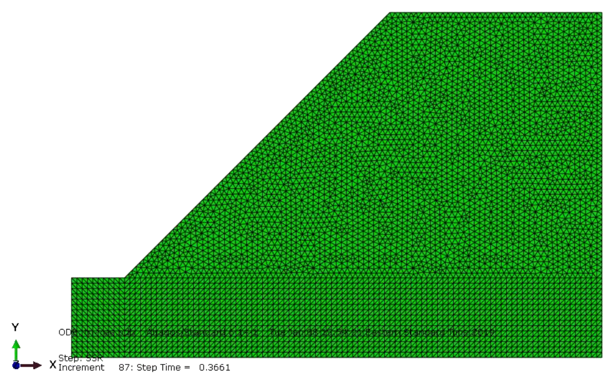

(a) triangular

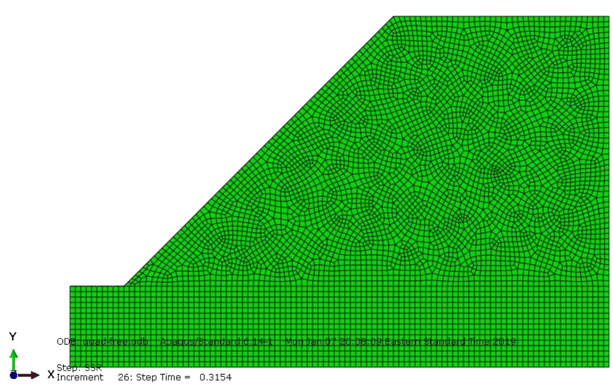

(b) quadrilateral

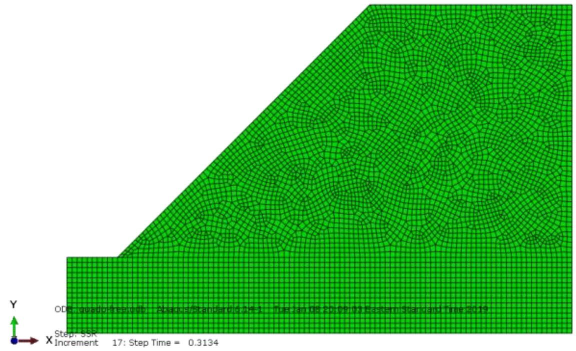

(c) quadrilateral-dominated

Figure IVb.15 – Three types of mesh available to model slope stability

The resulted shear band (plastic zone) of each test is shown in Figure IVb.16. It can be seen that both quadrilateral and quadrilateral – dominated mesh types presented a reasonable shear band.

Figure IVb.17 indicates that the factor of safety given by SRM was close to the closed form solution by limit equilibrium method. It was determined that quadrilateral-dominated was the most appropriate mesh strategy that was closest to the theoretical solution.

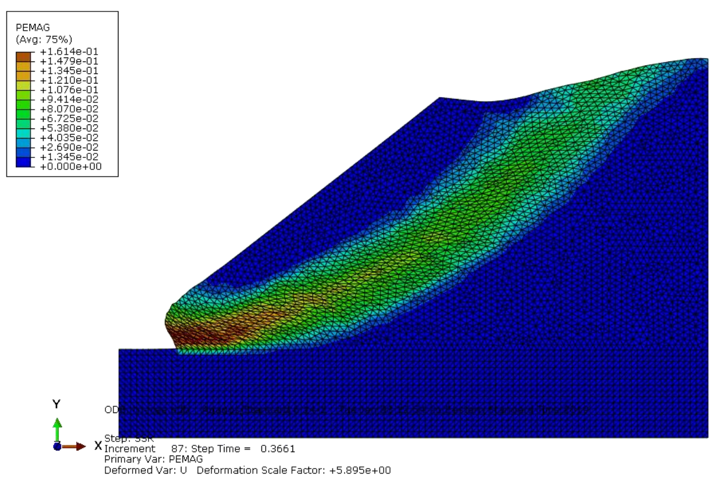

(a) triangular

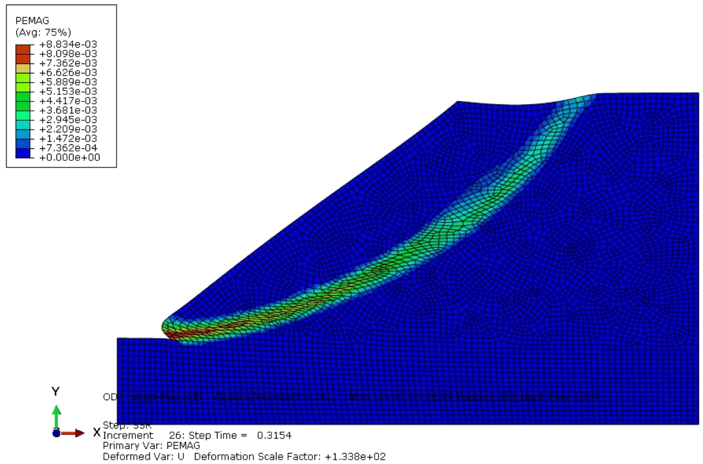

(b) quadrilateral

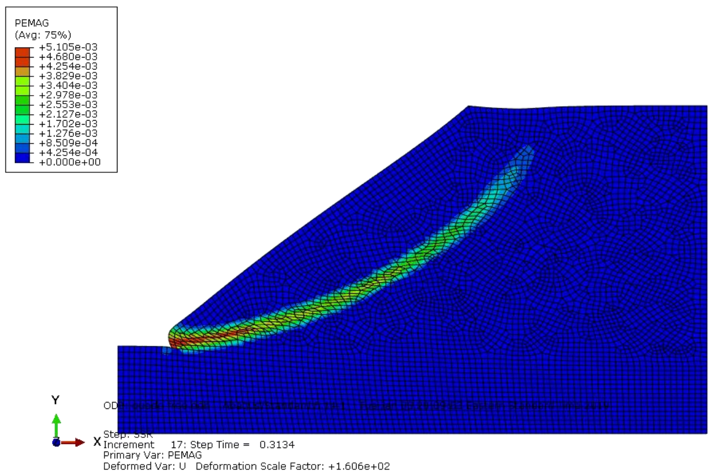

(c) quadrilateral – dominated

Figure IVb.16 – Comparison of three types of mesh in the resulted shear band in slope stability test

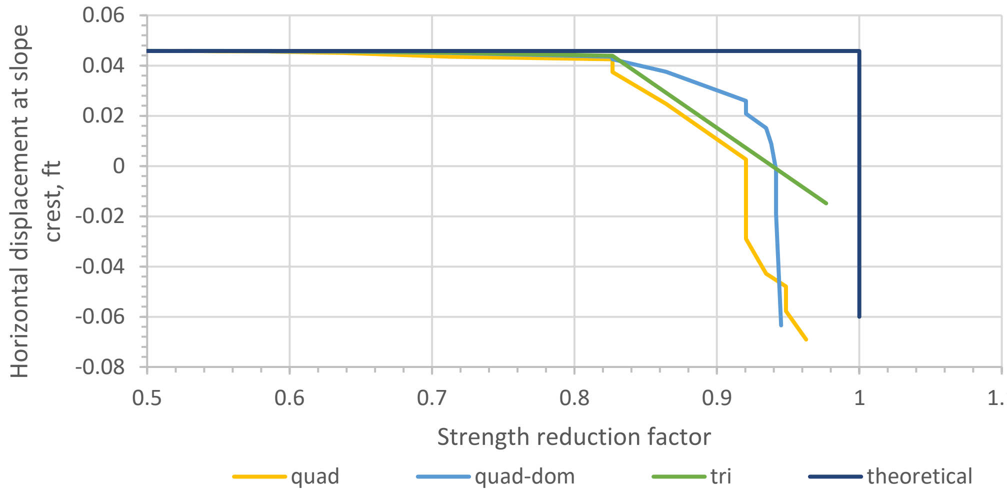

Figure IVb.17 – Comparison of three types of mesh in determining the factor of safety

In conclusion, quadrilateral and quadrilateral-dominated mesh types were more accurate in shear strength reduction test than triangular mesh.

5.0 Mesh Refinement Tests

5.1 <u>2D Convergence Test</u>

Experiments were performed to test for the most appropriate FEM model mesh type and size. Proper mesh selection increases the FEM model accuracy and lowers run time costs. Four sizes were evaluated, i.e. grid size of 6, 3, 1.5 and 0.75-ft. The maximum stress in vertical direction with four mesh sizes are shown in Figure IVb.18a to d and summarized in Table IVb.4. These experiments indicated that a mesh with size 1.5 and 0.75 are most appropriate for 2D analysis.

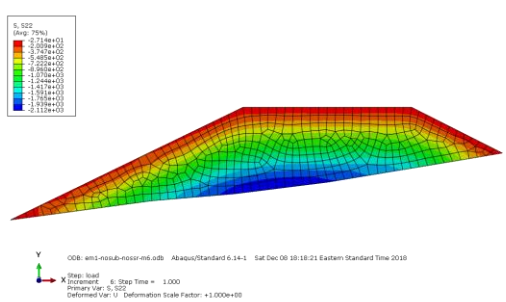

(a) mesh size = 6

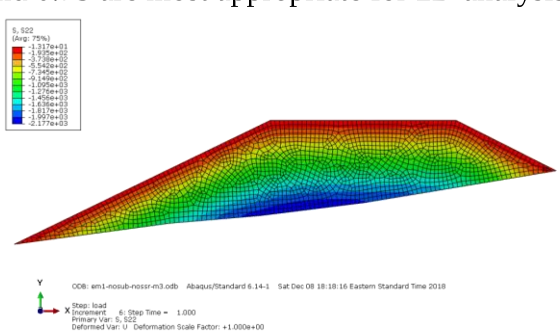

(b) mesh size = 3

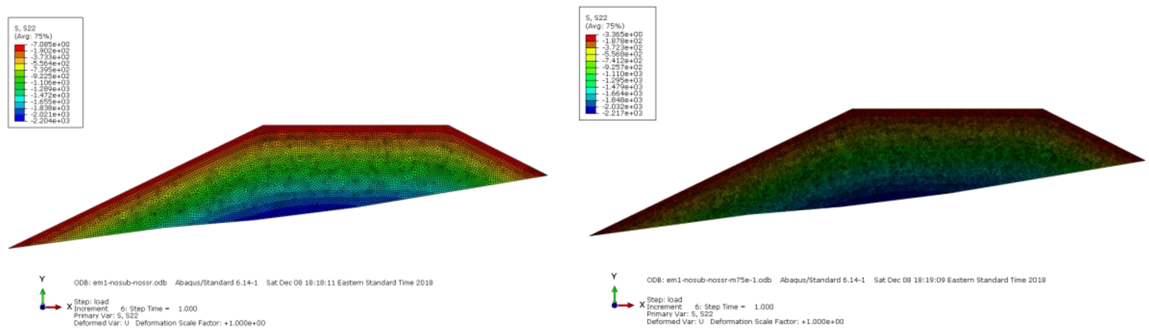

(c) mesh size = 1.5 *(d) mesh size* = 0.75

Figure IVb.18 – σ_{yy} contour with different mesh sizes of (a) 6-ft; (b) 3-ft; (c) 1.5-ft; (d) 0.75-ft

Table IVb.4 – Mesh refinement results

Mesh size, ft	**Maximum σ_{yy} (compression), psf**	**Difference**
6	-2110	3.175E-02
3	-2177	1.240E-02
1.5	-2204	5.898E-03
0.75	-2217	

5.2 3D Convergence Test

Experiments were performed to test for the most appropriate FE model mesh size. Three mesh sizes are evaluated, i.e., 16, 12, and 8-ft. The maximum vertical stress with three mesh sizes are shown in Figure IVb.19a to c and summarized in Table IVb.5. These experiments indicated that the test of a three-dimensional embankment converges at a mesh size of 12-ft. But in order to obtain more detailed results, 8-ft might be the most appropriate mesh size for this test.

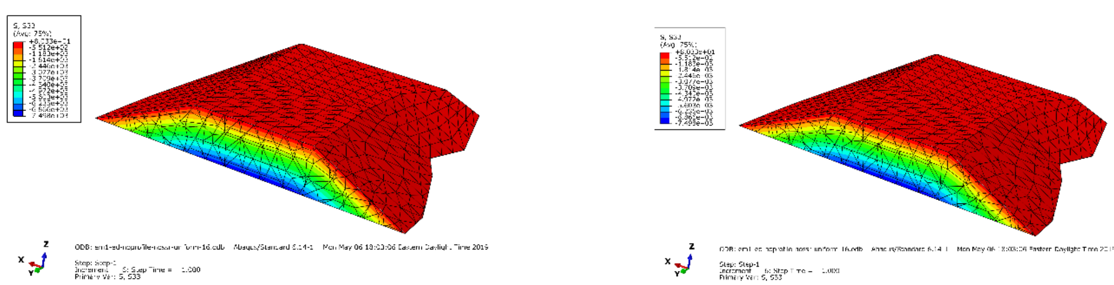

(a) Mesh size = 16 *(b) Mesh size* = 12

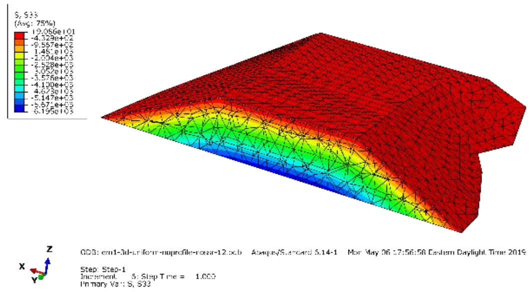

(c) *Mesh size* = 8

Figure IVb.19 – σ_{zz} *contour with different mesh sizes of (a) 16-ft; (b) 12-ft; (c) 8-ft*

Table IVb.5 – Mesh refinement results

Mesh size, ft	Maximum σ_{zz} (compression), psf	Difference, pct
16	7498	17.4
12	6195	0.04%
8	6192	

6.0 Analysis

This section consists of two parts including the results from the two-dimensional as well as three-dimensional model. Two tests were conducted on each model. First, normal tests were conducted to analyze the stress and strain field in the embankment. Second, slope stability analysis was carried out using shear strength reduction method (SRM). In the shear strength reduction test, the university analyzed the initial slope stability of the embankment under gravity before the longwall mining subsidence happens. The university figured out a method to obtain the factor of safety of the embankment. The university also made the contour of the plastic strain which induced the shear failure in the slope to predict the potential rupture surface in the embankment. In this way, it is possible to predict which part of the slope was more dangerous and how the embankment failed when the shear strength was reduced.

6.1 Analysis of Embankment #11 before Mining in 2D

6.1.1 *Normal Test without Shear Strength Reduction*

Normal stress in horizontal direction (σ_{xx}), vertical direction (σ_{yy}) and shear stress (σ_{xy}) contour at two cross sections 720+50 and 720+00 are shown in Figure IVb.20a to c and Figure IVb.21a to c, respectively.

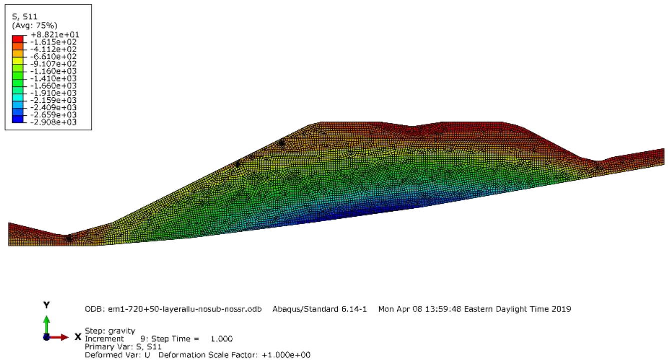

(a) σ_{xx}

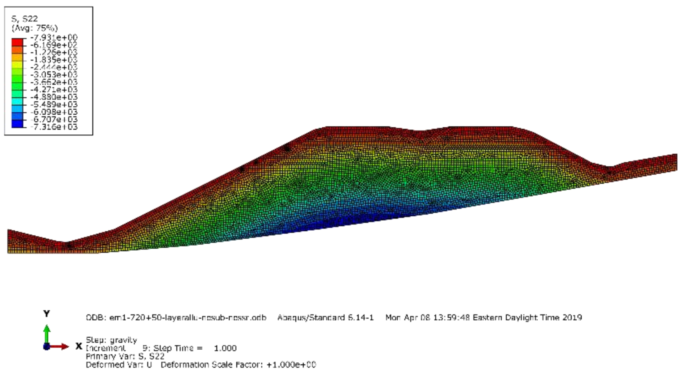

(b) σ_{yy}

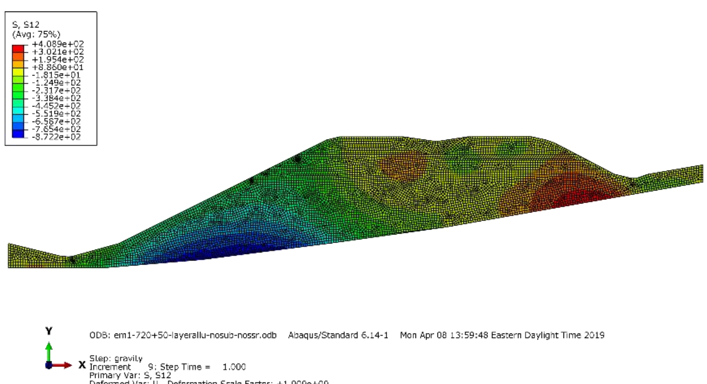

(c) σ_{xy}

Figure IVb.20 – Stress (a) σ_{xx}; (b) σ_{yy}; (c) σ_{xy} due to gravity at cross section 720+50

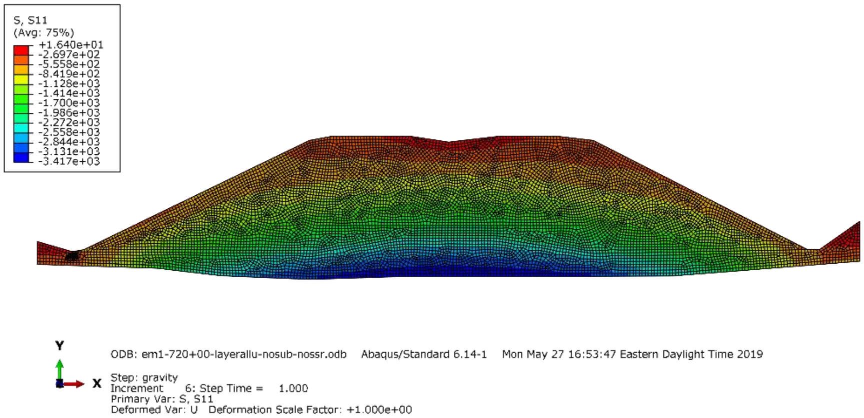

(a) σ_{xx}

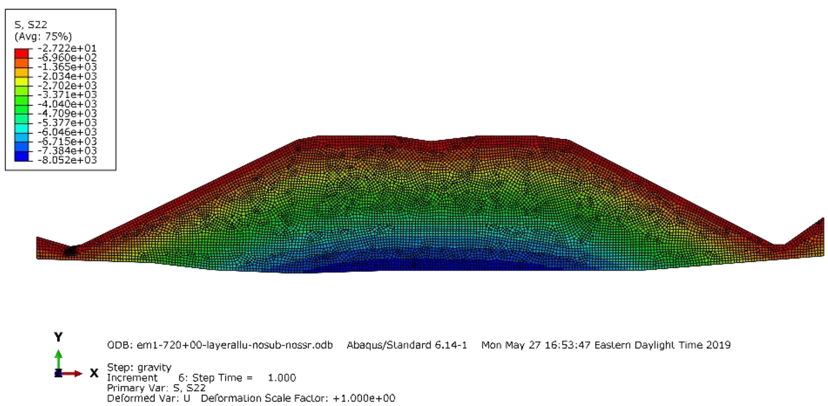

(a) σ_{yy}

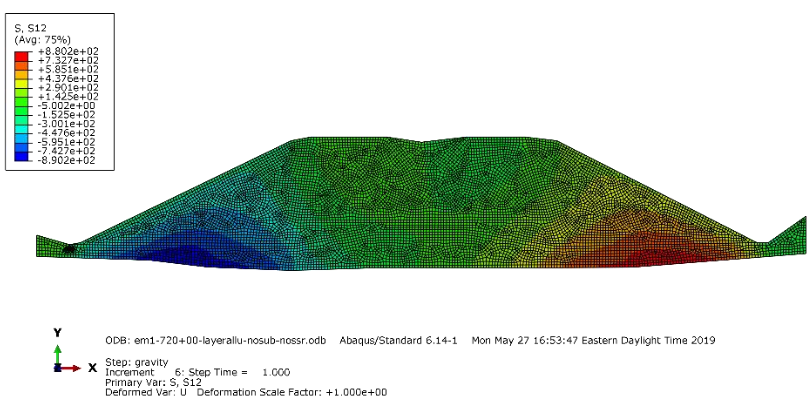

(a) σ_{xy}

Figure IVb.21 – Stress (a) σ_{xx}; *(b)* σ_{yy}; *(c)* σ_{xy} *due to gravity at cross section 720+00*

Horizontal normal stress is plotted on the surface of the embankment from the left toe to the right toe, including the north face, top face, and the south face, at cross sections 720+50 and 720+00 shown in Figure IVb.22a and b, respectively. At cross section 720+50, north part of top face is in tension, as well as the crest of the north face, which indicates that this part of road has potential of existence of crack. Compression reaches the largest value in the middle of the south slope. At cross section 720+00, the stress contour was symmetric due to the geometry of the embankment at this location. The stress reached highest magnitude of tension in the middle of the top face.

(a) 720+50

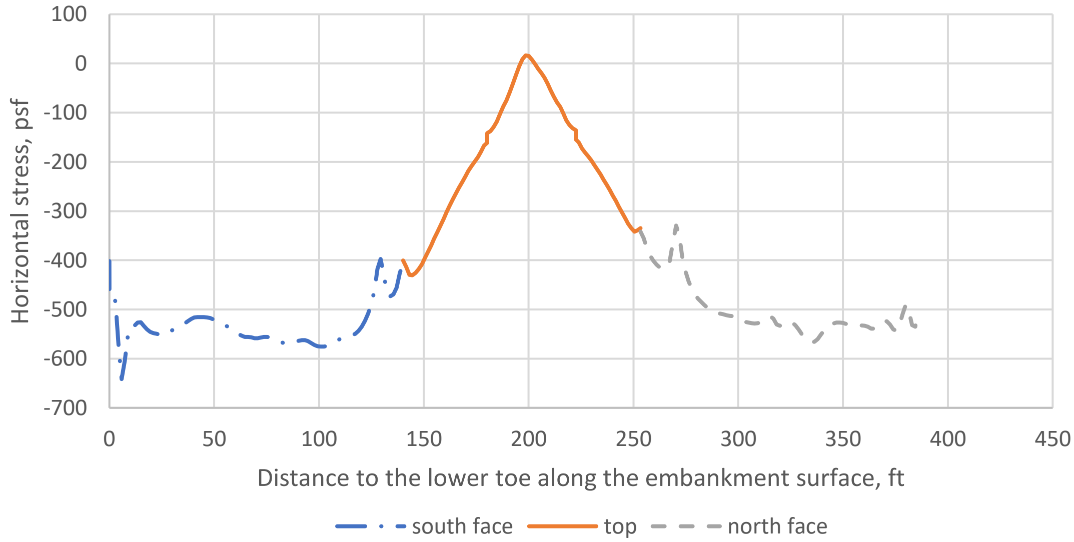

(b) 720+00

Figure IVb.22 – Horizontal stress perpendicular to the direction of highway along the surface of the cross section (a) 720+50 and (b) 720+0

Normal strain in horizontal direction (ϵ_{xx}), normal strain in vertical direction (ϵ_{yy}) and shear strain (ϵ_{xy}) contour at cross sections 720+50 and 720+00 are shown in Figure IVb.23a to c and Figure IVb.24a to c, respectively. These figures show that two zones under the left and right crest of the embankment are in high tension strain compared to other zones.

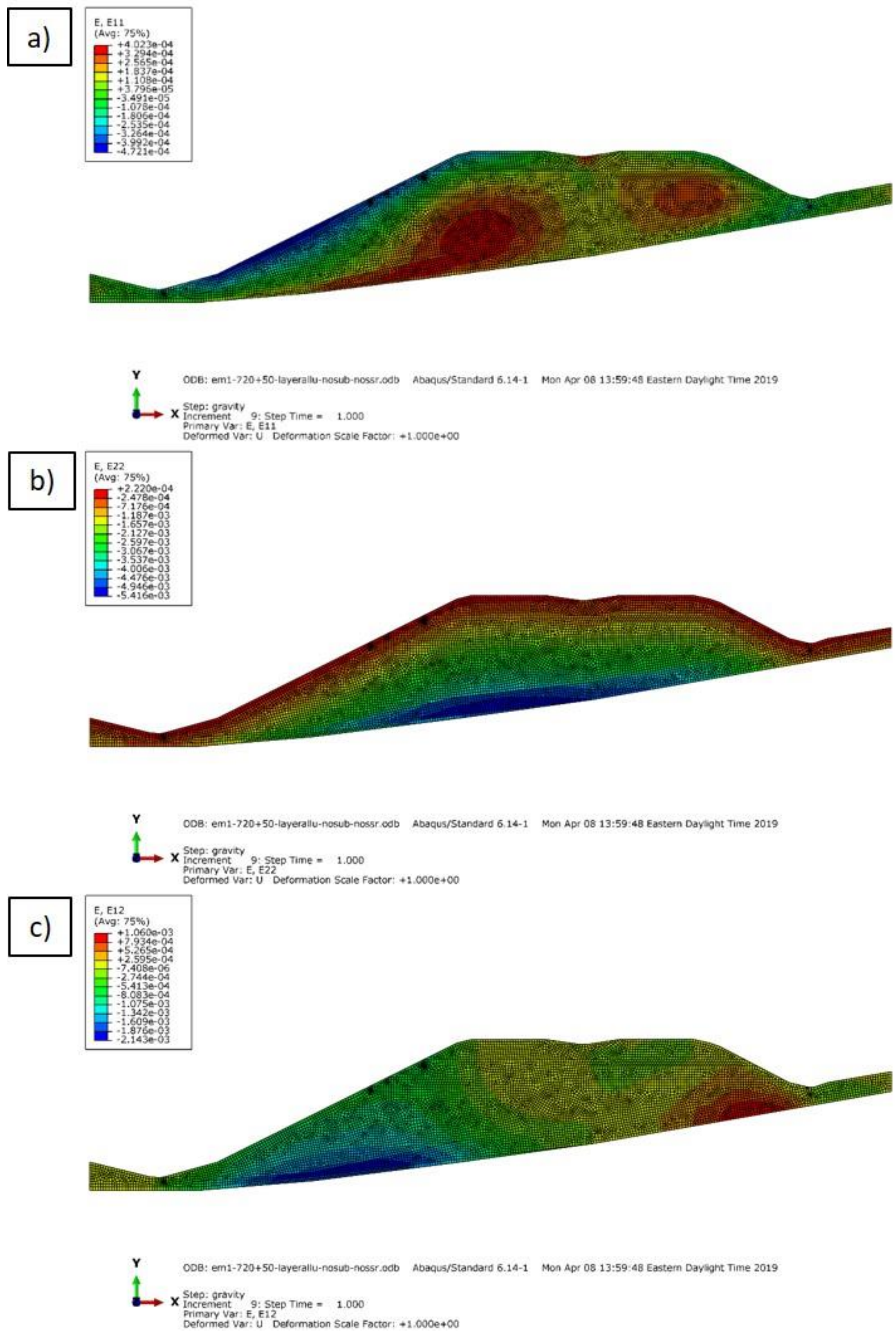

Figure IVb.23 – Strain (a) ϵ_{xx}; (b) ϵ_{yy} ; (c) ϵ_{xy} at cross section 720+50 due to gravity

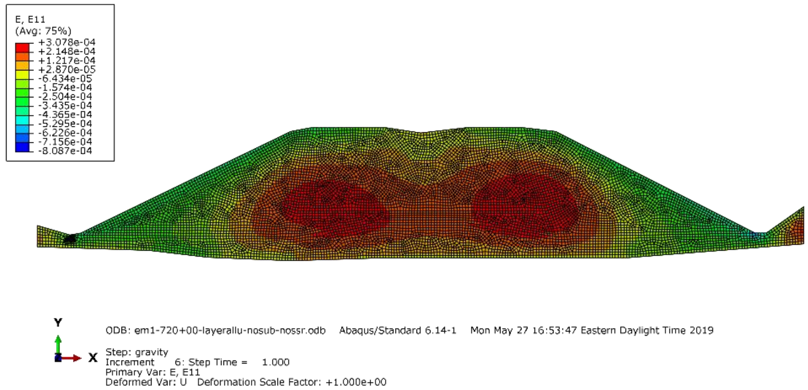

(a) ϵ_{xx}

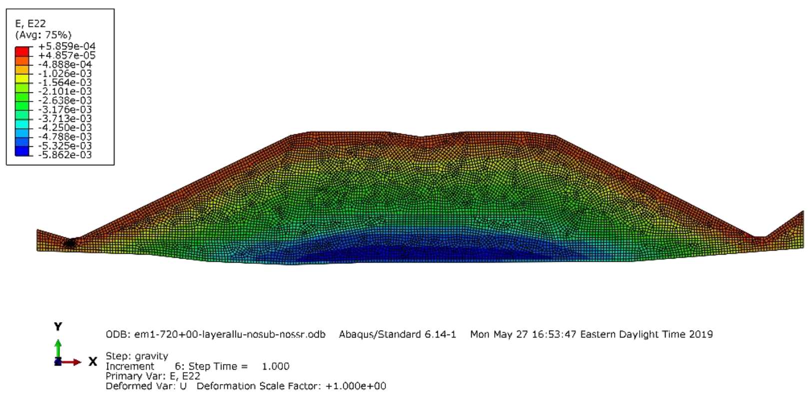

(a) ϵ_{yy}

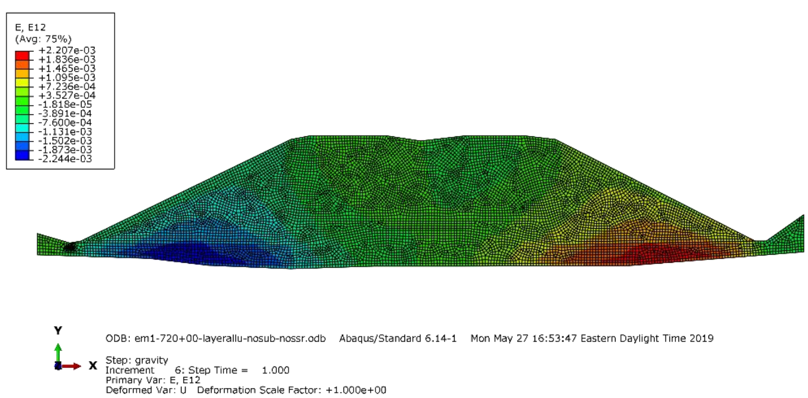

(a) ϵ_{xy}

Figure IVb.24 – Strain contour of (a) ϵ_{xx}*; (b)* ϵ_{yy} *and (c)* ϵ_{xy} *due to gravity at cross section 720+00*

Horizontal normal strain is plotted on the surface of the embankment at cross sections 720+50 and 720+00 from the left toe to the right toe shown in Figure IV.25a and b. At cross section 720+50, north part of the top face was in tension, as well as the crest of the north slope. Compressive strain reached the largest value in the middle of the south slope. Tensile strain was largest in the middle of the top surface, although the magnitude was in a rather small range. At cross section 720+00, the strain contour was similar to the stress contour.

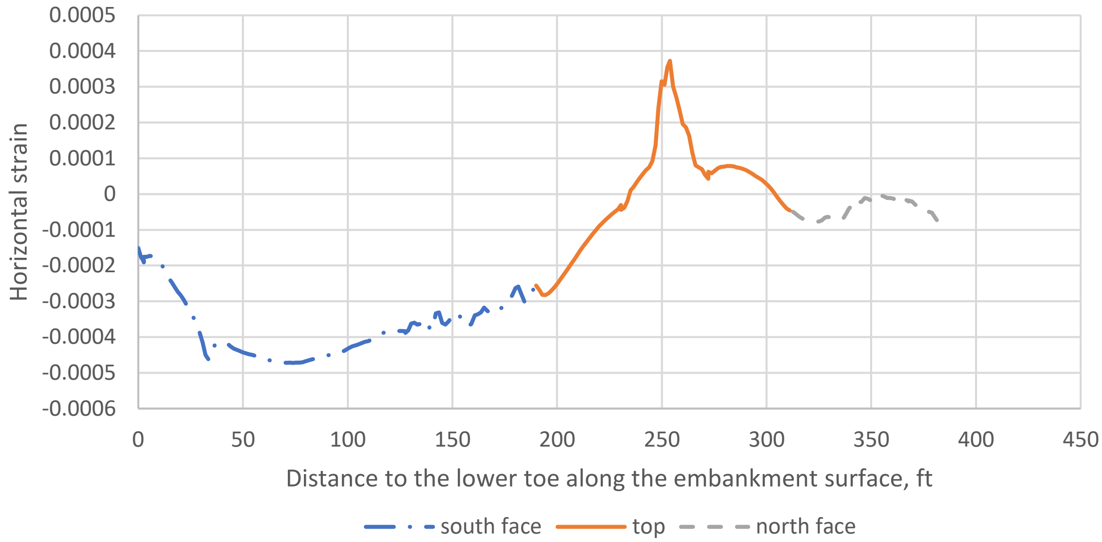

(a) 720+50

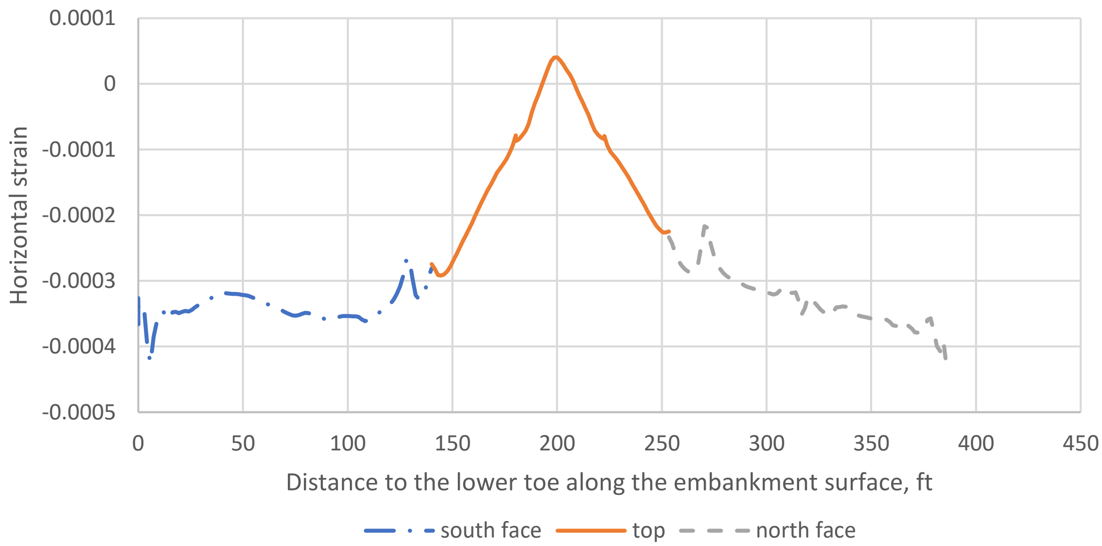

(b) 720+00

Figure IVb.25 – Horizontal strain perpendicular to the direction of highway along the surface of the cross section (a) 720+50 and (b) 720+00

Displacement in the horizontal direction (u_x), Displacement in the vertical direction (u_y) and the total displacement (u_t) contour at cross sections 720+50 and 720+00 are shown in Figure IVb.26a to c and Figure IVb.27a to c. At cross section 720+50, the horizontal displacement in the embankment is larger in the south slope compared to the north slope.

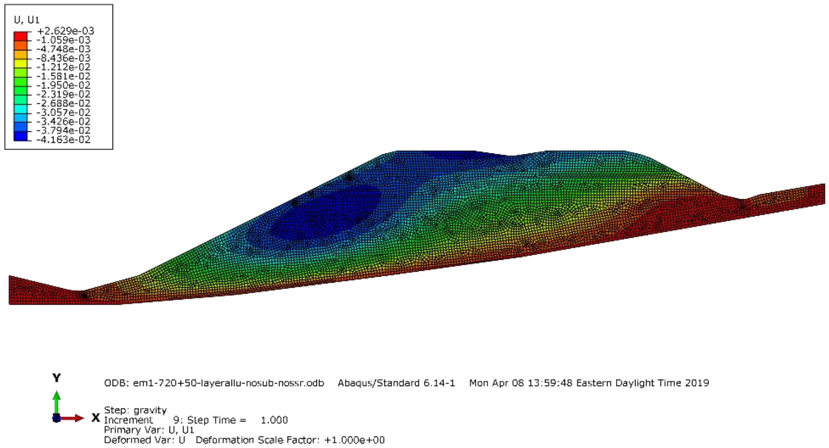

(a) u_x

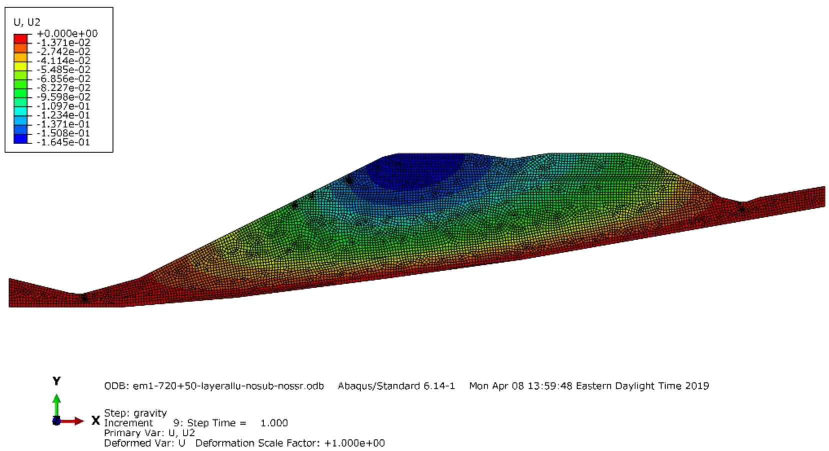

(b) u_y

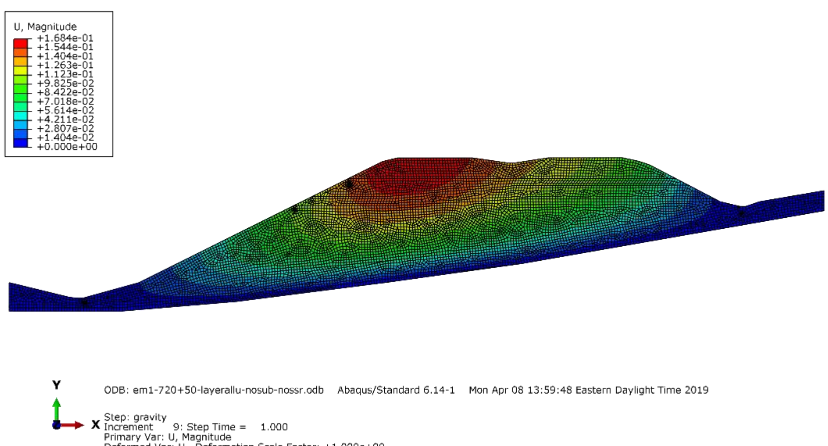

(c) u_t

Figure IVb.26 – Displacement contour of (a) u_x*; (b)* u_y *and (c)* u_t *at cross section 720+50 due to gravity*

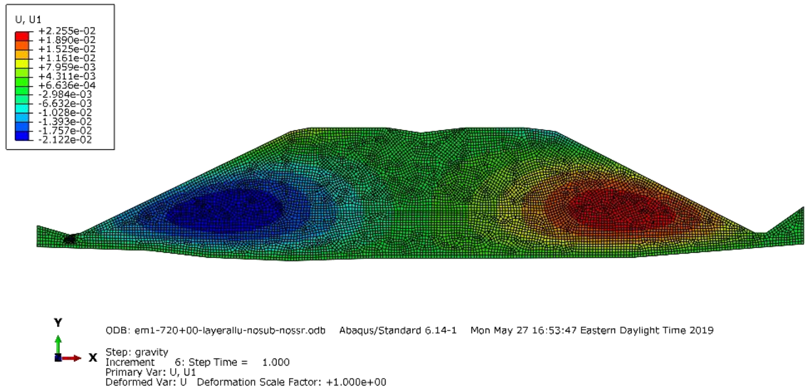

(a) u_x

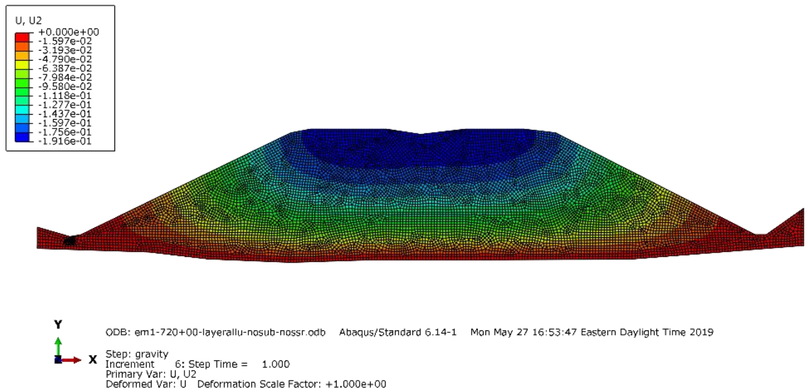

(a) u_y

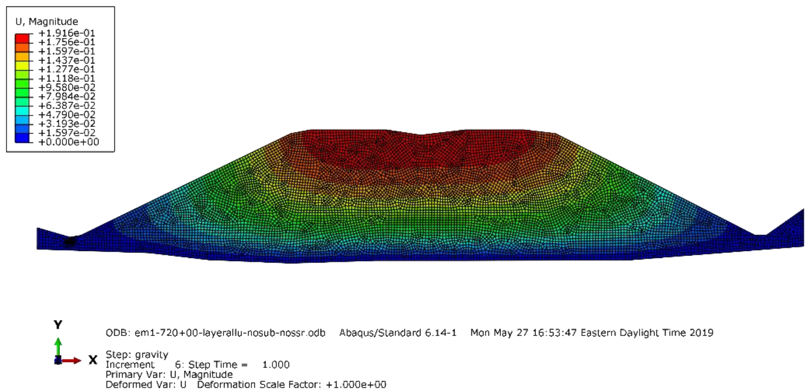

(a) u_t

Figure IVb.27 – Displacement contour of (a) u_x; (b) u_y and (c) u_t due to gravity at cross section 720+00

As shown in Figure IVb.28a and b, the horizontal displacement is plotted along the surface of the embankment at cross sections 720+50 and 720+00. At cross section 720+50, it was comparatively large from the south crest to the north crest. It reached the maximum value, albeit small, at the middle of the top face. At cross section 720+00, the magnitude of the displacement in the north-facing slope is symmetric to that in the south-facing slope, but the direction is opposite.

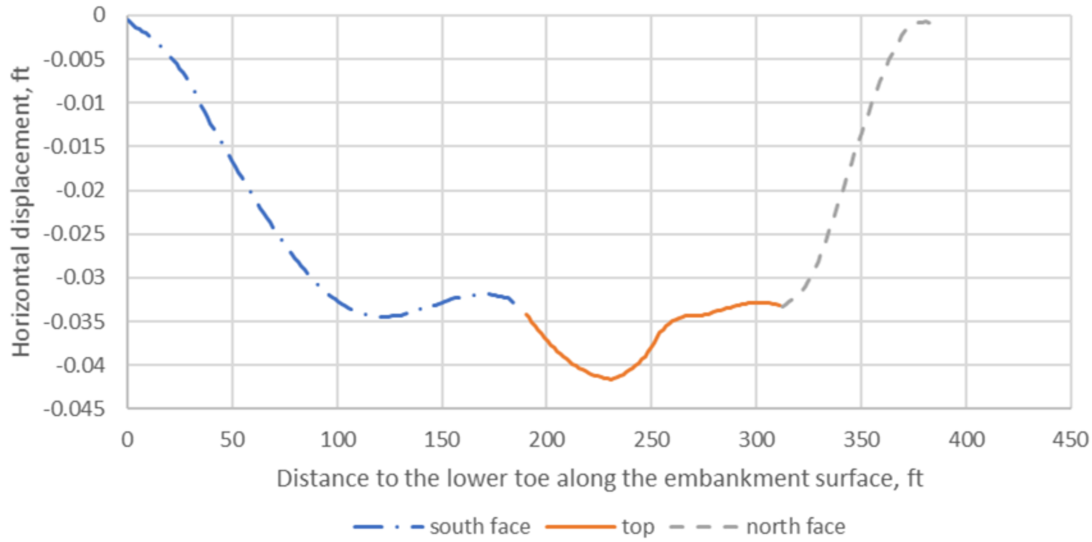

(a) 720+50

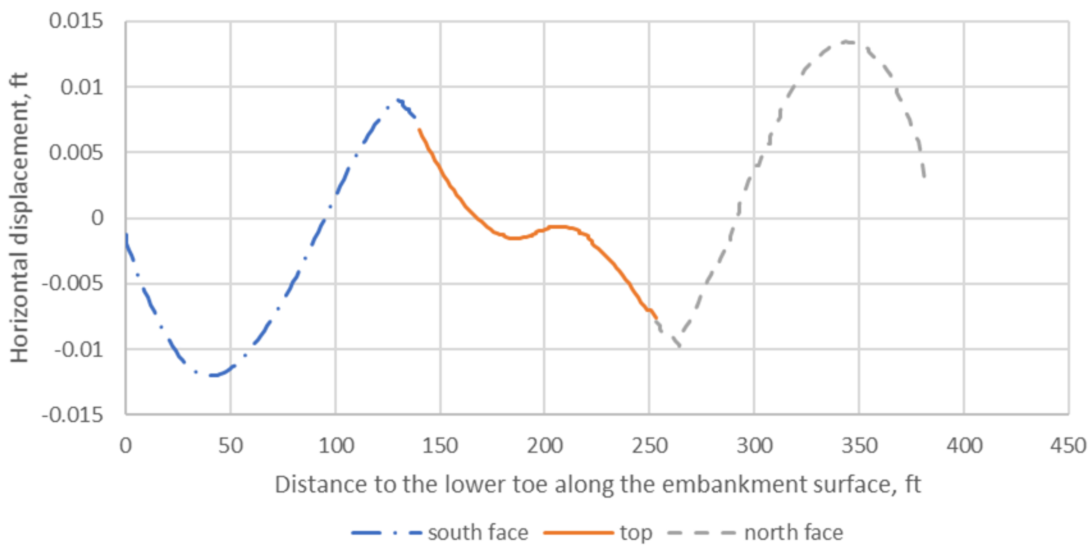

(b) 720+00

Figure IVb.28 – Horizontal displacement perpendicular to the direction of highway along the surface of the cross section (a) 720+50 and (b) 720+00

Figure IVb.29 indicates the directions of the total movement within the embankment at two cross sections before mining. Though the magnitude was rather small, these plots indicate the direction the embankment would tend to move with no failure in the embankment before mining.

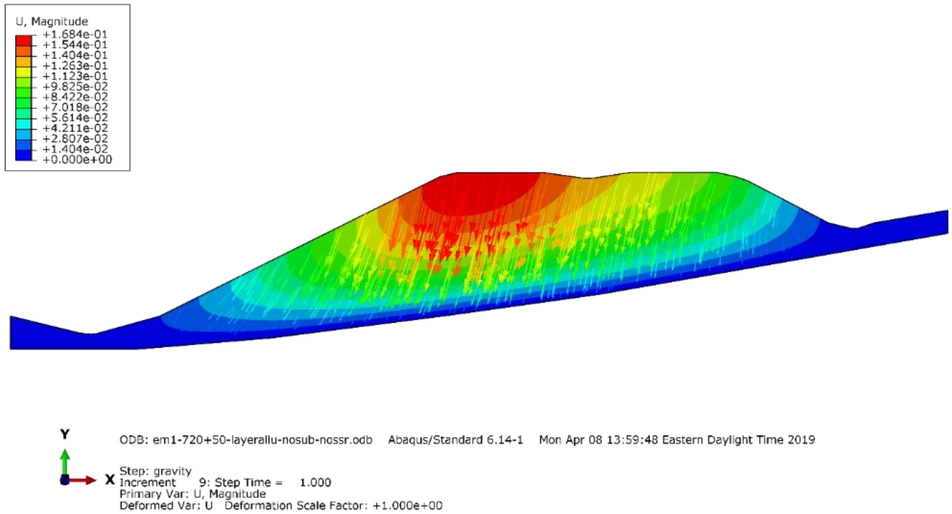

(a) 720+50

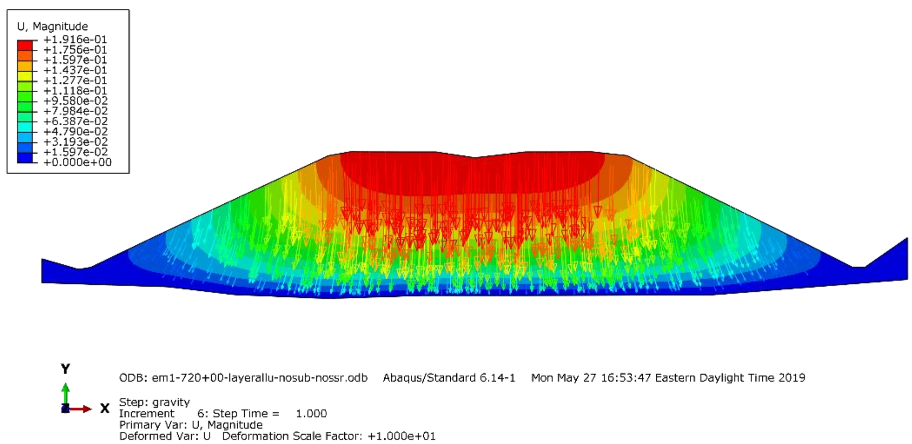

(b) 720+00

Figure IVb.29 – Directions of total displacement in the embankment due to gravity at cross section (a) 720+50 and (b) 720+00

6.1.2 *Slope Stability Analysis using the SRM*

Plotting the total displacement at the crest against the shear strength factor, yields a factor of safety for each cross section. For the cross section 720+50 (Figure IVb.30a), the south-facing slope was the more dangerous part according to the total displacement contour. Contrarily, for the cross-section 720+00 (Figure IVb.30b), the total displacement was almost same at two sides. The total displacement began to grow almost simultaneously in both slopes at this cross-section. The factor of safety for cross section 720+50 is 1.31 and 1.27 for cross-section 720+00.

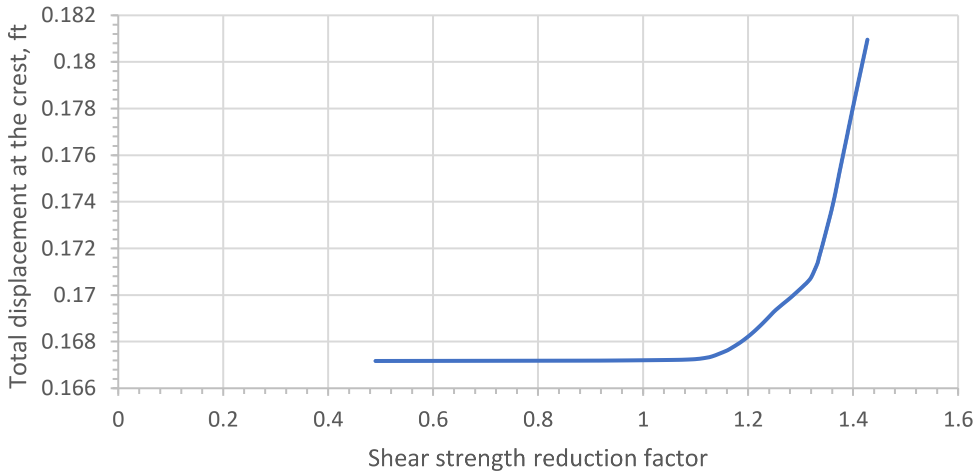

(a) 720+50, Fs = 1.31

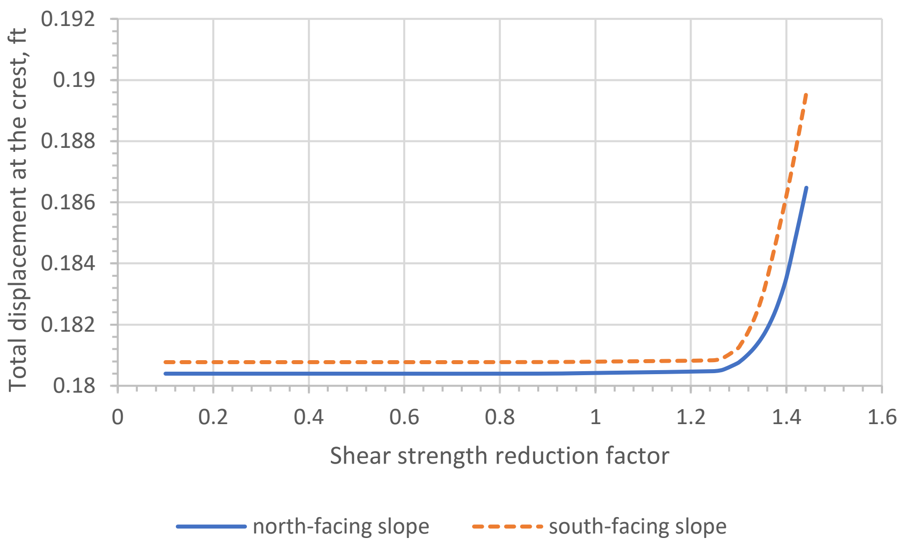

(b) 720+00, Fs = 1.27

Figure IVb.30 – Determination of factor of safety at (a) 720+50 and (b) 720+00 by plotting the total displacement versus the shear strength reduction factor

Total displacement at two cross sections shown in Figure IVb.31a and b show how the embankment may move during failure. At either of these two cross sections, total displacement is higher on the top than on the bottom. At cross section 720+50, the total displacement reaches highest value at the left crest and vertical displacement dominate in the magnitude. While at cross section 720+00, similar displacement are observed on both side due to the symmetric geometry of the embankment at this cross section. By comparing the angle of direction of total displacement with respect to vertical, the ratio of horizontal displacement to the vertical displacement can be analyzed.

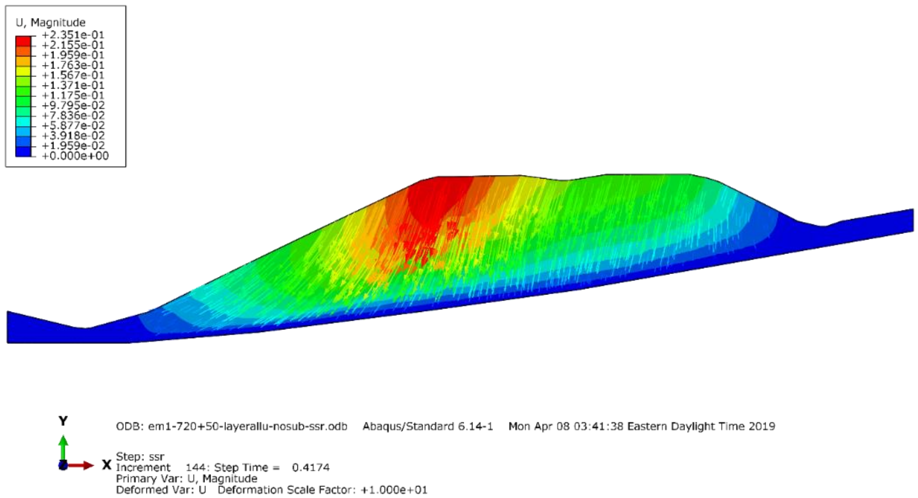

(a) 720+50

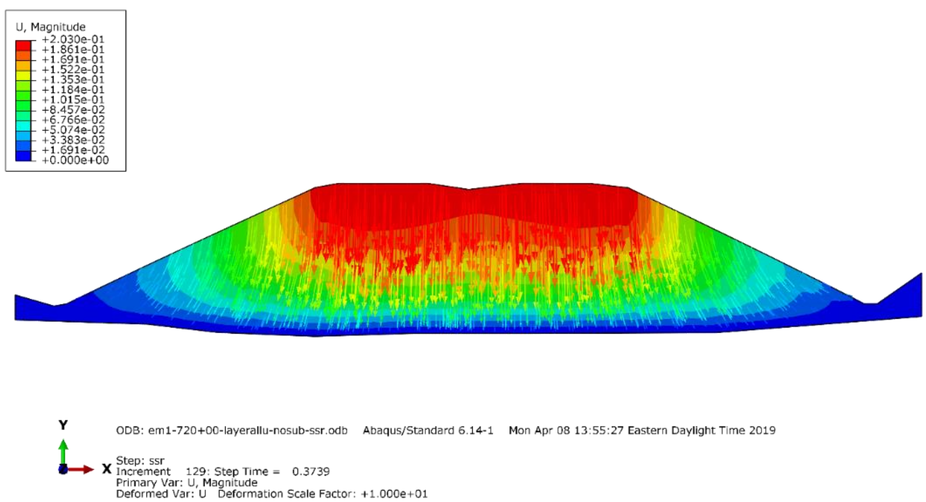

(b) 720+00

Figure IVb.31 – Potential total displacement at failure at cross section (a)720+50 and (b) 720+00 (unit: ft)

The distribution of horizontal displacement at cross section 720+50 and 720+00 is shown in Figure IVb.32a and b. Both cross sections exhibit large deformation at the lower part of the embankment when sliding failure occurs. At cross section 720+50, the horizontal displacement distribution is influenced by the layer of sandy silt (a-2-5), which has higher value of cohesion, on the bottom of the fill. It is indicated that the region of large displacement did not extend to the bottom due to the existence of this layer. At cross section 720+00, the zone of large horizontal displacement located closer to the bottom. The soil stopped showing large displacement before touching the bottom due to the existence of a thin layer of gravelly sand located on the bottom of the embankment.

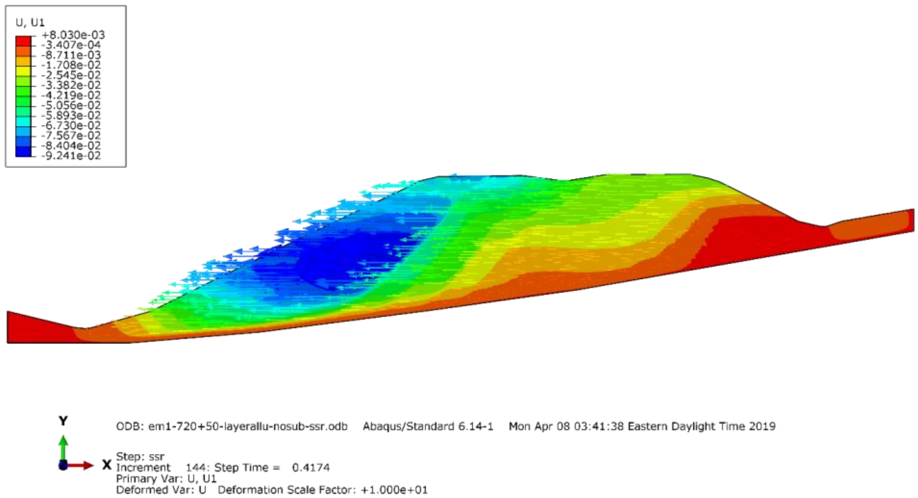

(a) 720+50

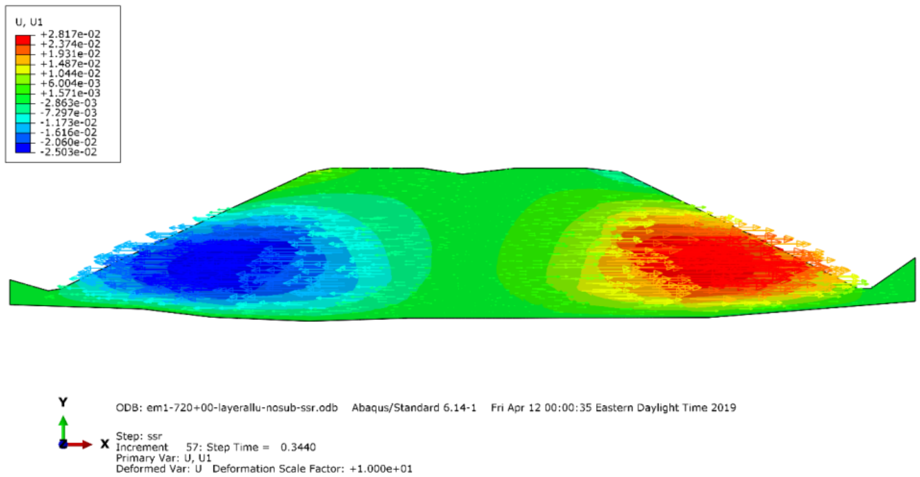

(b) 720+00

Figure IVb.32 – Potential horizontal displacement at failure at cross section (a)720+50 and (b) 720+00 (unit: ft)

In order to explore the mechanism of the sliding failure, the plastic strain contour was plotted, identifying the rupture surface inside the slope. Both cross sections present that the potential sliding surface consists of several minor curves (Figure IVb.33). In addition, the induced shear band in this nonuniform slope did not penetrate the whole slope. But in the uniform slope, the shear band went through the embankment reaching the bottom and the top. The difference in the plastic strain resulted from the existence of gravelly silt/sand layers at the bottom of the embankment with higher shear strength which provided a stronger resistance to the shear stress and prevented the extension of the plastic strain. In addition, the thin layer between the bottom of the plastic zone and the bottom of the embankment is roughly identical with that layer of the gravelly silt/sand.

The development of plastic zone did not contact the top of highway (Figure IVb.33b). This is caused by the existence of core material sandy silt (a-2-5) in the middle with higher shear strength. The ending point of two sliding surfaces lie on the edge of this core region shown in Figure IVb.IVb.33b, indicating that the shear band is prevented from propagating to the top by the core material (sandy silt). Also, there is almost no plastic strain in the region of clayey gravel on the two lateral parts of the slope, proving that this material is good for keeping the stability of the slope.

The weaker layer of alluvium results in the development of plastic zone, especially at cross section 720+50. At the area near the toe, there is a shear band extending along the alluvium, but don't penetrate to the very bottom of the embankment. The orientation of the extension of plastic zone is altered by that thin layer of gravelly silt (a-4 in AASHTO) on the bottom.

In conclusion, the nonuniformity of the material properties in the embankment had both positive and negative influences on the slope stability of the embankment. Weaker material like alluvium near the bottom of the slope decreased the slope stability especially in the case of 720+50 with an inclined bottom surface where plastic zone had more possibility to extend in such weak layers. However, the slope was still stable and the sliding surface did not penetrate all through the embankment due to the existence of a strong layer on the bottom that resisted the induced shear stress in the slope and prevented the formation of a complete sliding surface. The middle material is squeezed in this process due to the resistance of the bottom layer and several minor rupture surfaces are induced. The factor of safety decreased a little bit due to the localization of plastic strain in weaker layers. The influence of such induced plastic strain in the alluvium was limited and no global sliding surface formed in this process due to the stronger layer on the bottom or in the center core region so that the embankment was stable as a whole before mining.

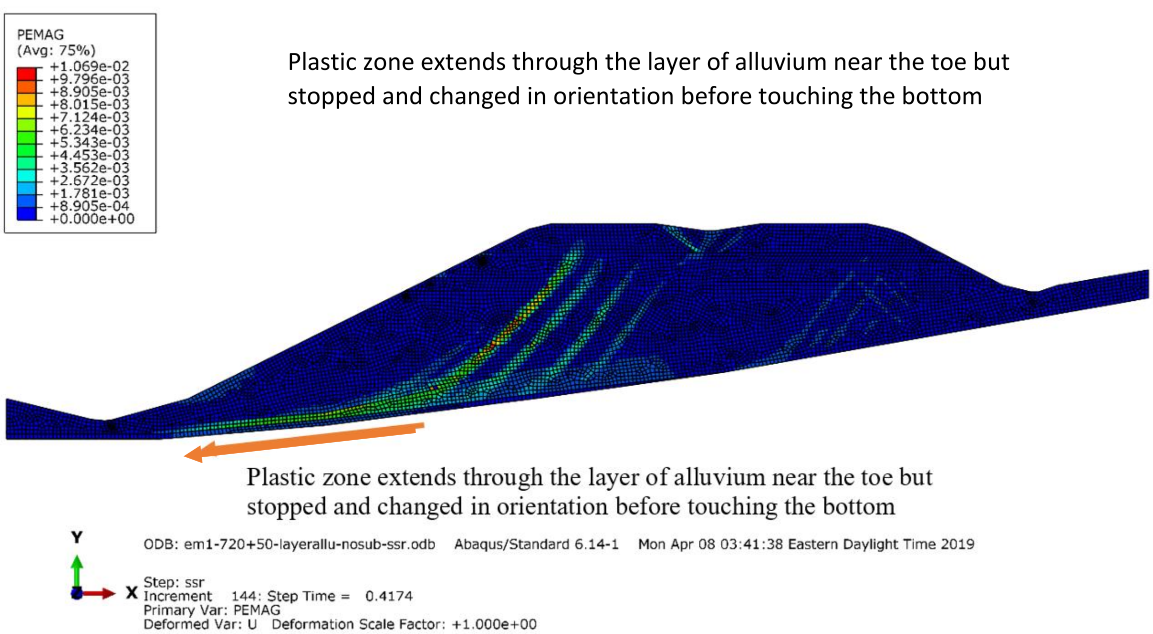

(a) 720+50

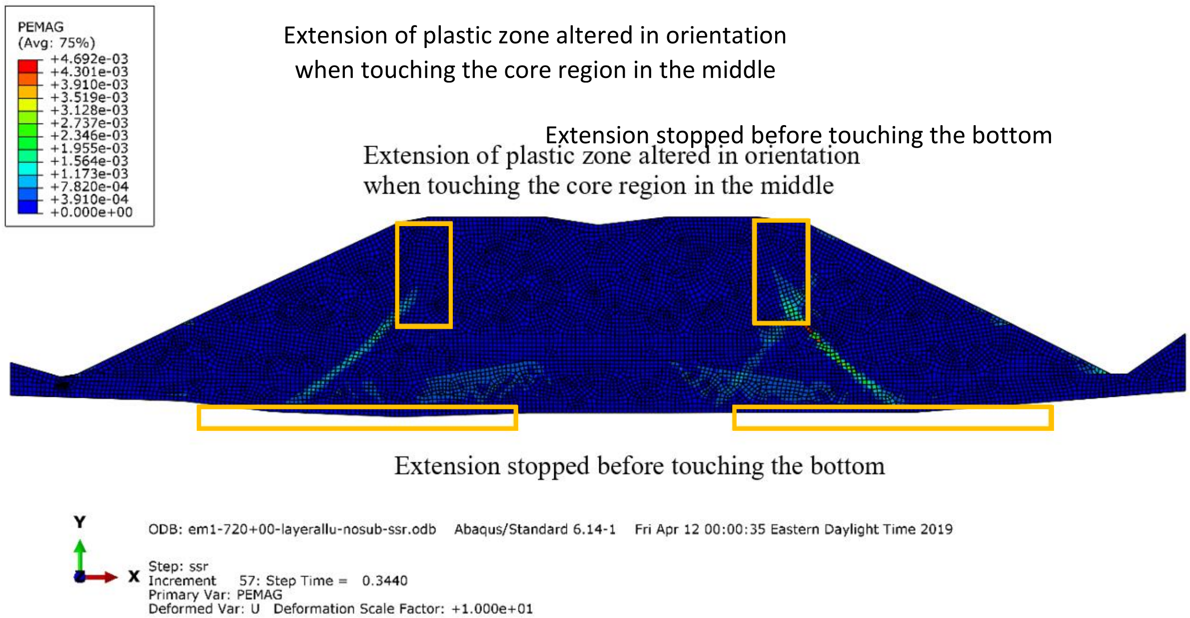

(b) 720+00

Figure IVb.33 – Plastic strain at cross section (a)720+50 and (b) 720+00

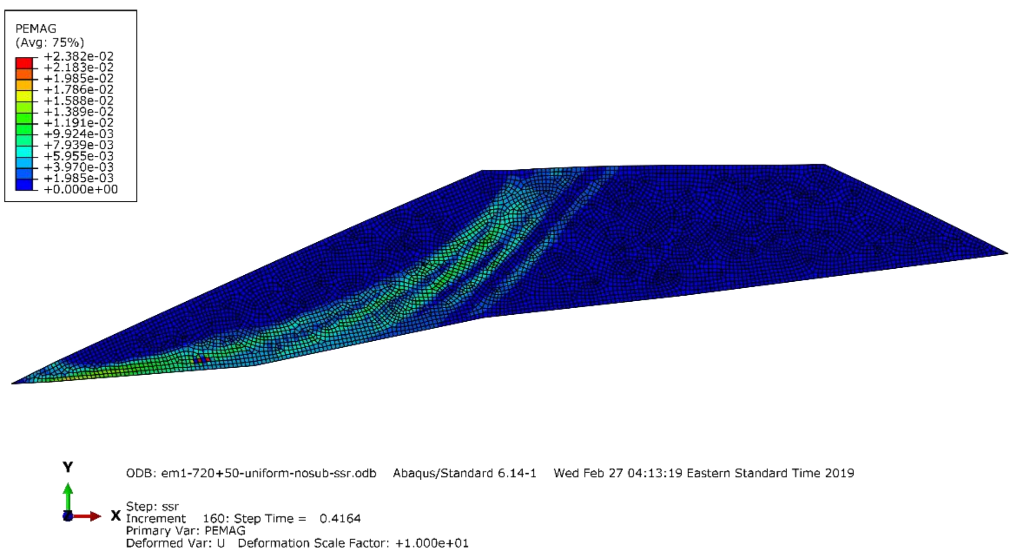

Figure IVb.34 – Plastic strain development of a uniform slope at cross section 720+50

6.2 Analysis of Embankment #1 before Mining in 3D

6.2.1 *Normal Test without SSR*

In this test, the University analyzed the initial stress and strain field as well as the displacement in Embankment #1 due to gravity. This pre-mining state of the embankment will be compared to the state during and after mining in the future to investigate the influence of longwall mining on the behavior of the embankment. Some parameters are plotted along the two paths south edge and north edge shown in Figure IVb.35. They are located on the edges of the top surface.

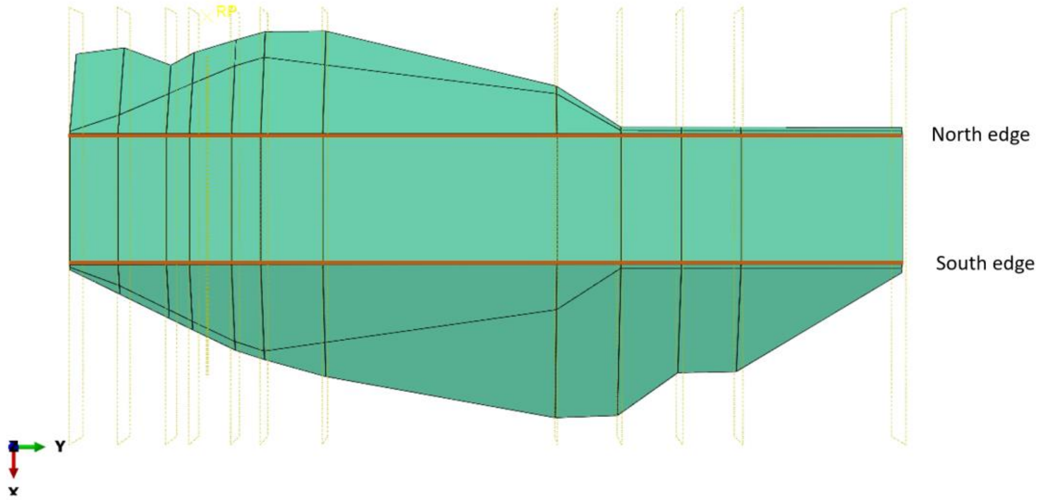

Figure IVb.35 – Locations of two paths on the North edge and South edge for plotting

Horizontal stress along the highway direction (s11), perpendicular to the highway direction (s22), and the shear stress (s12) are shown in Figure IVb.36. The horizontal stress is observed to be perpendicular to the direction of highway, reaching the highest value in the lower parts of two slopes with the color of yellow.

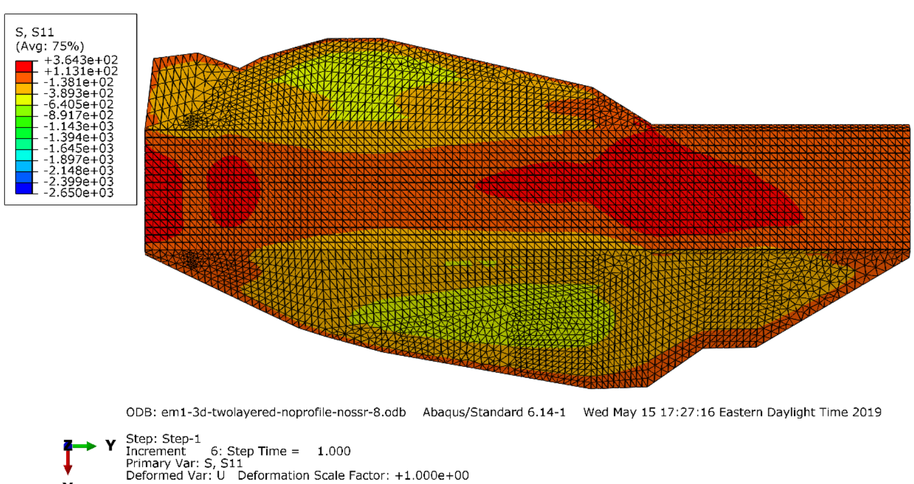

(a)

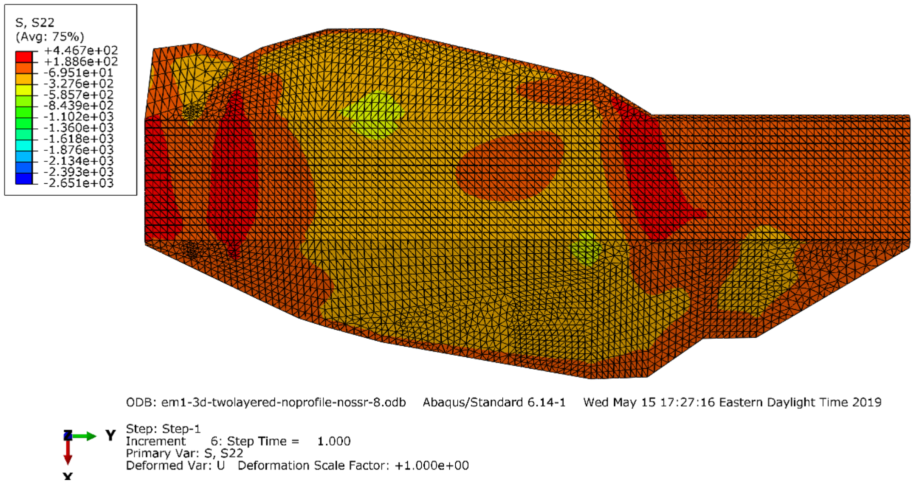

(b)

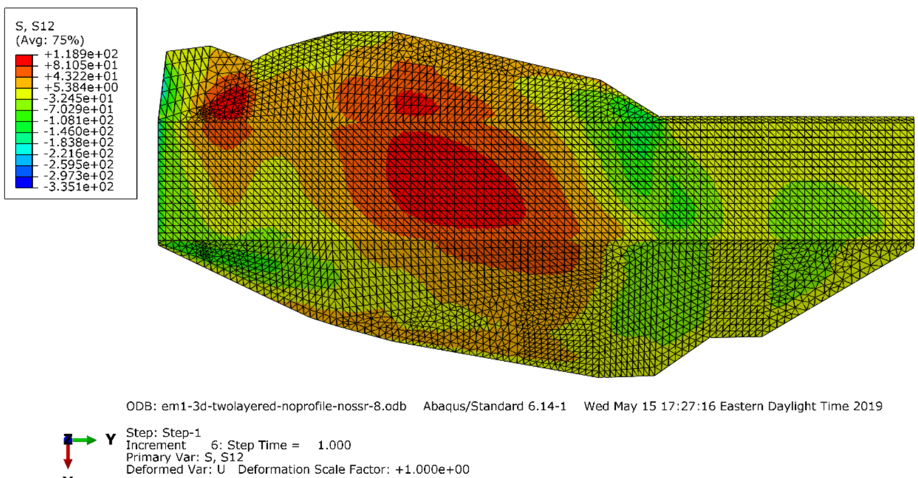

(c)

Figure IVb.36 – Stress contours of (a) s11; (b) s22; (c) s12 (unit: psf)

Figure IVb.37 indicates the horizontal shear stress parallel to the direction of highway along the two paths. When looking at the path of north edge, the shear stress switches from positive to negative in the middle of the path, which means that the shear stress changes the direction here.

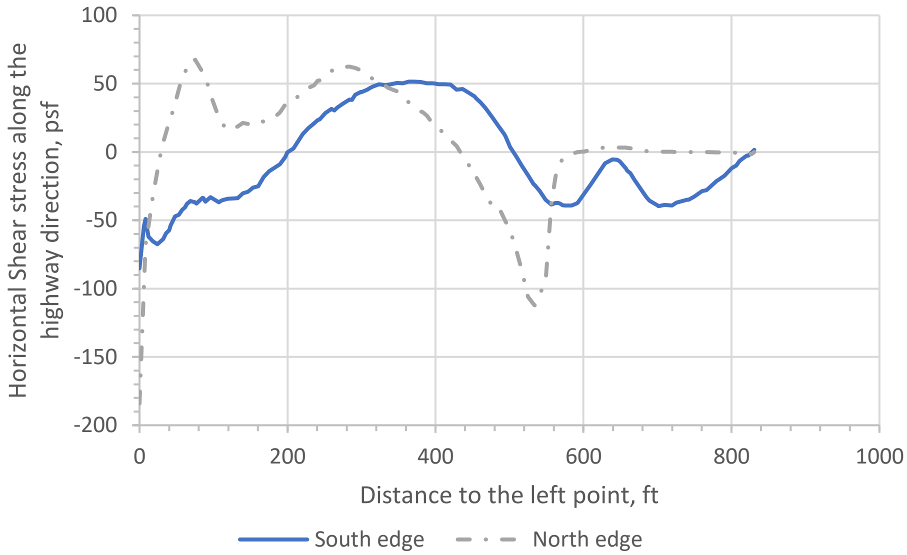

Figure IVb.37 – Horizontal shear stress parallel to the direction of highway along two longitudinal edges

Horizontal strain along the highway direction (E11), perpendicular to the highway direction (E22), and the shear strain (E12) are shown in Figure IVb.38. The shape of strain contours was similar to that of stress.

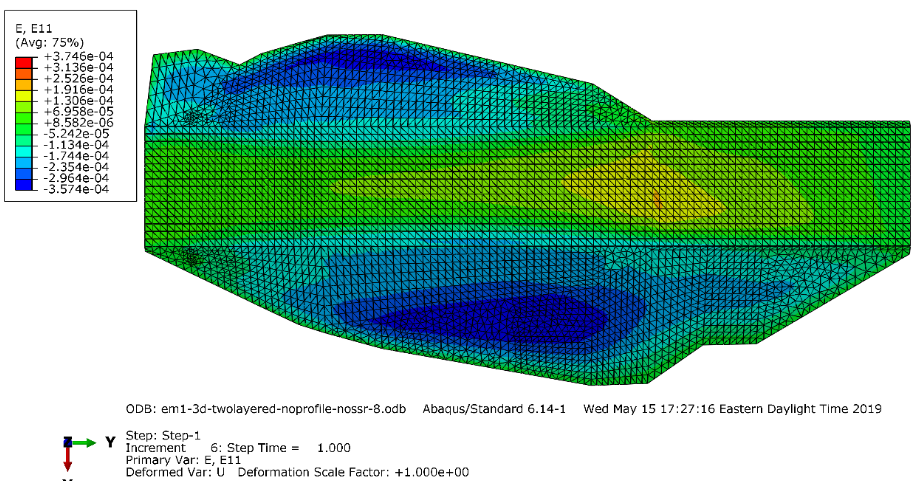

(a)

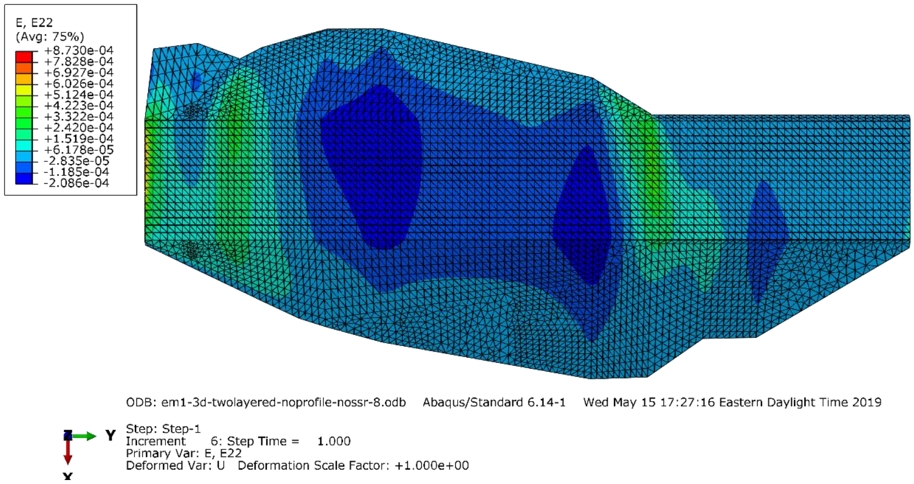

(b)

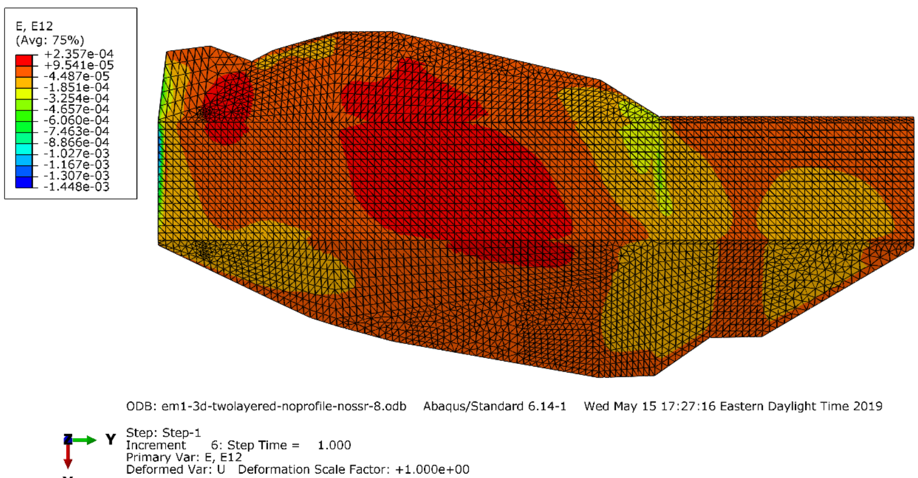

(c)

Figure IVb.38 – Strain contours of (a) E11; (b) E22; (c) E12

Figure IVb.39 indicates the horizontal strain parallel to the direction of highway along the two paths. The two peak values of negative strain on the two edges indicated these areas are in high compression compared to other parts.

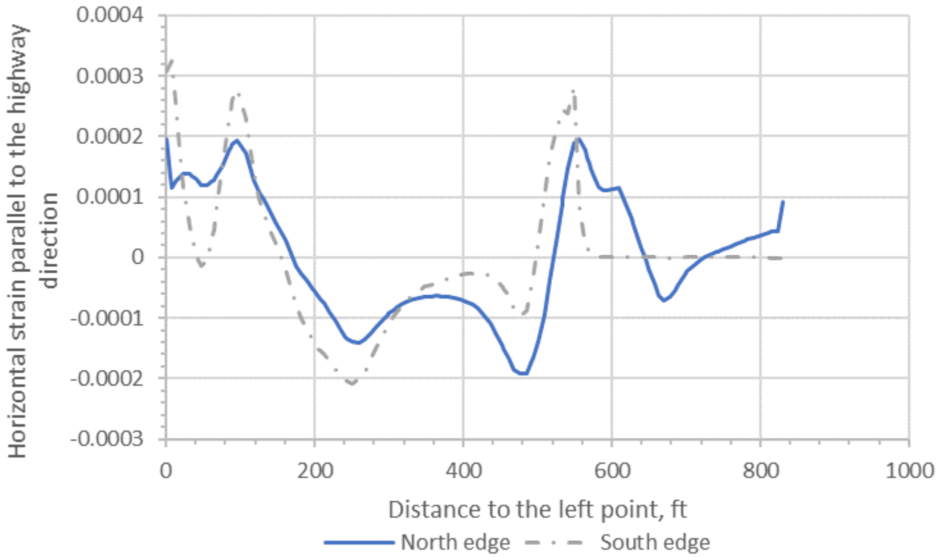

Figure IVb.39 – Horizontal strain parallel to the direction of highway along two longitudinal edges

Horizontal displacement along the highway direction (U1), perpendicular to the highway direction (U2), and the vertical displacement (U3) are shown in Figure IVb.40. The vertical displacement was plotted along the two edges (Figure IVb.41). It indicates that the vertical displacement on the south side of the highway is higher than that on the north side of highway in Embankment #1 before mining.

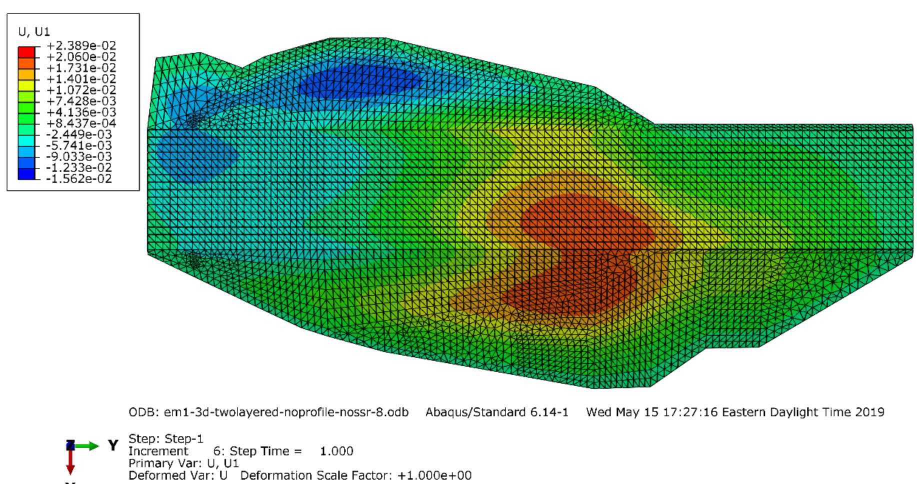

(a)

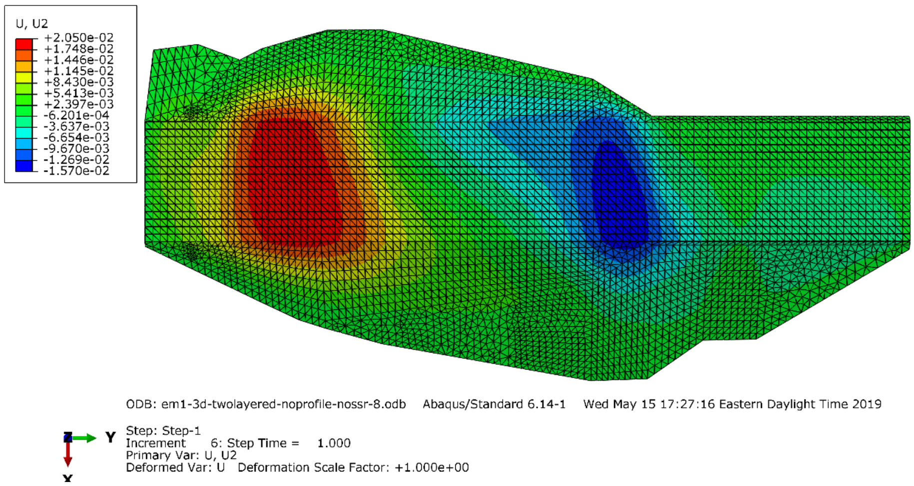

(b)

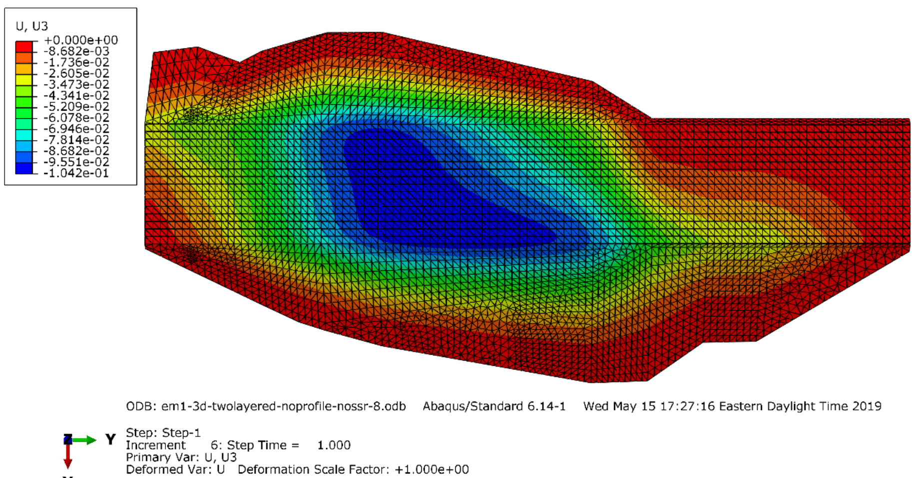

(c)

Figure IVb.40 – Displacement contours of (a) U1; (b) U2; (c) U3 (unit: ft)

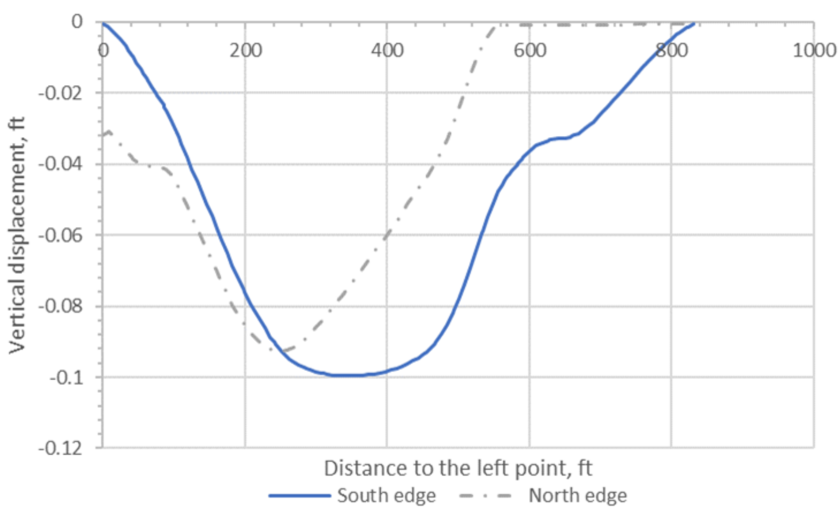

Figure IVb.41 – Vertical displacement along two longitudinal edges of highway

6.2.2 *Slope Stability Analysis*

Total displacement at the crest was plotted against the SRF in order to find the factor of safety at failure (Figure IVb.42). An obvious bending point can be observed in the plot where the total displacement begins to change dramatically. The shear strength reduction factor is located at the point of significant change to the factor of safety. Therefore, the factor of safety of the embankment is 1.9, which means that the embankment is stable.

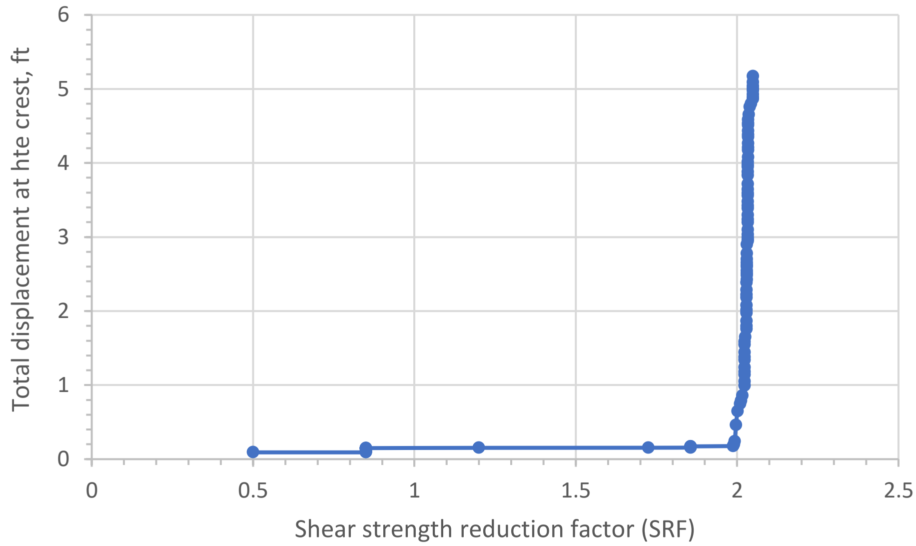

Figure IVb.42 – Determination of factor of safety by plotting the total displacement versus the shear strength reduction factor

The total displacement can be used to determine which part of the embankment is more unstable. As shown in Figure IVb.43a, more dramatic displacement occurred along the north-facing slope compared to the south-facing slope. From the Figure IVb.43b, deformation inside the embankment occurs at cross section 720+00 near the lowest toe, indicating the slipping surface in the slope. From the Figure IVb.43c, the deformation inside the embankment occurs at cross section 720+50 with some displacement on the shallow area from the crest to the toe of the slope.

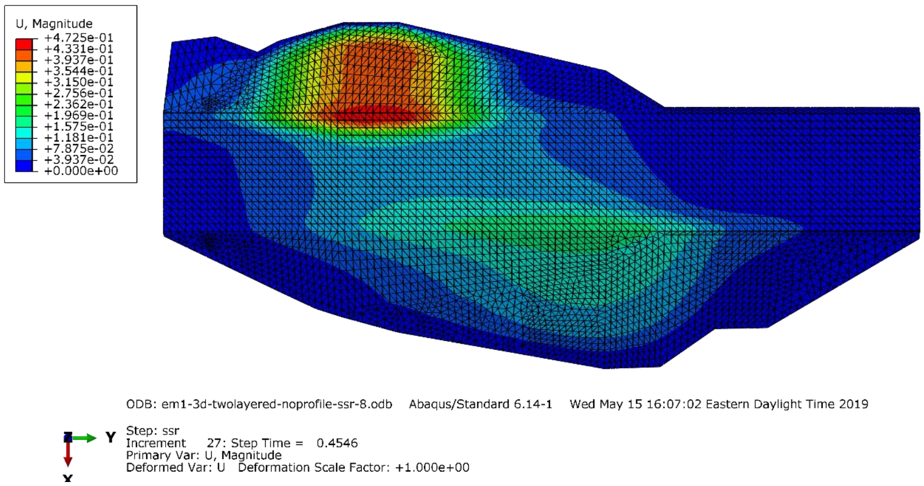

(a)

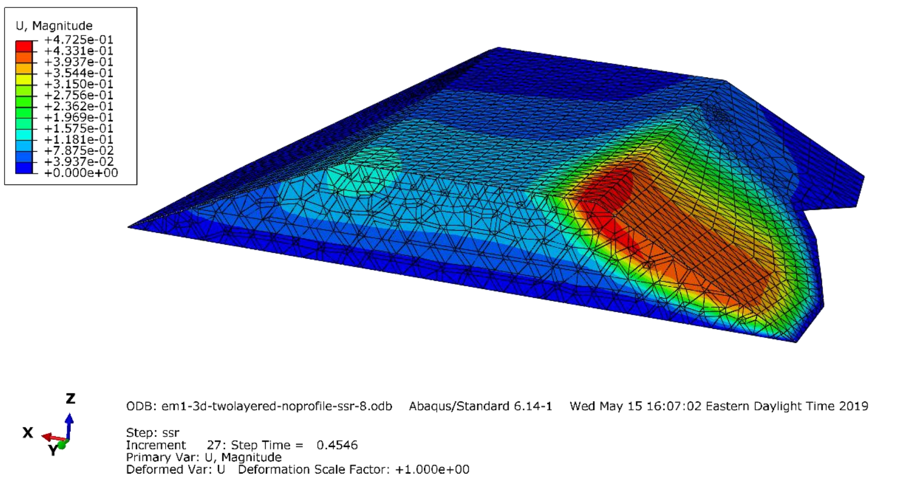

(b)

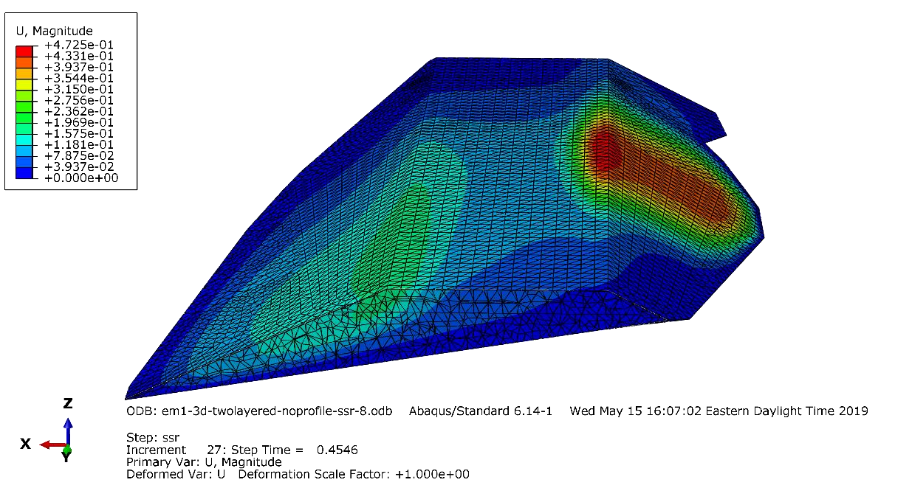

(c)

Figure IVb.43 – Total displacement at failure (a) on the surface of Embankment #1on the surface of Embankment #1; (b) inside Embankment #1 at 720+00; (c) inside Embankment #1 at 720+50 for layered model (unit: ft)

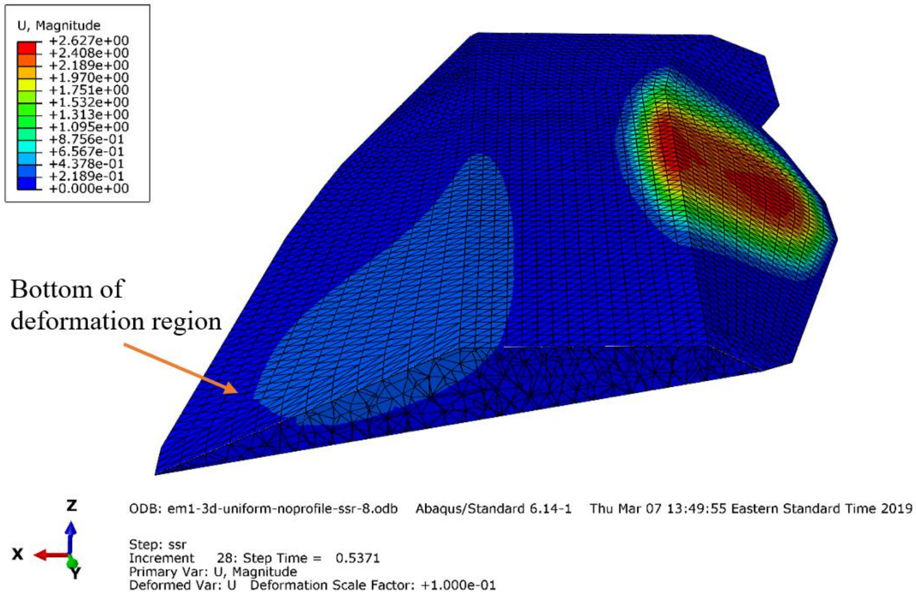

Figure IVb.44 – Total displacement inside the Embankment #1 at 720+50 of uniform model (unit: ft)

The part of slope capable of significant displacements provides an indication of the failure mode. Centrifuge tests have indicated that the plastic shear strain zone in unstable slopes coincided with the rupture surface (Roscoe, 1970). In other words, the development of plastic shear strain reflects the potential failure and the stability of the slope is dependent on the shear strength of the soil in the slope. Instead of using centrifuge tests, the SRM is applied to see in which part of the slope the plastic strain will develop.

The magnitude of plastic strain presents is shown in Figure IVb.45. The potential plastic zone on the surface of the embankment is shown in Figure IVb.45a, which is located at the north slope corresponding to the lowest part of toe. It shows that the plastic zone is located at the narrow area at the edge of the top on the north side as well as the toe at the north facing slope, indicating the potential damage and deformations will happen in these areas.

The mechanism of the slope failure can be illustrated plotting the interior plastic strain at cross section 720+00 in Figure IVb.45b. Plastic strain is maximum at the toe and goes through to the top of slope near the crest area. The part at the right of the plastic zone move downward due to gravity and shear band forms in this process. There is no plastic strain along the surface of the south facing slope (Figure IVb.45c).

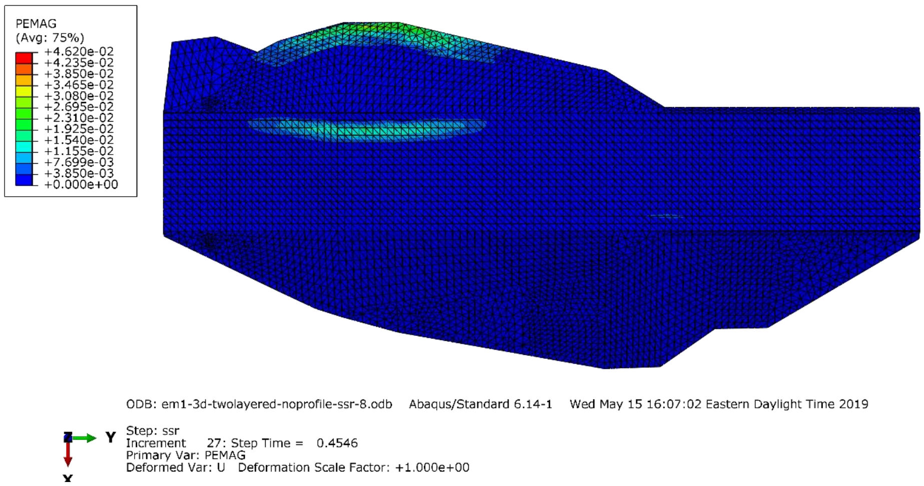

(a)

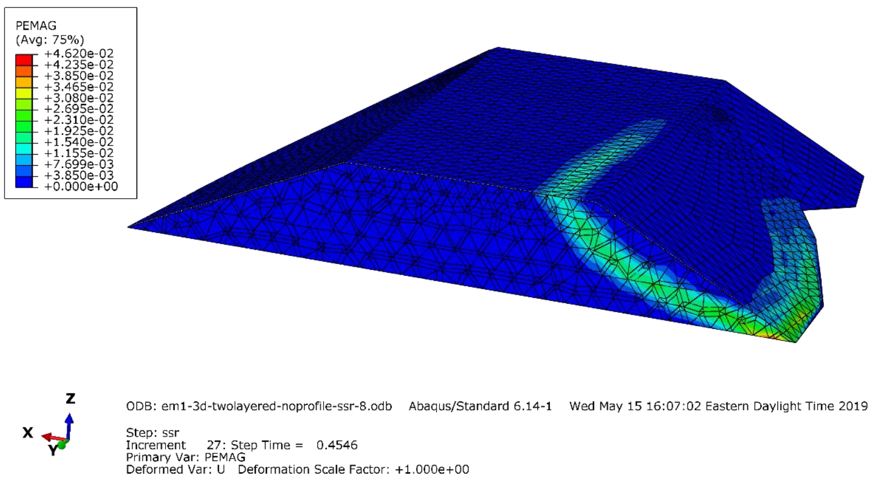

(b)

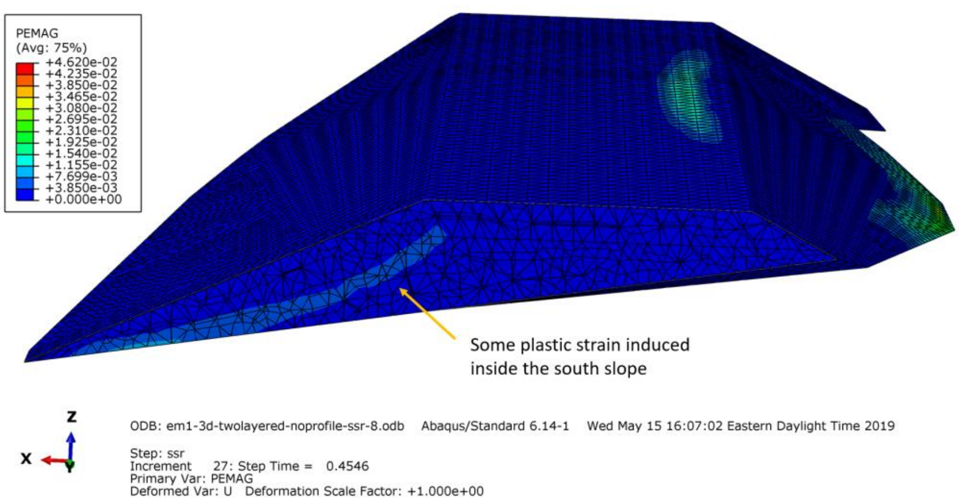

(c)

Figure IVb.45 – Plastic strain at failure (a) on the surface of Embankment #1; (b) inside Embankment #1 at 720+00; (c) inside Embankment #1 at 720+50 for layered model

Minor amounts of plastic strain occur on the south slope. This interior plastic strain accounts for the displacement at the south slope. Because the rupture surface did not penetrate all through the slope nor reach the surface of the embankment, the displacement is not as much as that in the north slope. The plastic strain at cross section 720+50 of the layered embankment is compared to the same location in Figure IVb.46. No plastic strain is observed in the uniform embankment at 720+50.

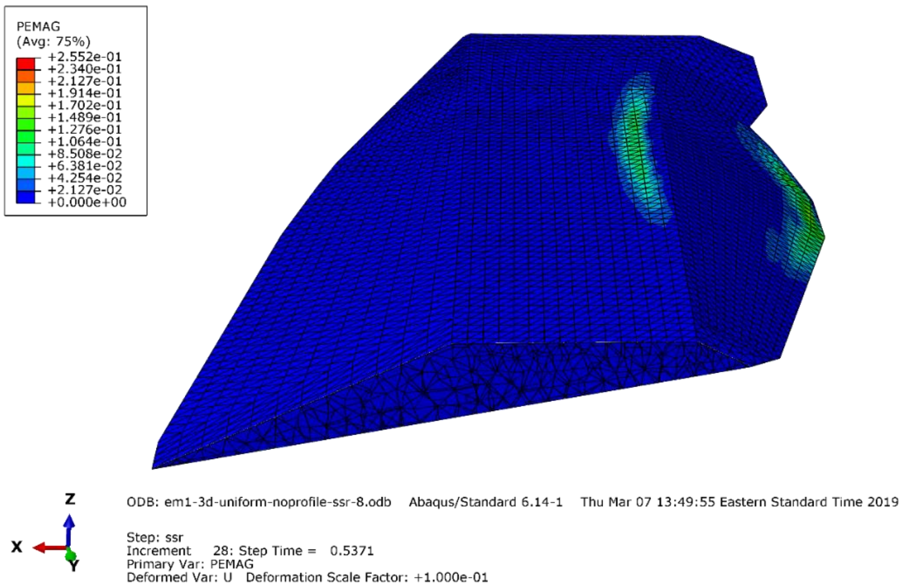

Figure IVb.46 – Plastic strain at failure inside Embankment #1 at 720+50 of the uniform model

7.0 Summary

The three-dimensional model of Embankment #1 was constructed to conduct the stress, strain, and the slope stability analysis before longwall mining. The exterior and interior contour of different layers were determined by the topography graph and test boring logs. Two sophisticated cross sections were constructed based on given information and the configuration of the 3D layered model was investigated based on these two cross sections. The failure behavior of this layered model was compared to that of the uniform model. Some displacement was observed in the south slope of the layered model at failure while none was observed in the same location of the uniform one. The results of stress, strain, and displacement analysis as well as the slope stability analysis will be compared to those using the measurements in the future to calibrate the model. Also, a subsidence basin will be applied on the bottom of this 3D model to investigate how the embankment behave when subjected to the longwall mining subsidence.

SECTION V – STUDY SITE MONITORING STRATEGIES

Subsection Va – Summary of Instrumentation Deployed to Monitor Highway Undermining

In preparation for undermining of I-70, a series of instruments were installed to monitor the behavior of the highway as the longwall face approached the study area. The behavior of the embankments was of particular interest, so the instruments were placed primarily on the embankment slopes. A total of 18 instruments were installed: nine tiltmeters, six inclinometers, and three piezometers.

1.0 Tiltmeters

PennDOT subcontracted Earth Inc. to supply nine tiltmeters in shallow boreholes to monitor the subsidence caused by Panel 15; eight of the tiltmeters were located along the berm of the eastbound lane of I-70 and one was located on the southern side of Embankment #1, towards the bottom of the slope (Figure 1). As only eight instruments were contracted for this project, on 24 January 2019, the instrument from TM-1 was removed and installed in TM-9's location at the bottom of the southern slope. These instruments allowed for the examination of change in tilt that occurred at different points along the highway as the undermining took place.

Each tiltmeter was installed in a casing and suspended 3-ft below the surface. These tiltmeters are described as "in place inclinometers". Readings, including the time, temperature, degree of tilt, and millivoltage, were taken for each instrument every ten minutes. Temperature readings are measured in Celsius and the degree of tilt and millivoltage are measured in both the X and Y planes. The degree of tilt can vary +/- 12 degrees and reportedly has an accuracy of 0.005 degrees. The locations and axes orientation of the tiltmeters are shown below in Figure Va.1.

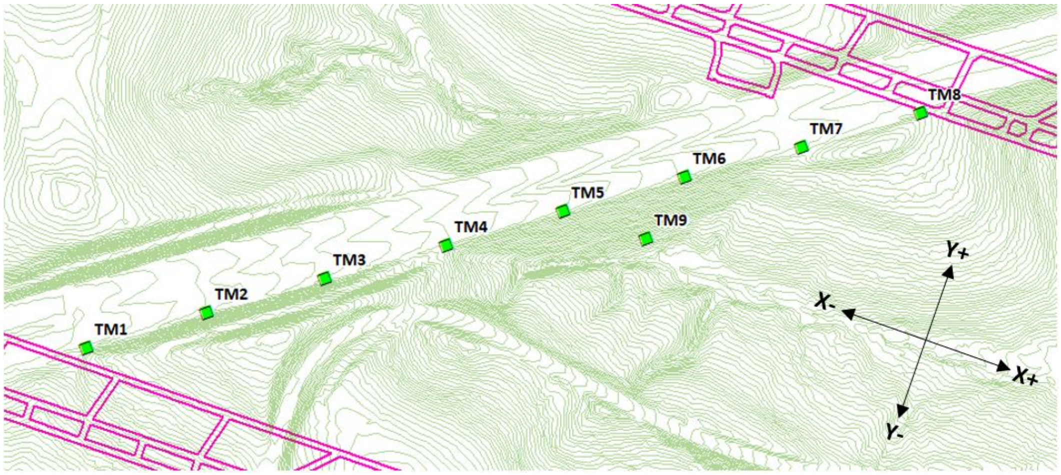

Figure Va.1 – Locations and orientation of the tiltmeters within I-70 study area

TM-1 (TM-9) through TM-8 used the "Model 906 Little Dipper" model tiltmeters. TM-1 (TM-9) through TM-5 are an older version of the model, while TM-6 through TM-8 are a newer version of this same model. The tiltmeters were connected to one another and continuous readings were transmitted to a central data reader, which is accessed remotely.

The software package Cambel Scientific (LoggerNet) was used by the tiltmeters and accessed the cell modem every 30 minutes to collect data. It contains a built-in alarm system to alert users via text or email if there is more than 0.5 degrees of movement between readings. This can be altered to any point but, for the purposes of this project, the alert was set so that once the 0.5 degree alarm is triggered, the alarm trigger is increased to 1.0 degrees. Conversely, it could also alert users when the direction of tilt is reversed.

Although the tiltmeters have not had data examined for the temperature impact, the specifications state that they can operate between -13 and 158 degrees Fahrenheit, meaning that variation in air temperature should not affect the accuracy of readings for this project.

All data gathered from the tiltmeters was to be put into a database, where the files were stored on a server with a local and offsite backup for storage and analysis. The data files are to be kept and looked at periodically to obtain the most critical results.

2.0 Inclinometers

PennDOT installed inclinometers in six boreholes within the study area and their survey crews were to take regular readings from these inclinometers throughout the undermining process. The RST Digital Inclinometer Probe, Model No. IC 35202 was used to take readings at these locations. These probes have an accuracy of +/- 0.1-in per 100-ft and can operate within +/- 30 degrees, and in temperatures ranging from -40 to 158 degrees Fahrenheit.

Figure Va.2 shows the locations and orientations of the borehole casings. Notice that the orientations differ based on their locations; TB-4 and TB-2 share an orientation, while TB-6, TB-8, TB-9 and TB-13 all share a different orientation. The orientation as installed shows the A+ direction pointing down the slope of the embankments and the B+ axis clockwise from the A+ orientation.

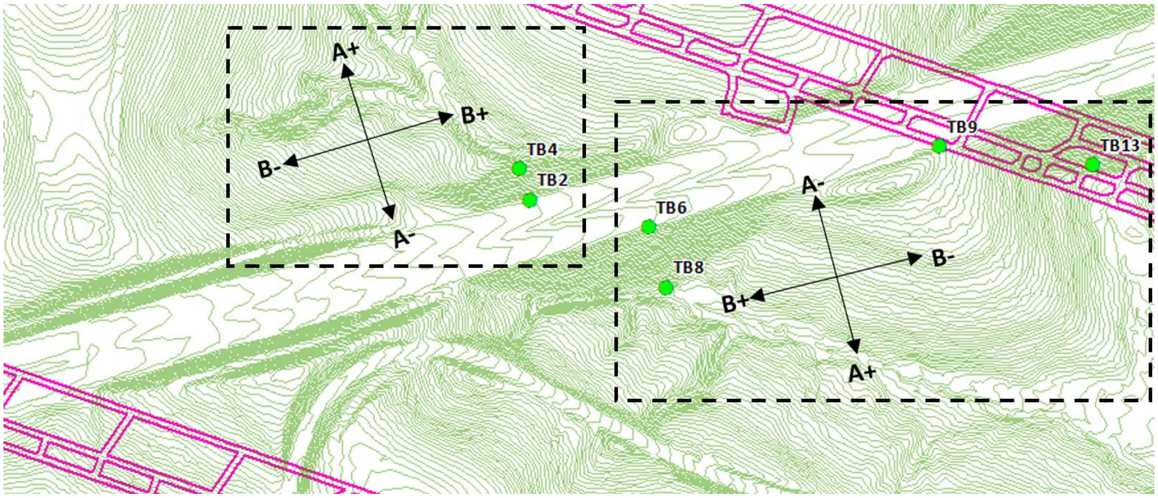

Figure Va.2 – Locations and orientations of the inclinometers within I-70 study area

The installation of the inclinometer is a multi-step process. Inclinometers are installed in boreholes, which were drilled to collect soil samples. An inclinometer casing is placed into the borehole and the area surrounding the casing is backfilled with granular material. This set up allows the casing to deform due to movement in the soil layers, as seen in Figure Va.3.

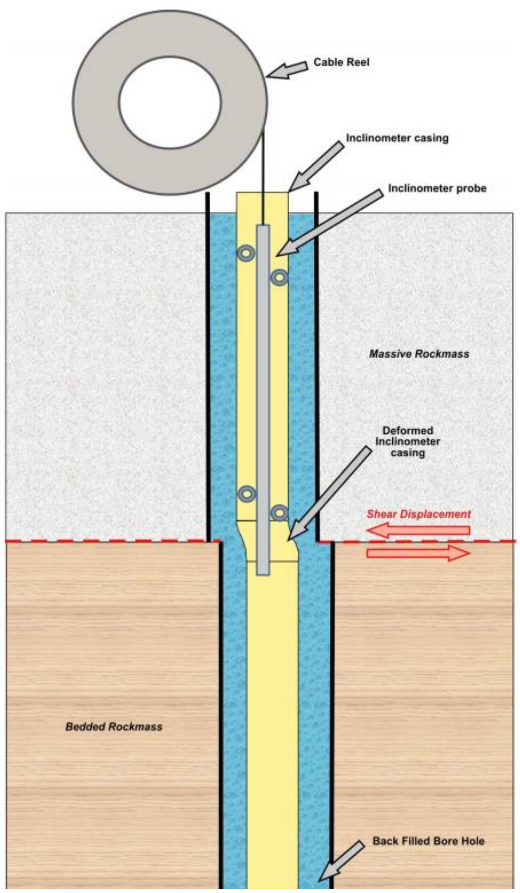

Figure Va.3 – Schematic view of inclinometer casing and inclinometer probe (Daigle and Mills, 2017)

Proper installation of the inclinometer casing attempts to align one set of grooves in line with the axis of expected movement. This set of grooves is referred to as the A axis. The perpendicular set of grooves is the B axis. For this site, movement is expected to run outward from the slope, so the A+ direction is facing outward from their respective slopes. The B+ axis runs along the slopes, clockwise from the A+ direction. To take a reading, the inclinometer is placed in the A axis groove and is lowered to the bottom of the hole with the wheels facing the A+ direction, as shown in Figure Va.4. The probe is then raised in 2-ft increments, with readings taken at each increment; at each position, the probe is stabilized before accepting the inclination reading. Results are accepted once the probe reaches the top. Once lifted, the probe is reversed and the process is repeated in the A-, B+, and B- directions.

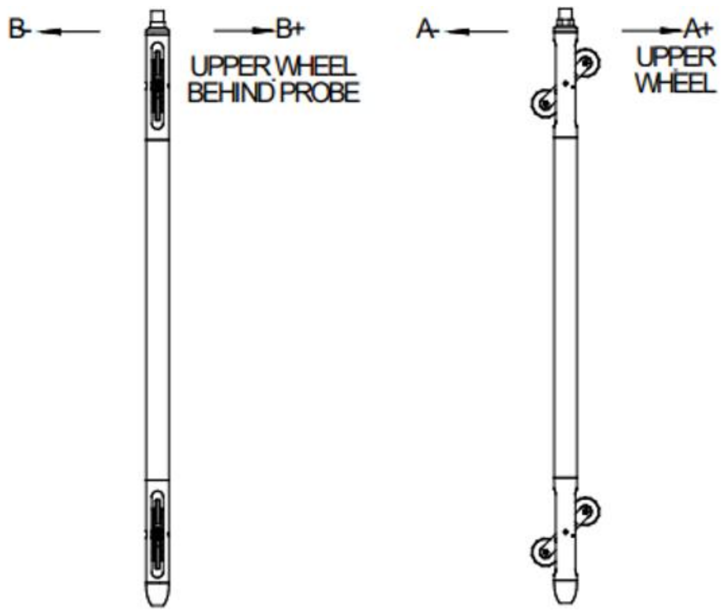

Figure Va.4 – Upper and lower wheel diagram

Readings taken from the inclinometer probe are deviations from the vertical over the distance between the upper and lower wheels, as can be seen in Figure Va.5. The deviation measurements for each reading were taken in feet and calculated using equation Va.1.

$$D = L * \sin(\alpha) \qquad \text{[Eq Va.1]}$$

where: L = inclinometer probe length

α = inclination angle of probe from vertical axis

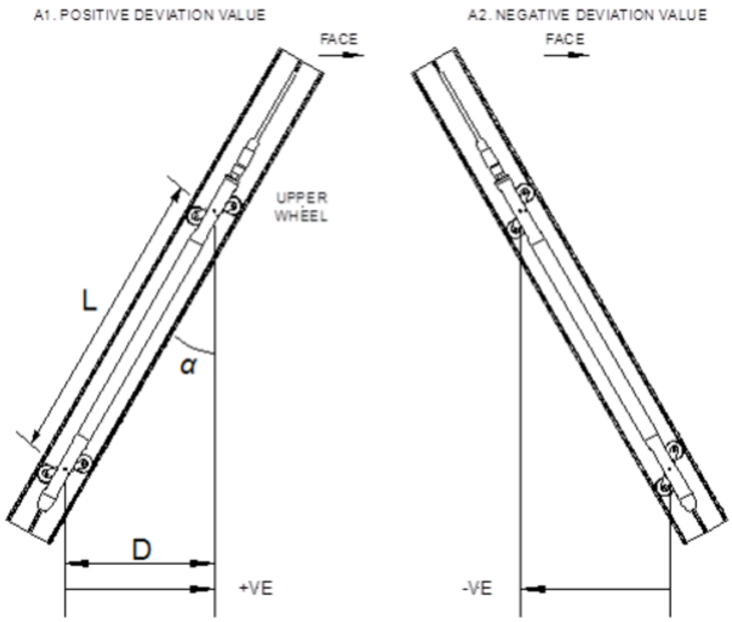

Figure Va.5 – Sign convention in the A-axis and deviation D measured by the inclinometer probe

These results are recorded on the portable instrument and on PennDOT's equipment calibration log in the office to be supplied to the University for analysis.

3.0 Piezometers

PennDOT installed three piezometers in TB-3, TB-7, and TB-12 for the duration of the undermining process. Two of these piezometers (TB-3 and TB-7) were installed in Embankment #1 on the north and south slopes respectively, and the final piezometer (TB-12) was installed in Embankment No. 2 on the south slope, as seen in Figure Va.6. These devices detect the level of the groundwater table.

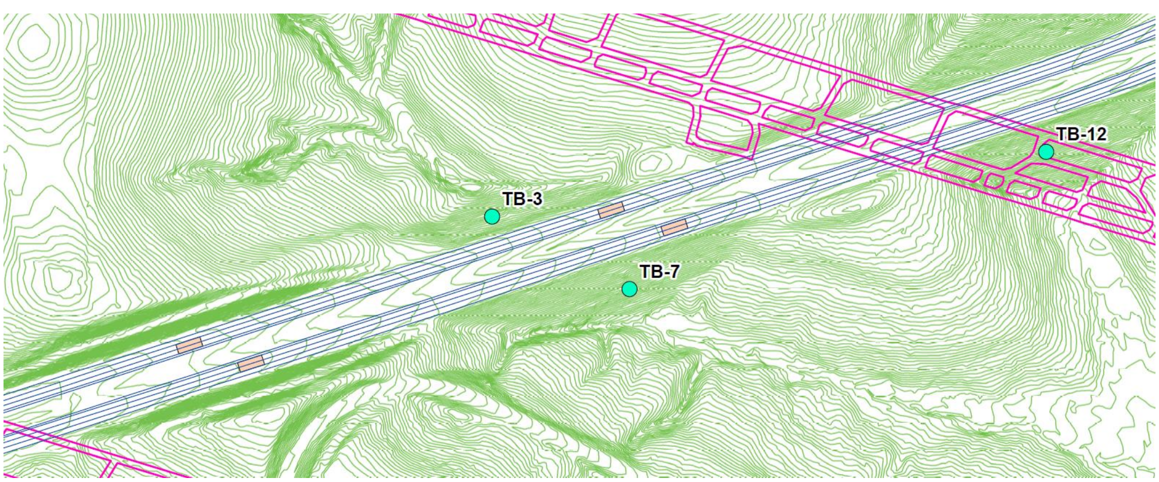

Figure Va.6 – Locations of piezometers within I-70 study area

These measurements show the distance from the ground surface down to the water table and are read manually. To take a reading, an inspector lowers a probe down the borehole and the monitor lights up red once the sensor has reached water. These distances are recorded and are to be supplied to the University for analysis.

Subsection Vb – Tracking of Ground Surface Movements

When Panel 15 undermined I-70, the ground movement occurred in all three dimensions due to the subsidence. To monitor this movement, a series of surveys including highway alignment surveys, slope surveys, and LiDAR surveys were employed.

1.0 Highway Alignment Surveys

The PennDOT survey crews tracked the movement of the highway alignment throughout the undermining process. This monitoring was necessary to redefine the highway's position once subsidence had concluded. The centerline alignment was staked for approximately 3,500-ft with 2,600-ft in Pennsylvania and 900-ft extending into West Virginia. The alignment was offset 62-ft right and left to create the two baselines with over 140 points along the alignment to be monitored. The location of the points surveyed can be seen in Figure Vb.1.

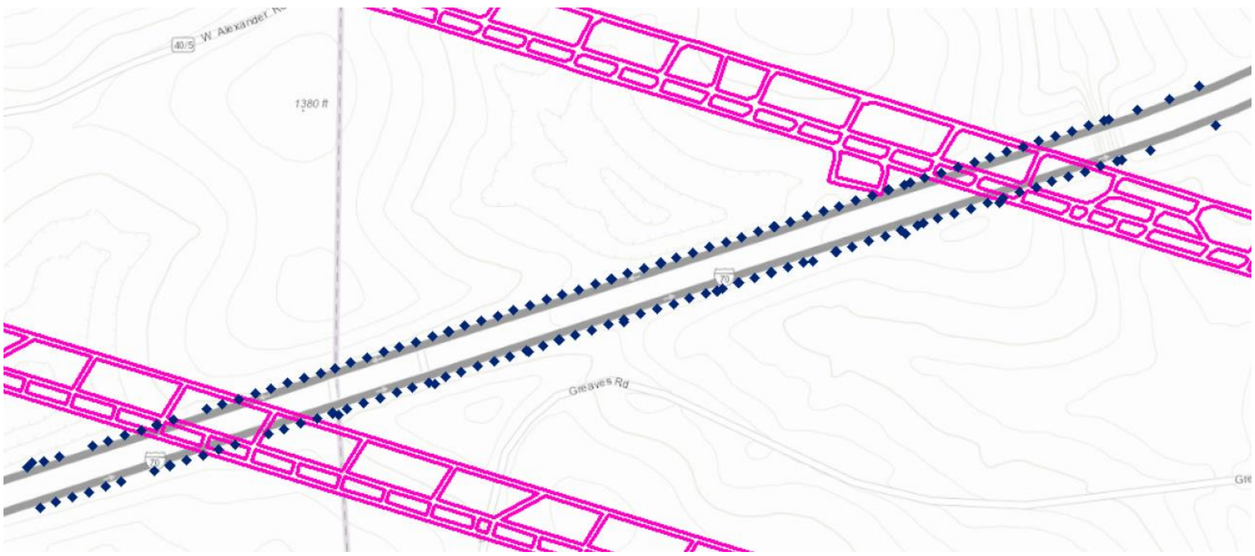

Figure Vb.1 – Points monitored by highway alignment surveys

This set of points was surveyed regularly during the undermining, for a total of 11 contracted monitoring surveys. PennDOT's survey crew performed 3D surveys using a Trimble R10 GPS unit with Virtual Reference Station (VRS) methodology. For this methodology, observational data is created from the data of surrounding, imaginary reference stations as though it had been observed by a GPS receiver. Vertical control was added using existing benchmarks and a differential leveling technique. This combination of survey techniques resulted in a horizontal accuracy of 0.02-ft and a vertical accuracy of 0.05 to 0.10-ft. The data collected through these surveys will be provided to the University of Pittsburgh and utilized to characterize the behavior of the road surface's behavior resulting from undermining.

2.0 Surveys of Cut Slopes and Embankments

PennDOT subcontracted SPK Engineering to monitor the movement of the cut slopes and embankments within the study area being undermined by Panel 15. The locations of over 590 points were collected twice a week to monitor the behavior of the slopes as the longwall panel undermined the road. These points were categorized into 11 survey stake groups, as can be seen in Figure Vb.2.

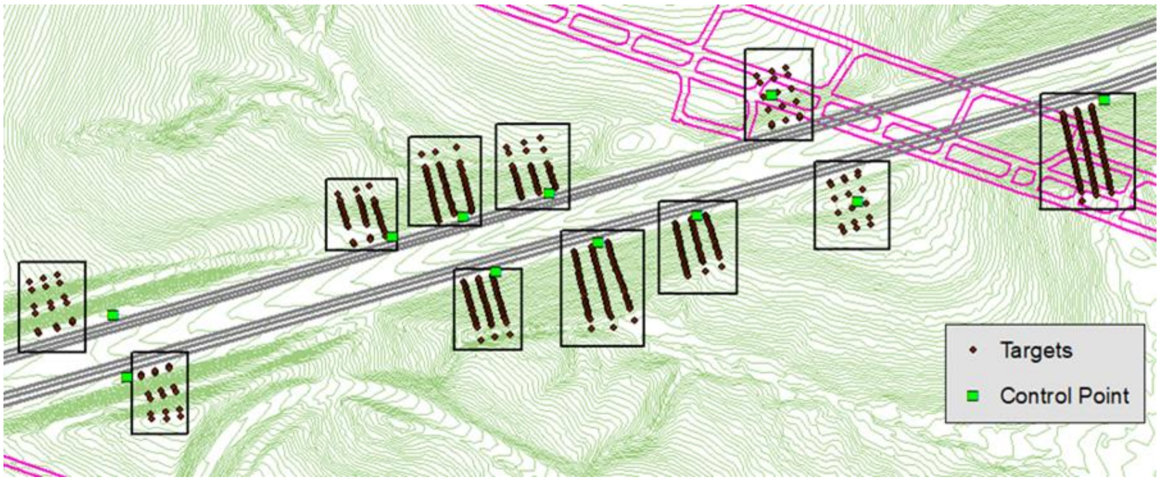

Figure Vb.2 – Points monitored by surveys of cut slopes and embankments

SPK Engineering utilized a Total Station to obtain angles and degrees from control points to the target points on the slopes. A Total Station utilizes trigonometry and triangulation to determine the location of surveyed points relative to a known point. There are 11 control points, or traverse points, located both inside and outside of Panel 15 that were used as known points to locate the other 590 target points. The horizontal location of these control points was identified using GPS and the elevation was determined using an engineer's level before each survey was performed. Though the GPS precision is approximately 0.026-ft, the elevation precision is approximately ±0.01-ft, and the Total Stations are accurate to ±0.02-ft, these surveys combining both methods are only accurate to ±0.05-ft. The data gathered from these surveys by SPK Engineering was provided to the University as it is collected and will be used to characterize the behavior of the slopes and embankments resulting from subsidence.

3.0 LiDAR Surveys

PennDOT contracted T3 Global Services to monitor the movement of the road surface as I-70 was undermined. T3 Global Services subcontracted ESP Associates to collect data and images to generate an engineering grade topographic survey. ESP deployed a Riegl VMX-1HA mobile LiDAR device based in Indianapolis to monitor this movement. This system is equipped with two Riegl VUX-1HA laser scanners, a POS LV 610 INS, and four 5 mp Riegl cameras.

Using this mobile LiDAR unit, the positions of millions of points were collected each time the road was driven. There were ten LiDAR scans contracted to be performed for this study. The points from these scans were processed using Riegl RiProcess. RiProcess uses plane to plane matching in conjunction with POS data to calculate errors in the POS solution to establish the most probable location for the LiDAR data. This was then used to analyze the provided control to search for potential errors in the provided control points. Once the LiDAR and control data were found to be consistent, the control points were held as fixed and RiPrecision was run to finalize the alignment of the LiDAR data to the controls.

For the scans of the highway alignment, the control points were located using the traverse method of land surveying. The traverse method uses a series of lines with predetermined and measured lengths to connect various points at determined locations. These traverse lines can be open or closed and can move easily around uneven terrain or obstacles. By using this method of control point surveying, T3 Global Services determined the LiDAR scans have an accuracy of 0.016 to 0.033-ft (5-mm to 10-mm) in the horizontal plane and 0.016-ft (5-mm) in the vertical plane.

T3 Global Services provided the University with the LiDAR surveys at the conclusion of the contract. This data will be used in conjunction with the highway alignment surveys to characterize the behavior of the road surface. Additional accuracy was maintained in the horizontal plane so that the University can analyze the change in movement and strains between concrete expansion joints.

Subsection Vc – Observational Protocol

To accurately observe the impact of longwall mining on the highway, a protocol was developed to ensure that all observations were properly recorded. Field observations were made by University of Pittsburgh employees once a week during the undermining period. Additional field observations were made by Pennsylvania Department of Transportation (PennDOT) Maintenance team that will be monitoring the highway as it is undermined. Approximately one mile of roadway was undermined by Panel 15 and the corresponding gate roads.

1.0 Safety Concerns

Safety was the priority and main concern of the University staff during field visits. To ensure that the inspectors on site remain safe, the inspectors were to use their judgement to find a safe place to pull off the road. Once the slow lane of the road was closed, the inspectors were to use the shoulder to pull off the road; until that lane was closed, the inspectors were to use their judgement to decide whether to use a side street or the shoulder to pull off to avoid interacting with traffic. In addition, someone from PennDOT was to be notified by the inspector prior to visiting the site so that the proper officials could be notified as necessary. Until the slow lane was closed, a shadow vehicle was to be provided to act as additional protection for the inspectors.

2.0 Grid Layout

To ease in locating any signs of failure that may occur on the highway surface, the University utilized a grid system marked on the roadway. A simplified layout for the gridwork can be seen in Figure Vc.1 below. The full layout shows that in the westbound direction the shoulder is “A”, the right lane is “B”, and the left lane is “C” and in the eastbound direction the left lane is “D”, the right lane is “E”, and the shoulder is “F”. The layout also has cross gridlines that match the PennDOT stations of the baseline median alignment. This allowed the inspectors to call out an identified feature in the section it occurred.

Figure Vc.1 – Gridwork on I-70 in study area

3.0 Mitigation Techniques

In order to mitigate the effects of undermining on the roadway, sections of concrete subbase were removed. These asphalt relief patches were installed in areas that were expected to see high concentrations of strain. There were four relief patches installed, each of which encompassed both lanes and were 60-ft in length. Traveling west bound, the relief patches were installed from Station 12+90 to Station 13+50 and from Station 2+40 to Station 3+00. Traveling east bound, the relief patches were installed from Station 14+25 to Station 14+85 and from Station 3+70 to Station 4+30. The location of the asphalt relief patches can be seen on the potential grid layout below in Figure Vc.2.

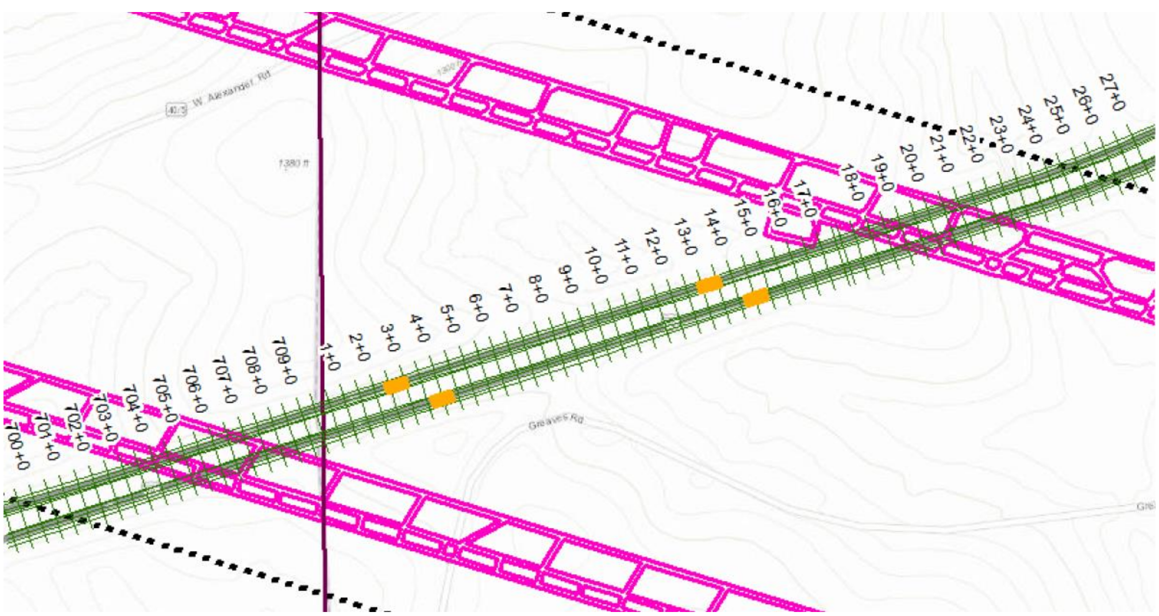

Figure Vc.2 – Location of asphalt relief patches denoted in orange

4.0 Observational Protocol for University Inspectors

Upon arriving at the site and finding a safe place to vacate his/her vehicle, the inspectors examined the highway surface for signs of failure. The inspectors carried a paper copy of the highway layout with the grid to the site. To the best of the inspector's ability, each sign of failure that was observed was sketched in the corresponding section on the paper grid. Special care was taken in sketching the observations to ensure that they were drawn to scale and in the correct location. Measurements were taken of the features documenting the width, length, height, and orientation as applicable and these measurements should be labeled on the sketch. Using the "Failure Type Sheet" as a guide, the inspector called out each observation with a description. The "Failure Type Sheet" can be seen below in Table Vc.1. Pictures were also be taken of every feature sketched, ideally in a manner that captured the characteristics and location of the feature.

Table Vc.1 – Failure Type Sheet (Miller and Bellinger, 2003)

Category	**Distress Type/ Photograph**
Cracking	<u>*Corner Breaks*</u> – A portion of the slab separated by a crack, which intersects with the adjacent transverse and longitudinal joints, describing approximately a 45-deg angle with the direction of traffic. The length of sides is from 1-ft to ½ the width of the slab on each side of the corner 
	<u>*Durability Cracking*</u> – Closely spaced, crescent-shaped hairline cracking pattern, occurring adjacent to joints, cracks, or free edges. Initiates in slab corners with dark coloring of the cracking pattern and surrounding area
	<u>*Longitudinal Cracking*</u> – Cracks that are predominately parallel to the pavement centerline 
	<u>*Transverse Cracking*</u> – Cracks that are predominately perpendicular to the pavement centerline 

Joint Deficiencies	*<u>Joint Seal Damage</u>* – Conditions which enable incompressible materials or water to infiltrate the joint from the surface. Typical types of joint seal damage are: extrusion, hardening, adhesive failure (bonding), cohesive failure (splitting), or complete loss of sealant; intrusion of foreign material in the joint; and weed growth in the joint
	<u>Spalling of Longitudinal Joint</u> – Cracking, breaking, chipping or fraying of slab edge within 0.3 m from the face of the longitudinal joint
	<u>Spalling of Transverse Joint</u> – Cracking, breaking, chipping, or fraying of slab edges within 0.3 m from the face of the transverse joint 
Surface Defects	*<u>Map Cracking and Scaling</u>* – Map cracking is a series of cracks that extend only into the upper surface of the slab. Larger cracks frequently are oriented in the longitudinal direction of the pavement and are interconnected by finer transverse or random crack. Scaling is the deterioration of the upper concrete surface, normally 3 to 13-mm, and may occur anywhere over the pavement
	<u>Polished Aggregate</u> – Surface mortar and texturing worn away to expose coarse aggregate
	<u>Popouts</u> – Small pieces of pavement broken loose from the surface, normally ranging in diameter from 25 to 100-mm, and depth from 13 to 50-mm
	<u>Blowups</u> – Localized upward movement of the pavement surface at transverse joints or cracks, often accompanied by shattering of the concrete in the area

Miscellaneous Distress	
	Faulting of Transverse Joints and Cracks – Difference in elevation across a joint or crack
	Lane-to-Shoulder Dropoff – Differences in elevation between the edges of slab and outside shoulder; typically occurs when the outside shoulder settles
	Lane-to-Shoulder Separation – Widening of the joint between the edge of the slab and the shoulder 
	Patch/Patch Deterioration – A portion, greater than 0.1 m^2, or all of the original concrete slab that has been removed and replaced, or additional material applied to the pavement after original construction
	Water Bleeding and Pumping – Seeping or ejection of water from beneath the pavement through cracks. In some cases, detectable by deposits of fine material left on the pavement surface, which were eroded (pumped) from the support layers and have stained the surface

In addition to observing the road surface, the inspectors also inspected the slopes of the embankments. An inspector went down the slopes to monitor for any signs of increased wetness or slope instabilities. Signs of slope instability may include bulges, tension cracks, and small scarps near the toe. Pictures were taken of any features that developed. Cut slopes were also observed for signs of instability during site visits, though only from the road surface as they cannot be traversed.

After returning from the field, the inspectors downloaded all of the pictures and scanned the paper grids with sketched features. The photographs were given descriptive names and placed into shared folders so that they could be easily found in the future. Photograph naming included the location and type of feature in addition to any measurements to characterize the feature. Using the ArcGIS software, the features observed and recorded on the paper grid in the field were digitized.

5.0 Requested Observational Protocol for Non-University Inspectors

An inspector from the University was unable to be on site at all times. As a result, the team requested cooperation from the maintenance personnel that remained on site for the duration of the undermining. The University provided a scroll map of the study area and requested that if the maintenance team noticed a feature indicating failure, he/she document the development of the feature. The documentation was to include photographs, measurements of length, width, height, and orientation of the feature as applicable, and the location of the longwall face at the time of development. In addition, if the maintenance team continued to be present on site during the subsequent days, it was requested that he/she continue to track the further development of the feature, such as if a tension crack began to close. All information collected should be provided to the University for analysis.

SECTION VI – FUTURE WORK

The Task 1 Report has focused on activities related to pre-undermining of I-70 by the Tunnel Ridge Mine. These activities are outlined in the scope of work and are connected to specific deliverables in the contract. Each of these Task 1 activities was addressed within this report.

Two more task reports will be delivered. The Task 2 Report will:

- Discuss and analyze the data collected during the undermining of I-70 by Panel 15,
- Identify the characteristics of the longwall subsidence basin, and
- Evaluate important trends in this data.

The analysis and evaluations of the subsidence data collected will increase our understanding of impacts to interstate highways, as well as their associated embankments and colluvium slopes. Matching the formation of these impacts with the transient surface deformation will provide the necessary background to aid in the future planning of engineering interventions.

Task 3 will take the experienced gained from the Panel 15 undermining episode (initial study area) and apply it to the I-70 alignment a distance of approximately 5 miles from the West Alexander to the Claysville interchanges in Washington County, Pennsylvania. Two important difference are expected between the interstate impact in the initial study area (Panel 15) and future longwall panels:

- The overburden is expected to be less, and
- The orientation of the longwall face to the overlying interstate alignment will vary.
  Both of these conditions have been observed to produce excessive levels of deformations and strains on the surface.

The University conducted a preliminary analysis of the overburden trends for the Tunnel Ridge Mine with a property limits provided by PennDOT (Figure VI.1). The accuracy of this property map could not be validated and is provided only to show the scale of the remaining coal reserves within Pennsylvania.

The average, minimum, maximum, and standard deviation of the measured overburdens within 1,000-ft of I-70 from the West Alexander to Claysville Interchanges are shown in Table VI.1. These overburden values are significantly less than the approximate average of 610-ft for Panel 15. If all other variables are left constant, less overburden will produce higher vertical subsidence and greater surface deformations and strains.

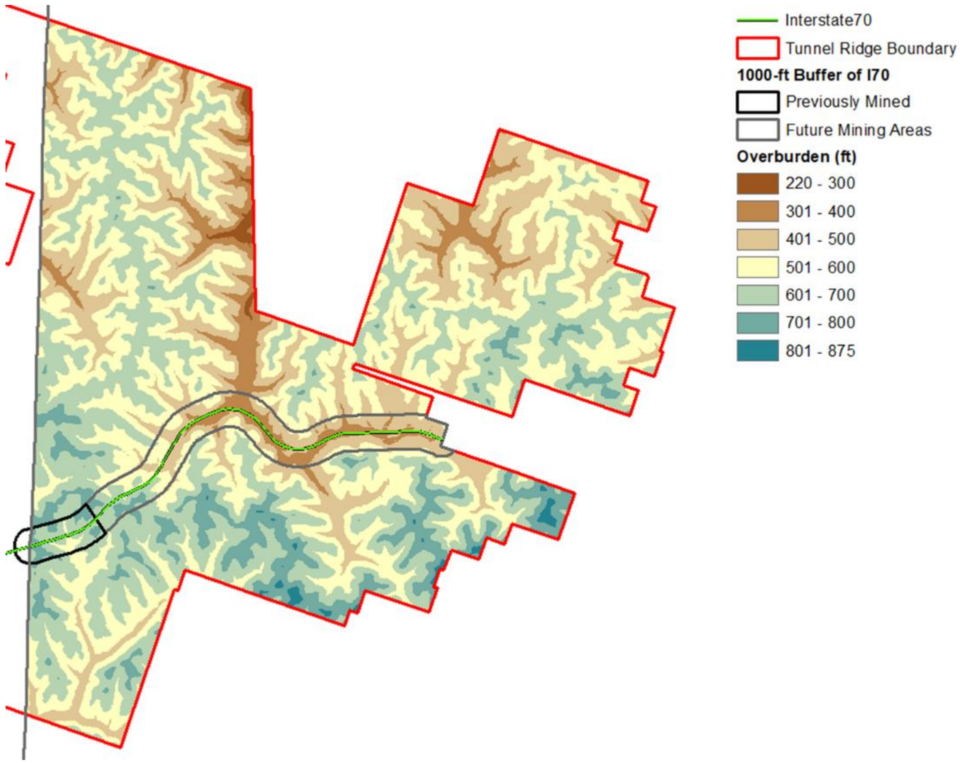

Figure VI.1 – Tunnel Ridge Mine assumed property limits and overburden trends along I-70 from the West Virginia State boarder to the Claysville Interchange

Table VI.1 – Overburden trends within 1,000-ft of I-70 from the West Alexander to the Claysville Interchanges

Boundary	Minimum, ft	Maximum, ft	Average, ft	SD, ft
I-70 1,000-ft Buffer	326	752	509	112

The orientation of the longwall face to the overlying interstate alignment within the study area is capable of producing a wide range of surface impacts. If the longwall face is oriented parallel to the interstate, impacts are expected to be greater than if the face is oriented perpendicular to the interstate. Figure VI.1 indicates a range of possible orientations, producing a assortment of surface impacts. These factors along with cut slope and embankment conditions will be evaluated as part of Task 3.

REFERENCE

Adelsohn, E., Iannacchione, A., and Winn, R. (2019). "Investigations on Longwall Mining Subsidence Impacts on Pennsylvania Highway Alignments," 38th International Conference on Ground Control in Mining, Morgantown, WV, 12 p .

Agioutantis, Z. and Karmis. M.K. (2008). "SDPS Surface Deformation Prediction System for Windows Version 6.0, Quick Reference Guide and Working Examples," Department of Mining and Minerals Engineering, Virginia Polytechnic Institute and State University, 2008, 248 p.

Brady, B.H.G., and Brown, E.T. (1985). *Rock Mechanics for Underground Mining.* George Allen & Unwin, London.

Briaud, J.L. (2001). Introduction to soil moduli. *Geotechnical News*, June Issue, pp. 1-8.

Bridgwater, J. (1980). On the width of the shear zone. *Geotechnique*, **30** (4): 533-536.

Daigle, L., & Mills, K. F. (2017). Experience of monitoring shear movements in the overburden strata around longwall panels. *Coal Operators Conference, University of Wollongong*. Pp. 125-137.

Dawson, E. M., Roth, W. H., & Drescher, A. (1999). Slope stability analysis by strength reduction. *Geotechnique*, *49*(6), 835-840.

Delano, H.L. and J.P. Wilshusen, (2001). "Landslides in Pennsylvania", Pennsylvania Geological Survey, 4th ser., Educational Series 9, 34 p.

Digital-Inclinometer-System-ICB0042C.pdf. (n.d.). Retrieved from https://www.rstinstruments.com/assets/brochures/Digital-Inclinometer-System-ICB0042C.pdf

Donaghe, R. T., & Torrey, V. H. (1979, September). Scalping and replacement effects on strength parameters of earth-rock mixtures. In *Proc. Conf. on Design Parameters in Geotechnical Engineering* (Vol. 2, pp. 29-34).

Edil, T.B., and Vallejo, L.E. (1980). Mechanics of coastal landslides and the influence of slope parameters. *Engineering Geology*, 16(1-2): 83-96.

Griffiths, D. V., & Lane, P. A. (2001). Slope stability analysis by finite elements. *GEOTECHNIQUE-LONDON-*, *51*(7), 653-654.

Hamel, J. and Flint, N. (1972). *Failure of Colluvial Slope,* Journal of the Soil Mechanics and Foundation Division, Proceedings of the American Society of Civil Engineers, Vol 98, No. SM2, Proc Paper 8731, February 1972, pp. 167-180.

Hamel, J. and Adams, W.R. (1981). Claystone Slides, Interstate Route 79, Pittsburgh, Pennsylvania, USA, Proceedings of the International Symposium on Weak Rock, Tokyo, 21-24 September 1981, pp. 549-553.

Highland, L.M. and Bobrowsky, P. (2008). "The Landslide Handbook – A Guide to Understanding Landslides", US Geological Survey, Circular 1325, 129 p.

Ho, I. H. (2017). Three-dimensional finite element analysis for soil slopes stabilisation using piles. *Geomechanics and Geoengineering*, *12*(4), 234-249.

Iannacchione, A., and Vallejo, L.E. (2000). Shear strength evaluation of clay-rock mixtures. In: Slope Stability 2000, American Society of Civil Engineers, *Geotechnical Special Publication 101*, pp. 209-223.

Iannacchione, A., Tonsor, S., Witkowski, M., Benner, J., Hale, A., and Shendge, M. (2011). "The Effects of Subsidence Resulting from Underground Bituminous Coal Mining on Surface Structures and Features and on Water Resources, 2003 to 2008," 3rd Five-Year Report, Bituminous Mine Subsidence and Land Conservation Act, Act 54 Amendments, PA Department of Environmental Protection, submitted by the University of Pittsburgh on January 10, 2011, 499 pages and 1 plate.

Johnson, A.M. (1970). *Physical Processes in Geology*. Freeman, Cooper and Co., San Francisco.

Karmis, M., Haycocks, C., Eitani, I., and Webb, B. (1981). *A Study of Longwall Subsidence in the Appalachian Coal Region Using Field Measurements and Computer Modeling Techniques.* 1st Annual Conference in Ground Control in Mining. Morgantown, WV: West Virginia University.

Lesny, P. (n.d.). *RST MEMS Digital Inclinometer Instruction Manual*. 60.

Matsui, T., & San, K. C. (1992). Finite element slope stability analysis by shear strength reduction technique. *Soils and foundations*, *32*(1), 59-70.

Miller, J.S. and W.Y. Bellinger. (2003). "Distress Identification Manual for the Long-Term Pavement Performance Program," 4th edition, U.S. Department of Transportation, Federal Highway Administration, Report No. FHWA-RD-03-031, 164 p.

Newmark, N.M. (1960). Failure hypothesis for soils. *Proceedings of Conference on the Shear Strength of Soils.* Boulder, Colorado, pp. 17-32.

O'Connor, K. (2001). *The Effects of Undermining Interstate Route 70, South Strabane Township, Washington County, Pennsylvania.* Pennsylvania Department of Environmental Protection.

PA DCNR website on Landslides
https://www.dcnr.pa.gov/Geology/GeologicHazards/Landslides/Pages/default.aspx

Painter, R. (2010). Personal communications.

Painter, R. (2019). Personal communications.

Peng, S. S., Ma, W. M., & Zhong, W. L. (1992). *Surface subsidence engineering*. Littleton, CO: Society for Mining, Metallurgy, and Exploration.

Pomeroy, J.S., and W.E. Davies, (1979)." Landslides and Related Features of the Donora, PA Quadrangle," US Geological Survey, Open File Map 79-1314 (B-2).

Rahn, P.H. (1996). *Engineering Geology.* Prentice Hall, New Jersey.

Roscoe, K. H. (1970). The influence of strains in soil mechanics. *Geotechnique*, *20*(2), 129-170.

Saeidi, A. Deck, O., Heib, M., Verdel, T., Rouleau, A. (2012). *Adjusting the Influence Function Method for Subsidence Prediction.* International Conference on Advanced Computational Engineering and Experimenting (ACE-X 2012). p. 59-66.

Scovazzo, V.A. (1999). *The Propagation Mechanics of Liquefied Sand Lenses due to Cyclic Loading.* Ph.D. Dissertation, University of Pittsburgh.

Vallejo, L.E. (1982). Development of a shear zone structure in stiff clays. *Proceedings of the 4th Int. Conference on Numerical Methods in Geomechanics, Canada*, **1***:* 255-262.

Vallejo, L.E., and Lobo-Guerrero, S. (2005). The elastic moduli of clays with dispersed oversize particles. *Engineering Geology*, 78(1-2):163-17

Vallejo, L.E. and Lin, J.S. (2010). *A Study of Highway Subsidence due to Longwall Mining using data collected from I-79.* Commonwealth of Pennsylvania: Department of Transportation.

Yancich, R. D. (1986). *Surface Subsidence in Longwall Mining – A Case Study*. Master's Thesis, Department of Mining Engineering, West Virginia University.

Wu, T. H., & Kraft, L. M. (1970). Safety analysis of slopes. *Journal of Soil Mechanics & Foundations Div*.

Zheng, Y. R., Zhao, S. Y., Kong, W. X., & Deng, C. J. (2005). Geotechnical engineering limit analysis using finite element method. *Yantu Lixue(Rock Soil Mech.)*, *26*(1), 163-168.

Zienkiewicz, O. C., Humpheson, C., & Lewis, R. W. (1975). Associated and non-associated visco-plasticity and plasticity in soil mechanics. *Geotechnique*, *25*(4), 671-689.

906-Little-Dipper-Jewell_2-Updated-Image.pdf. (n.d.). Retrieved from http://jewellinstruments.com/wp-content/uploads/2015/04/906-Little-Dipper-Jewell_2-Updated-Image.pdf